

UNIVERSITÉ DU QUÉBEC À CHICOUTIMI

MÉMOIRE PRÉSENTÉ À

L' UNIVERSITÉ DU QUÉBEC À CHICOUTIMI

COMME EXIGENCE PARTIELLE

DE LA MAÎTRISE EN INGÉNIERIE

BY

SHIMAA ELHADAD

**EFFECT OF TRACE ELEMENTS ON THE MICROSTRUCTURE
AND POROSITY FORMATION IN 319 TYPE AL-SI-CU ALLOYS**

JULY 2003



Mise en garde/Advice

Afin de rendre accessible au plus grand nombre le résultat des travaux de recherche menés par ses étudiants gradués et dans l'esprit des règles qui régissent le dépôt et la diffusion des mémoires et thèses produits dans cette Institution, **l'Université du Québec à Chicoutimi (UQAC)** est fière de rendre accessible une version complète et gratuite de cette œuvre.

Motivated by a desire to make the results of its graduate students' research accessible to all, and in accordance with the rules governing the acceptance and diffusion of dissertations and theses in this Institution, the **Université du Québec à Chicoutimi (UQAC)** is proud to make a complete version of this work available at no cost to the reader.

L'auteur conserve néanmoins la propriété du droit d'auteur qui protège ce mémoire ou cette thèse. Ni le mémoire ou la thèse ni des extraits substantiels de ceux-ci ne peuvent être imprimés ou autrement reproduits sans son autorisation.

The author retains ownership of the copyright of this dissertation or thesis. Neither the dissertation or thesis, nor substantial extracts from it, may be printed or otherwise reproduced without the author's permission.

*Dedicated to my parents,
Waleed and my little Abdo*

RÉSUMÉ

Les alliages d'aluminium-silicium Al-Si ont connu nombreuses applications dans l'industrie grâce à leur haute résistance mécanique, leur poids faible, leur bonne résistance à la corrosion et à leur excellente coulabilité. Un des traitements du métal liquide, appliqué sur ces alliages, est la modification par certains éléments comme le strontium (Sr) et le sodium (Na). Avec la modification, la morphologie du silicium eutectique change d'une forme aciculaire à une forme fibreuse ou globulaire. Cette dernière améliore les propriétés mécaniques, particulièrement la ductilité.

Les alliages 319, appartenant au système Al-Si-Cu, sont très populaires pour les applications de l'automobile, surtout avec une haute teneur en magnésium (Al-6.5%Si-3.5%Cu-0.4%Mg). Ces applications couvrent une gamme assez large incluant des pièces critiques comme les blocs de moteur, têtes de cylindre, etc.

Afin d'optimiser les propriétés de ces alliages, il est nécessaire de prendre compte les impuretés et les éléments de trace, comme le bismuth (Bi), le calcium (Ca), le phosphore (P), etc. Puisque le strontium est fréquemment utilisé dans ces alliages, il est important de savoir l'effet de ces éléments sur l'efficacité du strontium comme agent de modification, et la possibilité de leur interaction avec le strontium sur la qualité du produit final.

Avec l'augmentation de l'usage des matériaux recyclés dans l'industrie de l'automobile et la faible connaissance de cet aspect, cette étude a été réalisée. Le but principal est d'améliorer les informations concernant l'effet de l'interaction Sr-Bi et Sr-Ca sur les caractéristiques des particules de silicium eutectique dans les alliages 319 contenant 0.04 et 0.4% Mg en poids. Comme la modification au strontium est presque associée à l'augmentation de la quantité de porosité dans l'alliage, cette dernière a un effet nuisible sur les propriétés mécaniques; l'étude de cet effet fait partie de ce travail de recherche.

Les deux alliages 319 utilisés dans ce projet sont modifiés par le strontium (~80 ppm). Par la suite, différentes concentrations de bismuth (50-9000 ppm) et calcium (50-200 ppm) sont ajoutées aux ces alliages. Les alliages fondus sont coulés dans un moule en graphite préchauffé à 600 °C avec un taux de refroidissement ~0.8 °C/s. Ce dernier est proche aux conditions de l'équilibre pour réaliser les différentes phases en utilisant la technique d'analyse thermique. D'autre part, le métal liquide a été coulé dans un moule métallique avec un angle variable (0.5 et 15°). Avant l'analyse métallographique, tous les

échantillons ont été coupés et polis selon une technique standard. L'analyse microstructurale fut réalisée en utilisant un microscope optique combiné à un logiciel analyseur d'images de type Leco 2001 dans le but de quantifier les diverses phases. Pour identifier la nature de ces phases, les échantillons sont examinés par une microsonde électronique combiné à un système de rayons-X et un système de spectrométrie des rayons-X par longueur d'ondes.

Les résultats montrent que l'effet de la modification au strontium diminue d'une façon continue avec l'addition du bismuth jusqu'à 2250 ppm. A cette concentration, on note l'absence de la surfusion de l'eutectique indiquant la non modification. Cette observation est attribuée à la réaction entre le Sr-Bi ou entre le Bi-Mg-Sr durant la solidification avant la réaction eutectique. Cette réaction diminue la quantité du Sr libre qui est nécessaire pour la modification des particules de silicium eutectique. En augmentant de plus la teneur en Bi jusqu'à 6500 ppm, on observe le retour du phénomène de la surfusion renseignant l'efficacité du bismuth comme agent de modification.

Le bismuth est précipité sous forme d'oxydes contenant quelques ppm en Sr avec une bonne quantité de magnésium (~ 5%), indépendamment du taux de refroidissement appliqué. Les additions en calcium de l'ordre de 17 ppm et plus, augmentent la taille des particules de silicium eutectique, due à la formation de composés Al-Si-Ca-Sr. La nature de ces composés, dont la forme est tiges ou plaquettes, correspond respectivement aux compositions chimiques $Al_7(Ca,Sr)Si_7$ ou $Al_2(Ca,Sr)Si_2$. Un autre paramètre à considérer est la présence du magnésium dans l'alliage en question. Les impuretés comme AlP, $MgAl_2O_4$ et MgO agissent comme site ou emplacement de nucléation pour la précipitation des plaquettes contenant de calcium. La croissance de cette phase aura lieu par un mécanisme de macles.

En coulant dans un moule variable, la vitesse du solidus est contrôlée par la réjection du soluté à l'interface solide-liquide. Cet effet est plus significatif, particulièrement avec un petit moule (0° angle), comparé au grand moule (15° angle), et ceci est dû à la grande vitesse de solidification associée au petit moule. Ce dernier montre la formation de points chauds surtout au fond du moule.

En ce qui concerne la formation de porosité, le pourcentage de porosité augmente avec l'addition de bismuth (~ 2000 ppm), résultant de la formation d'oxydes de bismuth ou d'oxydes de bismuth et de strontium. Avec une concentration assez élevée en bismuth (~ 6000 ppm), le bismuth est partiellement oxydé. Cependant, la porosité est toujours associée à la partie de bismuth oxydée. Dans le cas du calcium, la porosité est toujours associée avec CaO qu'avec les composés en calcium mentionnés auparavant. Les oxydes de bismuth et de calcium forment de microporosité trop fine (~1 μm ou moins). Cette observation explique le faible pourcentage de porosité mesurée dans ces alliages. Pour les alliages coulés en petit moule (0° angle), la porosité est fréquemment observée au voisinage de points chauds.

ABSTRACT

Aluminum-silicon (Al-Si) alloys find numerous applications in industry on account of their high strength, light weight, good corrosion resistance and excellent castability. One of the melt treatment procedures normally applied to Al-Si casting alloys is that of modification where, by the addition of certain elements such as sodium (Na), strontium (Sr), *etc.*, the acicular eutectic silicon usually observed in the non-modified alloy is converted or “modified” to a fibrous form that is beneficial to the mechanical properties of the alloy, in particular, its ductility.

The 319 alloy, belonging to the Al-Si-Cu system, is a commercially popular alloy that finds extensive use in automotive applications. A higher magnesium-containing version (Al-6.5%Si-3.5%Cu-0.4% Mg) is frequently employed in such applications. The applications cover a broad range that includes critical components such as engine blocks and cylinder heads.

In order to optimize the properties of these alloys, it is necessary to take into consideration the presence of impurities and trace elements such as bismuth, calcium, phosphorus, *etc.*, which can possibly affect the properties. In this respect, since Sr-modified alloys are invariably employed in the production of automotive castings, it is important to have knowledge of the effect of such impurities on the Sr-modification process in terms of any interactions between them, and the consequent effect on the final product.

With the increased use of secondary materials in production, and in view of the fact that information in this area is scarce, this aspect becomes important enough to require a detailed study. The present work was therefore undertaken to quantify the effects of Sr-Bi and Sr-Ca interactions and their impact on the eutectic silicon particles characteristics (which would provide a measure of the effectiveness of the modification treatment) in Sr-modified 319 alloys containing 0.04 and 0.4wt% Mg. As Sr modification is almost always associated with an increase in the porosity level of the alloy, and since the presence of porosity is known to be detrimental to the alloy properties and casting quality, the effect on porosity formation was also studied.

The two 319 type alloys used were modified with strontium (~80 ppm), to which various concentrations of bismuth (50-9000 ppm) and calcium (50-200 ppm) were added. The alloy melts were poured into (i) a preheated graphite mold (600°C, cooling rate ~0.8°C/s) that provided close-to-equilibrium cooling conditions and could be

simultaneously used to conduct thermal analysis experiments, and (ii) a variable angle wedge mold that provided a range of solidification conditions with the use of 0°, 5° and 15° angle mold configurations. Metallographic samples were sectioned from the castings obtained from these molds and polished for examination. Microstructural analysis was carried out using optical microscopy, in conjunction with image analysis for quantification purposes. Phase identification was carried out using electron probe microanalysis (EPMA), coupled with EDX and WDS facilities.

The results showed that the modification effect of strontium diminishes continuously with Bi addition, up to 2250 ppm Bi, at which point no eutectic undercooling (indicating no modification) is observed. This is attributed to Bi-Sr or Bi-Mg-Sr interactions taking place during solidification (prior to the eutectic reaction), which reduce the amount of free Sr available for Si modification. With further increase in Bi addition, undercooling again commences, until at 6500 ppm Bi addition, an undercooling of $\sim 0.7^\circ\text{C}$ is observed, indicating that the Bi is acting as a modifier.

Bismuth is found to precipitate in the form of oxides- containing a few ppm of Sr and an appreciable amount of Mg ($\sim 5\%$), irrespective of the cooling rate. Calcium additions in the order of 17 ppm and higher coarsen the eutectic Si particles, due to the formation of Al-Si-Ca-Sr compounds, the morphology (rod- or plate-type) and chemical composition ($\text{Al}_7(\text{Ca},\text{Sr})\text{Si}_7$ or $\text{Al}_2(\text{Ca},\text{Sr})\text{Si}_2$) of which are strongly related to the Mg content of the alloy. Impurities such as AlP, MgAl_2O_4 , and MgO act as nucleation sites for the plate-type Ca-containing phase. Growth of the latter occurs via an impurity-induced twinning mechanism.

The solidus velocity is affected by the rejection of solute atoms in front of the moving solid/liquid interface, and is more significant in the small mold (0° angle) castings compared to the large mold (15° angle) castings, due to the much higher velocities obtained with the small mold configuration. The latter castings are also found to display hot spots frequently.

With respect to porosity formation, the percentage porosity is found to increase at Bi additions of ~ 2000 ppm, due to the formation of Bi- and (Bi,Sr)-oxides. At high Bi additions (~ 6000 ppm), the Bi is only partially oxidized. The porosity, however, is always associated with the Bi-oxides. In the case of Ca, while the porosity is mainly associated with CaO rather than the Ca-containing compounds, it is dependent to some extent on the particle size (*cf.* a particle size of $\sim 10\text{-}15\ \mu\text{m}$ for the Ca-compound with $1\text{-}3\ \mu\text{m}$ for the CaO particles). Both Bi- and Ca-oxides form very fine microporosities ($\sim 1\ \mu\text{m}$ or less). This would explain the low percentage porosity values observed with Bi and Ca additions. In the case of the small mold castings, such microporosity is frequently observed to occur in/near the hot spot regions.

ACKNOWLEDGMENTS

I would like to sincerely acknowledge the guidance of my supervisors, Professors F.H. Samuel and A.M. Samuel, who gave me the opportunity to undertake this research study. I would also like to thank all members of the TAMLA group for their help and assistance during various stages of my work, in particular, Mr. Alain Bérubé, technician, TAMLA-UQAC, for his assistance with the castings and sample preparation.

Financial support in the form of scholarships received from the Natural Sciences and Engineering Research Council of Canada (NSERC), the Fondation de l'Université du Québec à Chicoutimi (FUQAC), General Motors Powertrain Group (U.S.A), and Corporativo Nematik (Mexico) is gratefully acknowledged.

Thanks are also due to MM Glenn Poirier and Shi Lang of the Microanalysis Laboratory, Earth and Planetary Science Department, McGill University for carrying out the EPMA work.

Finally, I would like to extend a special acknowledgment to my husband for his continuous encouragement and support during my work.

PUBLICATIONS

Two research articles have been published and two others have been prepared for submission from this work. The details are provided below.

1. Influence of Bi-Sr and Ca-Sr Interactions on the Si Particle Characteristics in 319 Alloy, S. El-Hadad, A.M. Samuel, F.H. Samuel, H.W. Doty, S. Valtierra.
Light Metals 2002, T.Lewis (Ed.), The Metallurgical Society of the Canadian Institute of Mining, Metallurgy and Petroleum, Montreal, **2002**, pp. 265-283.
2. Effects of Bi and Ca Addition on the Characteristics of Eutectic Si Particles in Sr-modified 319 alloys.
S. El-Hadad, A.M. Samuel, F.H. Samuel, H.W. Doty, S. Valtierra.
International Journal of Cast Metals Research (**2003**), in Press.
3. Effects of Bi and Ca Additions on the Microstructure of Sr-Modified 319 Type Alloys Under Variable Cooling Conditions.
S. El-Hadad, A.M. Samuel, F.H. Samuel, H.W. Doty, S. Valtierra.
Prepared for publication in *AFS Transactions*, vol. 112 (**2004**), Paper No. **04-008**, 13 p.
4. Influence of Bi and Ca Additions on Thermal and Microstructure Characteristics of Sr-modified 319 Type Alloys Under Variable Cooling Conditions.
S. El-Hadad, A.M. Samuel, F.H. Samuel, H.W. Doty, S. Valtierra.
Prepared for submission to *Metallurgical and Materials Transactions A* (**2003**).

Conference Presentations

1. Influence of Bi-Sr and Ca-Sr Interactions on the Si Particle Characteristics in 319 Alloy, S. El-Hadad, A.M. Samuel, F.H. Samuel, H.W. Doty, S. Valtierra.
Presented at the *Int. Conf. on Enabling Technologies for Light Metals and Composite Materials and Their End-Products* (COM 2002), Montreal, Aug 11-14, 2002.
Casting and Solidification II. Session 13B: Paper 13B.1.
2. Effects of Bi and Ca Additions on the Microstructure of Sr-Modified 319 Type Alloys Under Variable Cooling Conditions.
S. El-Hadad, A.M. Samuel, F.H. Samuel, H.W. Doty, S. Valtierra.
To be presented at the *108th AFS Metalcasting Congress*, Rosemont, IL, June 12-15, 2004. Paper No. 04-008, pp. 1-13.

TABLE OF CONTENTS

RÉSUMÉ	i
ABSTRACT	iii
ACKNOWLEDGMENTS	v
PUBLICATIONS	vi
TABLE OF CONTENTS	vii
LIST OF FIGURES	x
LIST OF TABLES	xv
 CHAPTER 1	
DEFINITION OF THE PROBLEM	1
1.1 INTRODUCTION	2
1.2 OBJECTIVES.....	3
 CHAPTER 2	
LITERATURE SURVEY	4
2.1 INTRODUCTION	5
2.2 MODIFICATION OF Al-Si ALLOYS.....	6
2.2.1 CHEMICAL MODIFIERS	6
2.2.2 EFFECTS OF MODIFICATION.....	10
2.2.2.1 EFFECT OF MODIFICATION ON MICROSTRUCTURE.....	10
2.2.2.2 EFFECT OF MODIFICATION ON CASTING SOUNDNESS	17
2.2.2.3 EFFECT OF MODIFICATION ON MECHANICAL PROPERTIES	18
2.3 POROSITY FORMATION IN Al-Si ALLOYS.....	19
2.3.1 TYPES OF POROSITY	19
2.3.2 FACTORS CONTROLLING POROSITY FORMATION	20
2.4 EFFECT OF TRAMP ELEMENTS	33
2.4.1 BISMUTH IN Al-Si ALLOYS.....	33
2.4.1.1 MICROSTRUCTURE EFFECTS.....	34
2.4.1.2 THERMAL ANALYSIS.....	40

2.1.4.3	POROSITY	41
2.4.1.4	MECHANICAL PROPERTIES.....	42
2.4.2	CALCIUM IN Al-Si ALLOYS.....	44
2.4.2.1	CA AS IMPURITY.....	44
2.4.2.2	CA COMPOUNDS	46
2.4.2.3	REMOVAL OF IMPURITY CALCIUM.....	48
2.4.2.4	EFFECT OF Ca AS A MODIFIER	48
2.4.2.5	INTERACTION OF CALCIUM WITH MODIFIERS	48
2.4.2.6	EFFECT OF CALCIUM ON IRON IMPURITIES.....	49
2.4.2.7	EFFECT OF CALCIUM ON MECHANICAL PROPERTIES.....	50
2.4.2.8	EFFECT OF CALCIUM ON CASTING CHARACTERISTICS	53
2.4.2.9	EFFECT OF CALCIUM ON POROSITY FORMATION.....	53

CHAPTER 3

EFFECT OF Bi AND Ca ADDITIONS ON THE EUTECTIC Si PARTICLE

CHARACTERISTICS IN Sr-MODIFIED 319 ALLOYS.....		55
3.1	INTRODUCTION	56
3.2	EXPERIMENTAL PROCEDURE	56
3.2.1	ALLOY AND MELT PREPARATION	56
3.2.2	THERMAL ANALYSIS.....	58
3.2.3	METALLOGRAPHY	59
3.3	RESULTS AND DISCUSSION	60
3.3.1	THERMAL ANALYSIS.....	60
3.3.2	IMAGE ANALYSIS: Si PARTICLE CHARACTERISTICS.....	67
3.3.3	MICROSTRUCTURAL ANALYSIS.....	72
3.3.3.1	OPTICAL MICROSCOPY.....	72
3.3.4	ELECTRON PROBE MICROANALYSIS	75
3.3.4.1	EFFECT OF BI ADDITION.....	75
3.3.4.2	EFFECT OF CA ADDITION	81

CHAPTER 4

EFFECT OF Bi AND Ca ADDITIONS ON POROSITY AND EUTECTIC Si PARTICLE CHARACTERISTICS IN Sr-MODIFIED 319 ALLOYS UNDER VARIABLE COOLING CONDITIONS.....

.....		89
4.1	INTRODUCTION	90
4.2	EXPERIMENTAL PROCEDURE	91
4.2.1	VARIABLE ANGLE WEDGE MOLD.....	94
4.2.2	THERMAL ANALYSIS.....	96
4.2.2.1	THERMAL GRADIENT.....	96
4.2.2.2	INTERFACE VELOCITY	96
4.3	RESULTS AND DISCUSSION	97
4.3.1	THERMAL ANALYSIS.....	97
4.3.1.1	EUTECTIC TEMPERATURE	97

4.3.1.2	TEMPERATURE GRADIENTS AND INTERFACE VELOCITIES ..	100
4.3.2	IMAGE ANALYSIS	108
4.3.2.1	Si PARTICLE MEASUREMENTS.....	108
4.3.2.2	POROSITY MEASUREMENTS.....	116
4.3.3	ELECTRON PROBE MICROANALYSIS	123
4.3.3.1	BISMUTH ADDITION	124
4.3.3.2	CALCIUM ADDITION.....	131
CONCLUSIONS		137
SUGGESTIONS FOR FUTURE WORK.....		141
REFERENCES.....		142

LIST OF FIGURES

Figure 1.	Effect of sodium and strontium modifiers as a function of time.	8
Figure 2.	Hydrogen content as a function of holding temperature for aluminum alloy 356 melts with various modifiers.	9
Figure 3.	Microstructural differences between a sodium-modified structure, and an antimony refined structure.	13
Figure 4.	Variation of average eutectic temperature with Sr content in 319 alloy.	14
Figure 5.	Modification rating as a function of holding time for various Sr levels.	17
Figure 6.	a) Pore morphology at 0.49 mL hydrogen/100 g Al, ts ~12.5 s b) Pore morphology at 0.49 mL hydrogen/100 g Al, ts ~71 s.	23
Figure 7.	(a) Total amount of porosity and (b) Shrinkage and gas porosity as a function of initial hydrogen content (Ho).	24
Figure 8.	Schematic representation of the Tatur mold.	25
Figure 9.	Summary of the variation of microporosity content with a freezing range for alloys with various melt treatments.	32
Figure 10.	Al-Bi phase diagram.	33
Figure 11.	Photomicrographs of cast Al-Si eutectic alloys a) unmodified; b) treated with 0.2 wt pct Bi, c) treated with 0.25 wt pct Bi.	35
Figure 12.	Microstructure of A356.2, cast in graphite mold, containing various percentages of Bi and modified with 0.015% Sr, 500X.	36
Figure 13.	Eutectic Si structure in (a) 0.01% Bi, modified with 0.05% Sr, and (b) 0.02% Bi, modified with 0.02% Sr.	36
Figure 14.	Addition of different modifiers to unmodified AL2 (Al-Si) alloy.	38
Figure 15.	Effect of Bi and Na addition on the refining of eutectic silicon a) 136 ppm Na, 38 ppm Bi, and b) 76 ppm Na, 115 ppm Bi	38
Figure 16.	a) Original alloy, b) Na treated, and c) Sr treated AL4 (Al-Si-Mg) alloy.	39
Figure 17.	Al-Si eutectic temperatures versus %wt Bi in a melt separated by wt% Sr.	40
Figure 18.	The alpha-aluminum-arrest and eutectic-arrest temperature of A356.2 alloy, modified with 0.015% Sr, obtained in conventional silica thermal analysis cups.	41
Figure 19.	Amount of Bi, ppm vs. percentage porosity.	42
Figure 20.	Effect of Bi on the mechanical properties of unmodified, Na-	43

	modified and Sr-modified Al casting alloy, A413.8.	
Figure 21.	Effect of the addition of modifier elements on mechanical properties in as-cast specimens.	44
Figure 22.	Al-Ca phase diagram.	45
Figure 23.	Calcium and silicon interactions in Al-5%Si alloys at 700 °C.	47
Figure 24.	Effect of Ca addition on %Bi.	47
Figure 25.	Calcium loss vs. holding time of SAE332 (Al-Si-Cu-Mg alloy) at 665.6 °C.	49
Figure 26.	Effect of calcium and iron additions on the eutectic silicon size.	50
Figure 27.	Effect of Ca on tensile strength and elongation of AC3A (Al-Si), AC2A (Al-Si-Cu), ADC12 (Al-Si-Cu) alloys.	51
Figure 28.	Effect of Ca on Vickers hardness of AC3A (Al-Si), AC2A (Al-Si-Cu), ADC12 (Al-Si-Cu) alloys.	52
Figure 29.	Effect of Ca on shrinkage cavity formation in Al-Si alloy: a) 0.0005% Ca, b) 0.014% Ca, and c) 0.026% Ca.	54
Figure 30.	Graphite mold.	59
Figure 31.	Cooling curves obtained for B alloys containing various amounts of Bi.	62
Figure 32.	Cooling curves obtained for C alloys containing various amounts of Bi.	63
Figure 33.	Cooling curves obtained for B alloys containing various amounts of Ca.	64
Figure 34.	Cooling curves obtained for C alloys containing various amounts of Ca.	65
Figure 35.	The effect of Bi addition on eutectic undercooling in the B alloy.	66
Figure 36.	Average Si particle area as a function of Bi content in B and C alloys.	68
Figure 37.	Average Si particle length as a function of Bi content in B and C alloys.	68
Figure 38.	Average Si particle roundness as a function of Bi content in B and C alloys.	69
Figure 39.	Average Si particle density as a function of Bi content.	69
Figure 40.	Average Si particle area as a function of Ca content in B and C alloys.	70
Figure 41.	Average Si particle length as a function of Ca content in B and C alloys.	71
Figure 42.	Average Si particle roundness as a function of Ca content in B and C alloys.	71
Figure 43.	Average Si particle density as a function of Ca content in B and C alloys.	72
Figure 44.	Eutectic Si structure obtained in (a) A, and (b) B, and (c) C alloys.	73
Figure 45.	Eutectic Si structure obtained in (a) BBE alloy (B + 1151 ppm Bi), and alloy (C + 1152 ppm Bi).	73
Figure 46.	Eutectic Si structure obtained in (a) BCD alloy (B + 129 ppm Ca),	74

	and (b) CCD alloy (C+ 221 ppm Ca).	
Figure 47.	Bi distribution in (319 + 300 Sr + 9000 ppm Bi) alloy.	75
Figure 48.	SEM micrographs obtained from CBJ alloy (C + 9600 ppm Bi)	77
	a) SEM micrograph;	
	b) Bi image of (Mg,Bi) oxide particles;	
	c) Mg image of (Mg,Bi) oxide particles;	
	d) O image of (Mg,Bi) oxide particles.	
Figure 49.	EDX spectrum and oxygen scan corresponding to Mg-Bi-O particles observed in the CBJ alloy samples (C alloy + 9600 ppm Bi).	78
Figure 50.	a) Backscattered image, and X-ray images of b) O, c) Sr, and d) Bi taken from CBE alloy sample (C alloy + 1152 ppm Bi).	79
Figure 51	EDX spectrum corresponding to a Mg-Sr-Bi-O particle observed in 319 alloy containing (0.4 % Mg + 300 ppm Sr + 9000 ppm Bi).	80
Figure 52.	Backscattered images taken from BCD alloy (B + 129 ppm Ca) showing the morphology of the rod-type Ca-containing particle	81
	a) plane view, and b) inside a pore	
Figure 53.	(a) Backscattered image, and X-ray images of (b) Si, and (c) Ca, (d) Sr in the rod-type Ca-containing particle observed in BCD alloy (B + 129 ppm Ca).	82
Figure 54.	EDX spectrum showing the elements observed in the rod-type, BCD alloy (B alloy + 129 ppm Ca).	83
Figure 55.	Backscattered image taken from the CCD alloy (C + 221 ppm Ca) showing growth through twinning in a plate-like Ca-containing phase particle, spot analysis of points 1 and 2 are given in Table 10.	84
Figure 56	a) Backscattered image, and X-ray images of b) Mg, c) P, and d) O elements in the plate-type Ca-containing phase particle observed in CCD alloy (C alloy containing 221 ppm Ca).	86
Figure 57.	a) Backscattered image showing a plate type Ca-containing phase particle in CCD alloy, and images of b) Ca, c) Sr, and d) P elements across the particle. Line scans taken across the image are superimposed in each case.	87
Figure 58.	EDX spectrum taken from the plate-type Ca-containing phase particle in CCD alloy showing Al, Si, Sr, P, and Mg reflections.	88
Figure 59.	Schematic diagram of the variable angle wedge mold and positioning of thermocouples used to determine various thermal parameters.	95
Figure 60.	Cooling curves obtained for (a) B alloy, (b) C alloy, large mold (15° angle).	98
Figure 61.	Cooling curves obtained for BB2 alloy (B alloy + 2186 ppm Bi, large mold).	99
Figure 62.	Cooling curves obtained for CC2 alloy (C alloy + 94 ppm Ca, large mold).	100
Figure 63.	Comparison of temperature, thermal gradient and cooling rates versus time for (a) B (Sr-modified 319), (b) BB2 (B+2186 ppm Bi),	101

	and (c) BC2 (B+103 ppm Ca) alloys (small mold).	
Figure 64.	Average vertical solidus interface velocities in the wedge mold as a function of the distance from the bottom of the mold for (a) B alloy, (b) BB2 alloy (B + 2186 ppm Bi) for small, medium and large molds.	103
Figure 65.	Average vertical solidus interface velocities in the wedge mold as a function of the distance from the bottom of the mold for (a) C alloy, (b) CB6 alloy (C + 3020 ppm Bi) for small, medium and large molds.	104
Figure 66.	Schematic diagram showing rejection of solute atoms in front of a growing α -Al dendrite in (a) B (Sr-modified 319 alloy), (b) Bi-containing B alloy.	105
Figure 67.	Average vertical solidus interface velocities in the wedge mold as a function of the distance from the bottom of the mold for (a) BC2 alloy (B + 103 ppm Ca), and (b) CC2 alloy (C + 94 ppm Ca), for medium and large molds.	107
Figure 68.	Dendrite arm spacing versus distance from mold bottom for B alloy for different mold configurations.	108
Figure 69.	Variation in the average Si particle area in B alloy as a function of Bi addition obtained in a) small mold, and b) large mold samples. Positions 1, 2 and 3 in the legend correspond to the thermocouple positions in the casting from which the samples for metallographic examination were sectioned.	110
Figure 70.	Variation in the average Si particle area in C alloy as a function of Bi addition obtained in a) small mold, and b) large mold samples. Positions 1, 2 and 3 in the legend correspond to the thermocouple positions in the casting from which the samples for metallographic examination were sectioned.	111
Figure 71.	Eutectic Si structure observed in B alloy with (a) 0 ppm, (b) 1555 ppm, and (c) 6060 ppm Bi additions. Note the well-modified Si particles in (a) in the Sr-modified alloy, and the demodification and modification effects of Bi in (b) and (c) at the respective Bi levels.	112
Figure 72.	Eutectic Si structure in the C alloy with (a) 0 ppm, (b) 874 ppm, and (c) 3020 ppm Bi additions.	113
Figure 73.	Eutectic Si structure in the B alloy with (a) 0 ppm, (b) 103 ppm, and (c) 465 ppm Ca additions. The circled area in (c) points to a Ca-compound particle.	114
Figure 74.	Eutectic Si structure in the C alloy with (a) 0 ppm, (b) 94 ppm, and (c) 486 ppm Ca additions. The circled areas point to a Ca-compound particle in each case.	115
Figure 75.	Variation in (a) percentage porosity, and (b) average pore length as a function of Bi addition in B alloy samples obtained from small and large castings.	117
Figure 76.	Variation in (a) percentage porosity, and (b) average pore length as a	118

	function of Bi addition in C alloy samples obtained from small and large mold castings.	
Figure 77.	Macrographs of hot spots (circled) in castings containing (a) < 5 ppm Ca; (b) 40 ppm Ca; (c) ~150 ppm Ca.	121
Figure 78.	Examples of hot spot formation in (a) B alloy, and (b) BC5 alloy (B+465 ppm Ca) (small mold, position 1 samples).	122
Figure 79.	X-ray radiographs obtained from the TiB ₂ grain refined (Al-9 wt% Si-3 wt% Cu) alloy samples, (a) cold mold, and (b) hot mold.	123
Figure 80.	Backscattered image taken from BB2 alloy (B alloy + 2186 ppm Bi), large mold-position 2 sample.	124
Figure 81.	Line scans showing (a) O, and (b) Bi distributions from Bi oxides observed in BB2 alloy (B alloy + 2186 ppm Bi).	125
Figure 82.	Backscattered image showing a Bi particle in BB6 alloy (B alloy + 6060 Bi, large mold sample).	126
Figure 83.	Backscattered image and X-ray images of O, Sr and Bi elements obtained from the Bi particle shown in Figure 82 (BB6 alloy).	128
Figure 84.	EDX spectrum obtained from the Bi particle shown in Figure 82 for BB6 alloy.	129
Figure 85.	Backscattered image taken from CB2 alloy (C alloy + 1034 ppm Bi, large mold sample), showing Bi oxide particles (arrowed) within and around a pore.	129
Figure 86.	EDX spectrum corresponding to Figure 85, obtained from CB2 alloy.	130
Figure 87.	Backscattered image obtained from CB2 alloy (C alloy + 1034 ppm Bi, small mold sample), showing the presence of microporosity and Bi oxide particles (white) in the vicinity of a hot spot region.	131
Figure 88.	Ca-compound particles observed in BC2 alloy (B alloy + 103 ppm Ca) showing (a) plate-type, and (b) rod-type particles.	132
Figure 89.	Backscattered images taken from (a) B, and (b) C alloy containing ~500 ppm Ca (large mold samples).	134
Figure 90.	Backscattered image showing the oxygen distribution for the same particles illustrated in Figure 89(b).	135

LIST OF TABLES

Table 1	Chemical composition of as cast alloys used for experimental work	22
Table 2	Volume percent porosity of treated and untreated samples	29
Table 3	Samples for the metallographic determination of the modification level	37
Table 4	Chemical composition of G- AlSi12 (Cu) (modified A413) (wt%)	43
Table 5	Chemical composition (wt %) of the alloys used in the present work.....	57
Table 6	Alloy codes for Bi-containing alloys	57
Table 7	Alloy codes for Ca-containing alloys.....	57
Table 8	The undercooling values obtained for alloy B from 4 identical experimental conditions	59
Table 9	Approximate composition (at%) of bismuth oxide particles observed in CBE alloy sample (C alloy + 1152 ppm Bi)	80
Table 10	Chemical composition of the examined Ca-containing phase particles obtained from WDS analysis	83
Table 11	Chemical compositions (wt%) of the two main alloys used.....	92
Table 12	Alloy codes for Bi- and Ca-containing alloys.....	92
Table 13	Average Si particle area and corresponding standard deviation obtained in B and C alloys with Ca addition	116
Table 14	Percentage porosity for B and C alloys* with Ca addition.....	119
Table 15	Approximate composition (at%)*of the plate- and rod-type Ca-containing particles observed in BC2 alloy obtained from WDS analysis of the particle surface	132
Table 16	WDS analysis* corresponding to Figure 89(a), obtained from BC5 alloy (B alloy + 465 ppm Ca).....	136
Table 17	WDS analysis* corresponding to Figure 89(b), obtained from CC5 alloy (C alloy + 486 ppm Ca).....	136

CHAPTER 1

DEFINITION OF THE PROBLEM

CHAPTER 1

DEFINITION OF THE PROBLEM

1.1 INTRODUCTION

Aluminum-silicon (Al-Si) alloys are widely used in numerous applications because of their high strength, light weight, good corrosion resistance and castability. It is well established that the addition of certain elements such as calcium (Ca), sodium (Na), and strontium (Sr) to hypoeutectic Al-Si alloys alters or 'modifies' the morphology of the eutectic silicon from its acicular plate-like form to a fibrous form. This change in the Si morphology enhances the mechanical properties of the alloy and, in particular, its ductility.¹In this regard, Sr-modification is one of the melt treatment procedures normally applied to (Al-Si) casting alloys.

To optimize the modification process, other factors controlling modification should also be considered, e.g., the presence of various tramp elements, such as Bi, Ca, P, etc. and any possible interactions with the modifier used. With respect to these elements, the presence of Bi is known to increase the machining speed and reduce the need for cutting fluids,² whereas Ca refines and spheroidizes the iron intermetallics as well as the eutectic silicon in Al-Si base alloys, resulting in improved mechanical properties.³⁻⁴

Although investigations have been carried out to study the influence of tramp elements on the microstructure and mechanical properties of hypoeutectic Al-Si alloys, there is not much information available on the effects of these elements on the modification of the eutectic silicon. Among commonly used Al-Si base alloys, 319 alloy is a commercially popular alloy used in diverse automotive applications including critical components such as engine blocks and cylinder heads.

In view of the fact that commercial alloys invariably contain a certain amount of impurity and trace elements, it was considered relevant to investigate these aspects in 319 alloys used in such applications. Both 319 alloys and its higher magnesium version (used in automotive applications) were employed in this study.

1.2 OBJECTIVES

The present research work was undertaken to study the effects of trace elements such as Bi and Ca on the changes in the microstructure of Sr-modified 319 type Al-Si alloys. The work was divided into two parts covering the following aspects:

- Correlation of Al-Si eutectic temperature with trace element additions;
- Evaluation and quantification of the eutectic Si phase;
- Evaluation of porosity
- Correlation of the new phases observed with the addition of trace elements.

CHAPTER 2
LITERATURE SURVEY

CHAPTER 2

LITERATURE SURVEY

2.1 INTRODUCTION

Aluminum alloys with silicon as the major alloying element are the most important of the aluminum casting alloys, primarily because of their excellent casting characteristics. Additions of Si to pure aluminum impart high fluidity, good feeding characteristics, low shrinkage and good hot cracking resistance. Hypoeutectic Al-Si alloys have a widespread use and are used extensively in structural, aerospace and automotive applications, which primarily require consistent strength-ductility properties throughout the casting.^{5, 6} Due to the importance of such kinds of alloys, hypoeutectic Al-Si alloys have been the subject of extensive research.⁷ As a result, several innovative molten metal processing techniques have been developed in recent years, including filtration, grain refinement, improved degassing techniques and the modification of eutectic silicon.^{8, 9}

Modification in Al-Si hypoeutectic alloys is a process whereby an element such as Na or Sr is added to the melt for the purpose of altering the acicular shape of the eutectic to a fibrous form.¹⁰ However, to attain the required properties for these alloys, the modification process must be optimized. For this optimization to be completed one should not only adjust the factors controlling the modification process, but also study the effect of

various tramp elements on the efficiency of the modifier used. This is due to the need for the addition of some tramp elements like Bi, which increases machining speeds and reduces the need for cutting fluids.² Furthermore Ca, which refines both iron intermetallic compounds and eutectic silicon in Al-Si alloys, results in improved mechanical properties.

Much research has been devoted to the study of the influence of these tramp elements on the structure and mechanical properties of hypoeutectic Al-Si alloys. However, information on the effects of these elements on the efficiency of different modifiers is not adequate. This makes it difficult to control the modification process so as to optimize the casting and service properties of the alloys.¹¹

2.2 MODIFICATION OF Al-Si ALLOYS

Hypoeutectic aluminum-silicon alloys can be improved by inducing the structural modification of the normally occurring eutectic. In general, the greatest benefits from this process were achieved in alloys containing more than 5 wt% Si in the eutectic concentration.

2.2.1 CHEMICAL MODIFIERS

In normal foundry practice, because of the ease in the addition and obtained reproducibility, modification is primarily achieved by the addition of foreign elements or compounds known as 'modifiers'.¹² It was found that the addition of elements such as calcium, sodium, strontium and antimony to hypoeutectic aluminum silicon alloys results in a finer lamellar or fibrous eutectic network.^{1,13} It is also understood that increased solidification rates are useful in providing similar structures. There is, however, no agreement on the mechanisms

involved. The most accepted explanation suggests that modifying additions suppress the growth of silicon crystals within the eutectic, providing a finer distribution of lamella relative to the growth of eutectic. The result of modification by strontium, sodium and calcium is quite similar. Sodium has been shown to be the superior modifier¹⁴, followed by strontium and calcium, respectively. Each of these elements is mutually compatible so that a combination of modification additions can be made without adverse effects. Eutectic modification is, however, transient when artificially promoted by the additions of these elements. Figure 1 illustrates the relative effectiveness of various modifiers as a function of time at a given temperature,¹⁵ and where the degree of modification increased from level A to level F (*i.e.* from under-modified (A) through well-modified (C) to overmodified (F)).

Antimony has been advocated as a permanent means of achieving structural modification. In this case, the modified structure differs in that a more acicular refined eutectic is obtained compared to the uniform lace-like dispersed structures of sodium-, or calcium- or strontium-modified metal. As a result, improvements in castability and mechanical properties offered by this group of elements are not completely achieved.

The structural refinement obtained is one that is time-independent when the two conditions are satisfied. First, the metal to be treated must be essentially phosphorous-free, and secondly, the velocity of the solidification front must exceed the minimum value approximately equal to that obtained in conventional permanent mold casting. Antimony is not compatible with other modifying elements. In cases in which antimony and other modifiers are present, coarse antimony-containing intermetallics are formed, which

preclude the attainment of an effectively modified structure and adversely affect casting results.

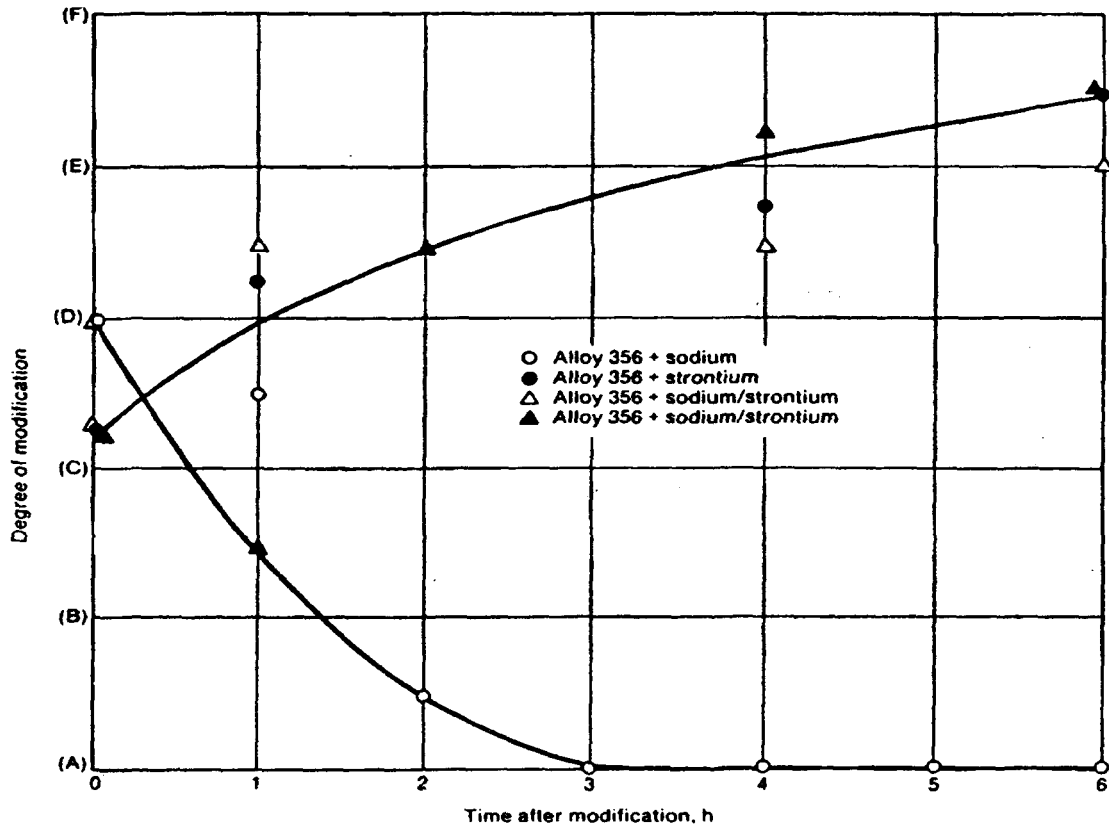


Figure 1. Effect of sodium and strontium modifiers as a function of time.¹⁵

Modifier addition is usually accompanied by an increase in hydrogen content (see Figure 2). In the case of sodium and calcium, the reaction involved in the solution of the elements is invariably turbulent or accompanied by compound reactions that increase dissolved hydrogen levels. In the case of strontium, a master alloy may be highly contaminated with hydrogen, and there are numerous indications that hydrogen solubility is increased after alloying.

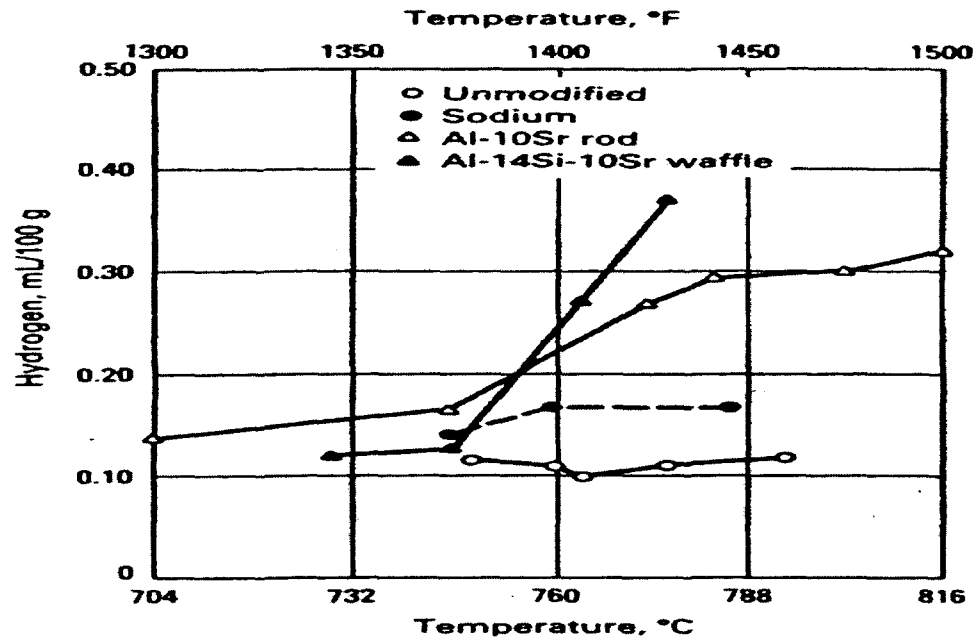


Figure 2. Hydrogen content as a function of holding temperature for aluminum alloy 356 melts with various modifiers.¹⁵

For sodium, calcium, and strontium modifiers, the removal of hydrogen by reactive gases also results in the removal of modifying elements added to well-processed melts, followed by inert gas fluxing to acceptable hydrogen levels. No such disadvantages accompany antimony use. Calcium and sodium can be added to molten aluminum in metallic or salt form. Vacuum prepackaged sodium metal is commonly used. Strontium is currently available in many forms, including aluminum-strontium master alloys ranging from approximately 10 to 90%Sr and Al-Si-Sr master alloys of varying strontium contents. Very low sodium concentrations (0.001%) are required for effective modification. More typically, additions are usually needed to obtain a sodium content of 0.005 to 0.015% in the melt. Remodification is performed, as required, to maintain the desired modification level.

It is to be noted that, due to the limited solubility of sodium in aluminum, the sodium must be plunged rapidly into the melt to avoid excess losses.

A much wider range of concentrations is used in the case of strontium. In general, addition rates far exceed those required for effective sodium modification. A range of 0.015 to 0.05% Sr is standard industry practice. Normally, good modification is achievable in the range of 0.008 to 0.015% Sr. Remodification, even though strontium additions may be required, and retreatment is less frequent than in the case of sodium.

To be effective in modification, antimony must be alloyed to approximately 0.06%. In practice, antimony is employed in the much higher range of 0.10 to 0.50% where it is possible to achieve a state of overmodification, in which eutectic coarsening occurs, as in the case when sodium and/or strontium are used in excessive amounts. The corollary effects of reduced fluidity and susceptibility to hydrogen-related problems are usually encountered well before overmodification may be experienced.¹⁵

2.2.2 EFFECTS OF MODIFICATION

2.2.2.1 EFFECT OF MODIFICATION ON MICROSTRUCTURE

The microstructural change from acicular to fibrous silicon is not a sharp one, and castings with an inadequate amount of either sodium or strontium will exhibit a mixed structure: one containing regions of fibrous silicon, lamellar silicon and acicular silicon. Modification with strontium is often less uniform than with sodium and, of course, antimony will only produce a lamellar (and never fibrous) structure. The entire range of microstructures seen in the modification of a hypoeutectic alloy has been divided into six

classes, with well-modified structures falling into class 5, unmodified ones into classes 2-4, and lamellar ones into class 2.¹⁶ Formation of the very fine structure is sometimes called supermodified.

In assessing the efficiency of modification, it is sometimes useful to quantify the microstructure. This can be readily accomplished by examining a polished section under a microscope and assigning to each class, the proportion of the sample surface, which has a particular type of modification. For example, suppose a given sample contains roughly 25% of class 3, 50% of class 4 and 30% of class 5, its modification rate (M.R.) would then be calculated as

$$M. R. = (0.2 \times 3) + (0.5 \times 4) + (0.3 \times 5) = 4.1 \dots^9$$

and the sample could be said to be reasonably well, but not perfectly, modified. Five variables determine the exact microstructure which will form:

- The type of modifier used;
- The impurities present in the melt;
- The amount of modifier used;
- The freezing rate; and
- The silicon content of the alloy.

Type of Modifier

Both sodium and strontium are capable of producing the full range of microstructures. Antimony has an effect on microstructure that is different than Na and Sr. Antimony additions simply refine the Al-Si eutectic, causing a fine lamellar eutectic to form instead of the fibrous one produced by sodium or strontium. The microstructural

differences that appear in Figure 3 are due to the inability of antimony to cause extensive additional twinning in silicon. Nevertheless, the eutectic refinement is so great that the improvements in properties due to antimony are similar to those with Na or Sr, and hence antimony should truly be regarded as a structural modifier.

The attraction of Sr and Sb is their considerably greater stability than sodium in the melt. While precise fading rates depend strongly on furnace and melting conditions, sodium concentrations are often reduced through vaporization by 50% in a matter of 10-20 minutes. Strontium, on the other hand, has a long-term modifying effect that persists over extended holding times, premodified ingots can be remelted and cast often with little loss of modifying power.¹⁷ In terms of stability, antimony is the best of the three. It has a very low vapor pressure and oxidation tendency, resulting in a virtually permanent effect.

Sodium additions are still made as metallic sodium or through salt fluxes, while the primary alloy manufacturer adds antimony to the ingot. Many different ways of adding strontium have been devised as a result of considerable research into the manufacture of Al-Sr master alloys. Both low and high Sr-containing master alloys have been developed so that the foundryman has a real choice of products that can be matched to his particular melting conditions. For example, high Sr-containing alloys undergo exothermic dissolution and are best used at low liquid temperatures, while the low-Sr alloys dissolve endothermically and should be used at higher melt temperatures.

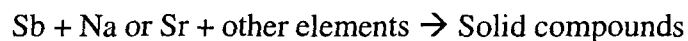
In contrast, strontium has been found to need a considerable "incubation time" (one to two hours have been reported)^{18,19} before its optimum modifying effect is reached.²⁰

Antimony is metallurgically incompatible with sodium or strontium and acts to destroy the modifying effect of these two elements.



Figure 3. Microstructural differences between sodium-modified structure and an antimony refined structure.⁹

For Na-or Sr-modified A356 alloy in the alloy containing the modifier at the level of (0.01-0.015%), poor modification is achieved if antimony is present, and many treatment levels are required to reach a reasonable modification rating (4 or better). The discovery of this effect has sparked interest in the chemical reactions that take place between the various elements within an Al-Si alloy melt. It was demonstrated that the negative interaction between Sb and other modifiers is due to melt phase reactions of the form:



These solid compounds effectively remove Na or Sr from the solution and prevent them from acting as modifiers by the twinning mechanism, as mentioned previously. Since the compounds contain antimony, a dense element, they tend to sink to the bottom of furnaces and crucibles to form sludge.²¹

Impurities Present in the Melt

Phosphorous in particular makes modification difficult, and alloys, which are easy to modify, have a low phosphorous content. Antimony interacts with both sodium and strontium in a negative fashion, and antimony-containing melts require exceptionally high levels of either modifier to produce structures of class higher than 2.

Amount of Modifier Used

For a given set of casting conditions and alloy composition, there is a critical modifier level required to produce a given microstructure. In general, a higher concentration of modifier will produce a higher microstructure class, at least. Too high a level is undesirable, as overmodification can occur. Many experiments were conducted using the Alu-Delta GS instrument to study the variation in eutectic temperature, as a function of strontium modifier content in 319 aluminum alloys.⁹ Different strontium levels were studied and the results are summarized in Figure 4.

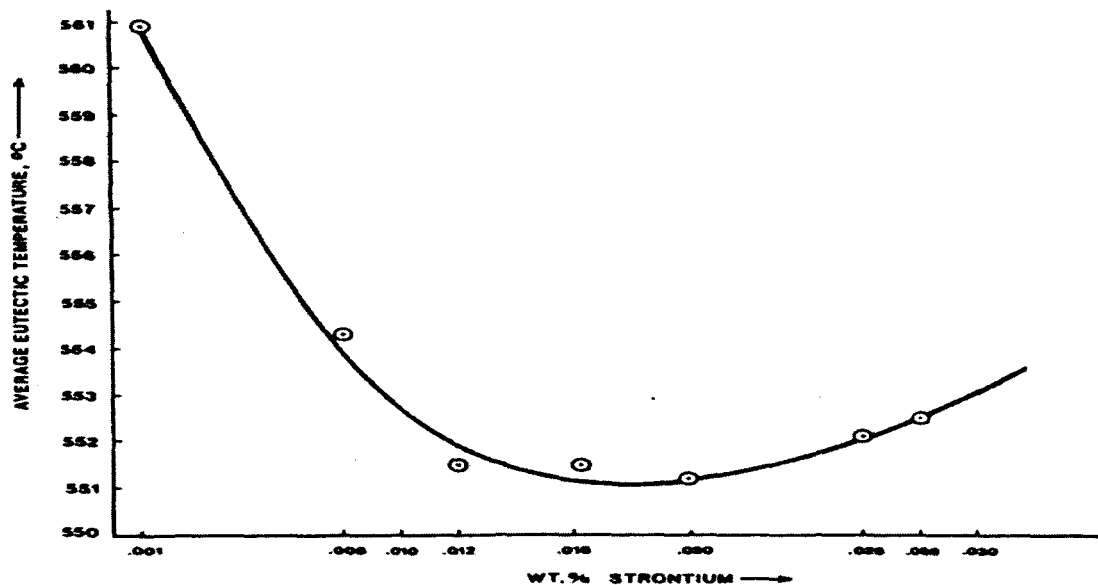


Figure 4. Variation of average eutectic temperature with Sr content in 319 alloy.⁹

As shown in Figure 4, the eutectic temperature decreases until about 0.016%Sr is reached; the eutectic temperature then increases again with a further increase in strontium concentration. The eutectic temperature-strontium relationship observed in this figure deviates from the previously published results that show the eutectic temperature to continuously decrease with increasing strontium content. The initial decrease in temperature noted in the figure may be attributed to the gradual refinement of the eutectic structure.

However, when the strontium content in the melt is raised to 0.008%, the drop in eutectic temperature from 560.9 °C to 554.3 °C is certainly accompanied by a change in the morphology of the eutectic silicon, in which evidently few fibrous silicon particles appear. When the eutectic temperature reaches a minimum at 0.016%Sr, both fibrous and plate-like silicon are present. The increase in strontium content beyond 0.016% contributes to a more fibrous silicon eutectic. The silicon structure appears to be fully fibrous when the strontium content reaches 0.013%.²²

Furthermore, the Sr content plays an important role in reducing the dangerous effect of the plate-like iron intermetallic β -Al₅FeSi phase, whose presence can reduce alloy properties and casting quality.^{23,24,25,26,27} It is also shown that Sr (250-350 ppm) is effective in reducing the β -platelet size through its fragmentation/dissolution effect on the latter. At higher Sr concentrations, both the coarsening of β -platelets (*i.e.* overmodification) and their decomposition (through Si rejection ahead of the platelets) occur. Generally, for a given Fe level, the optimum Sr content depends on the cooling rate and Si content of the alloy.²⁸

Freezing Rate

Higher solidification rates assist the modification process and so lower modifier levels are required in permanent mold castings than in heavy section sand-castings. Modification has never been pursued in die-casting because it is often said that die-castings freeze so quickly as to produce microstructures, which are fine enough. However, some recent experiments on the use of strontium in die-casting have indicated the potential beneficial effect of modification. Additions of 0.02% or 0.03% strontium to 380.0 alloys lead to a noticeably finer microstructure, which could result in improved machining properties.

Silicon Content

Higher silicon concentrations require larger amounts of modifier to produce complete modification. An increase of up to 50% in the amount of strontium needed is observed, when the silicon level is changed from 7% to 11%.⁹

There is also another variable which must be considered in the modification process, which is the holding time through which the modifier carries out its role. Pan *et al.*²⁹ studied the effect of holding time on the modification of A356 alloy by Sr and Sb. Figure 5 shows the change in silicon morphology as a function of holding time at 710°C for various Sr levels. At 0.02% Sr, the modification effect of Sr reaches its maximum after a holding time of about 5-10 minutes, and then fades gradually during the holding period. The eutectic silicon degrades from a fibrous structure to a partially modified one 15 minutes after the addition of Sr, then further deteriorates to a lamellar structure after a holding time of 50 minutes. For 0.03 and 0.04%Sr, not only can full modification be achieved after an

incubation period of about 15 minutes, but also the fading of Sr modification is substantially delayed. During the whole isothermal holding period of 50 minutes, little fading occurs and the modified silicon structure remains. When a higher level of modifier is added, (0.05% Sr), full modification appears almost instantaneously after Sr introduction.

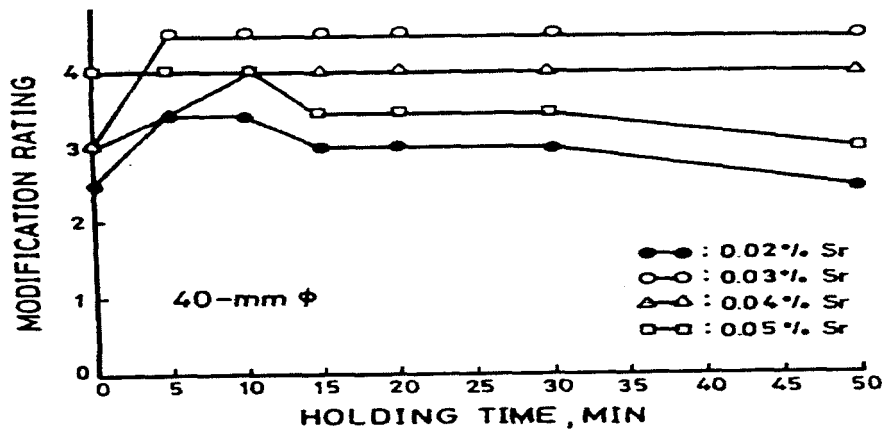


Figure 5. Modification rating as a function of holding time for various Sr levels.²⁹

2.2.2.2 EFFECT OF MODIFICATION ON CASTING SOUNDNESS

As determined by radiographic examination,⁹ the chemical modification treatment, with Sr or Na, does have an adverse effect on quality. In the permanent mold, the level of casting rejection, based on X-ray analysis, was always much higher for modified alloys. For the unmodified alloy, the rejection percentage of the tensile bars was relatively low at 16%, while it increased significantly to 49, 53 and 65% for 0.002, 0.02 and 0.08% Sr, respectively.³⁰

Sodium had a similar effect on the casting soundness, leading to a rejection rate of 54%. In terms of mechanical properties, the elongation is certainly the parameter most

affected by unsoundness, dropping 35-40% in the presence of porosity. The defects in unmodified test bars were very localized and well defined, appearing as spots on the X-ray films. Strontium addition not only caused an increase in the number of the defects detected radiographically, but also the changes in their shape and size, with the flaw being larger, more dispersed and spongy. However, the porosity level is substantially higher (by 1.0-1.5 %) for the modified alloy than for the unmodified alloy. This ensures the fact that modification yields an increase in porosity and is thought to be a result of increased hydrogen pickup and change in the eutectic solidification mode brought about by modification.³⁰

2.2.2.3 EFFECT OF MODIFICATION ON MECHANICAL PROPERTIES

From the previous discussion relating to the effect of the modification process on microstructure, heat treatment, and casting soundness, it clearly appears that the modification process must have optimum conditions to avoid side effects on other properties. Garat *et al.*³¹ stated that every modifier improved tensile strength and elongation, *i.e.*, the quality of the alloy, given by a quality index Q defined as:

$$Q = UTS + 150 \log E$$

The Q value indicated, in every case, an improvement with the presence of Na, Sb or Sr. Antimony showed itself to be superior to the two other modifiers. This is due to the fact that the benefit of the absence of porosities with respect to the mechanical properties is more important in critical areas than the benefit due to a finer silicon morphology in the T6 condition.

2.3 POROSITY FORMATION IN Al-Si ALLOYS

Porosity in aluminum alloy castings occurs because of the rejection of gas from the liquid metal during solidification and/or the ability of the latter to feed through the interdendritic regions to compensate for the volume shrinkage associated with solidification.

2.3.1 TYPES OF POROSITY

Porosity in aluminium alloys can be divided into two main categories: dispersed microporosity and shrinkage porosity.

Dispersed Microporosity

The dispersed form of porosity, which is especially prone to occur in long-freezing range alloys, is often difficult to detect and requires the control of a number of metallurgical variables for best product quality. Particularly important are the quantity of gas dissolved in the liquid metal, the freezing rate in the casting and the absence of oxides or other inclusions, which act as sites for the heterogeneous nucleation of pores.

Shrinkage Porosity

Macroscopic shrinkage cavities, such as under-riser and centerline shrinkage, are generally associated with short freezing range alloys that contract during freezing. The potential presence of dispersed porosity or shrinkage cavities in cast metals represents a problem that is responsible for more than half of the scrap loss in the production of commercial castings, which prevents the widespread use of net-shaped castings in many critical load-bearing applications. This is because of the deleterious effects of such porosity,

which include lack of pressure tightness, limited strength and ductility, variable fracture toughness, and irregular crack initiation and propagation characteristics.³²

2.3.2 FACTORS CONTROLLING POROSITY FORMATION

The increase of hydrogen content makes the production of a sound casting more difficult, even for a casting designed with a high volume ratio and low freezing ratio.³³ Hydrogen is the main gas which is appreciably soluble in aluminum and its alloys.³⁴ The dramatic decrease in its solubility at the solidification point of aluminum, resulting in outgassing, leads to the formation of porosity, reduced mechanical properties and corrosion resistance.

Besides hydrogen as the strongest determinant for porosity, the formation of porosity is also controlled by other factors such as the grain refining and inclusion content.³⁵ Grain refiners are added in small amounts to molten aluminum alloys to control the grain structure in the casting. Al-Ti, Al-Ti-B master alloys are usually employed, where TiAl_3 particles act as nucleation sites for the formation of primary α aluminum dendrites and promote uniform, equiaxed grain structure. This leads in some cases to a reduction in the amount of porosity.

Hydrogen

Hydrogen porosity formation is controlled by several parameters other than its high solubility limit. Laslaz and Laty³⁶ summarized these parameters as follows:

- The local pressure during solidification, on which the enthalpy of the bubble formation depends;

- The chemical composition of the alloy, since alloying elements modify the hydrogen activity;
- The solidification range of the alloy; and
- The solidification rate and temperature gradient.

Cleanliness of the Metal

The formation of porosity in Al-9% Si-3%Cu-X alloys studied by Samuel *et al.*³⁷ as a function of factors controlling the porosity formation in alloys listed in Table 1. It was observed that, at very low hydrogen level, i.e., 0.06 mL/100g Al (h1 alloy), samples solidified at a high rate ($t_s = 12.5$ s) exhibited almost no pores in the casting except for the central portion where fine pores were located along the dendrite arms. In non-grain refined alloy, with a hydrogen content of about 0.49 mL/100g Al (h3 alloy containing approximately 170 ppm Sr), elongated and rounded pores were observed at $t_s = 12.5$ s, Figure 6(a). Increasing the solidification time to 71 s resulted in a significant change in pore morphology. Figure 6(b) reveals that all pores are almost rounded, as opposed to elongated. When the hydrogen content of the melt exceeds the solubility limit, the resultant excess hydrogen forms gas bubbles, leading to porosity. The pores nucleate and grow in the presence of proper nucleants, their size and distribution depending on local solidification conditions.

Porosity formation is described by the relation $\Delta P = 2\sigma/r$, where σ is the surface tension, and ΔP is the critical pressure that must be exceeded in the pore for a pore nucleus of radius r to grow. Higher hydrogen content in the melt will increase ΔP and decrease r , resulting in an increase in the amount of porosity in the casting. Pores may form prior to or

during solidification. Pores of the former type are spherical and relatively large. The ones formed during solidification are small, irregularly shaped (elongated), and attributed to shrinkage porosity. The hydrogen enrichment and shrinkage pressure in the interdendritic area influence their formation.

Table 1 Chemical composition of as cast alloys used for experimental work³⁷

(mL/100 g Al)										
Alloy	Si	Cu	Zn	Fe	Mg	Mn	Ti	Sr	P	H ₂
f1	—	3.08	0.01	0.22	0.32	0	0.14*	0.013	0	0.22
f2	—	3.18	0.01	0.16	0.35	0.6	0.15*	0.023	0.0019	0.25
f3	—	3.19	0.10	1.19	0.31	0	0.15*	0.090	0	0.20
f4	—	3.31	0.06	1.06	0.33	0.62	0.14*	0.022	0	—
f5	—	3.23	0.7	0.19	0.29	0	0.137*	0.012	0.0033	0.25
f6	—	2.77	0.7	0.19	0.28	0.6	0.148*	0.014	0	0.31
f7	—	2.78	0.8	1.0	0.28	0	0.11*	0.014	0	0.31
f8	—	2.94	1.13	0.95	0.27	0.6	0.14*	0.015	—	0.25
h1	—	3.02	1.48	0.54	0.08	0.35	0.13	0.024	0	0.06
h2	—	3.32	1.51	0.60	0.09	0.20	0.19*	0.022	0	0.52
h3	—	3.06	1.49	0.55	0.08	0.30	0.13	0.017	0.0030	0.49
h4	—	3.05	1.47	0.55	0.08	0.28	0.14*	0.017	0.0033	0.13
h5	—	2.98	1.50	0.55	0.66	0.29	0.13	0.024	—	0.57
h6	8.93	3.41	1.56	0.57	0.77	0.26	0.19*	0.024	0	0.12
h7	—	3.68	1.56	0.57	0.61	0.36	0.14	0.017	0.0037	0.13
h8	—	3.12	1.47	0.53	0.66	0.30	0.19*	0.027	0.0011	0.45
s1	—	3.40	0	0.57	0.02	0.3	0.04*	0.002	0.0020	0.28
s2	—	3.16	0	0.56	0.01	0.3	0.27*	0.043	0.0025	0.24
s3	—	3.06	0	0.43	0.33	0.31	0.05*	0.042	0.0025	—
s4	—	3.35	0	0.53	0.24	0.3	0.29*	<0.002	0.0025	0.23
s5	—	2.84	1.8	0.56	0.01	0.31	0.03*	0.0300	0.0025	0.26
s6	—	2.90	1.9	0.79	0.01	0.31	0.09*	<0.002	0.0025	0.21
s7	—	3.16	1.7	0.54	0.67	0.3	0.03*	<0.002	0.0025	0.21
s8	—	2.87	1.8	0.97	0.30	0.3	0.06*	0.038	0.0025	0.29

* Grain refined alloys

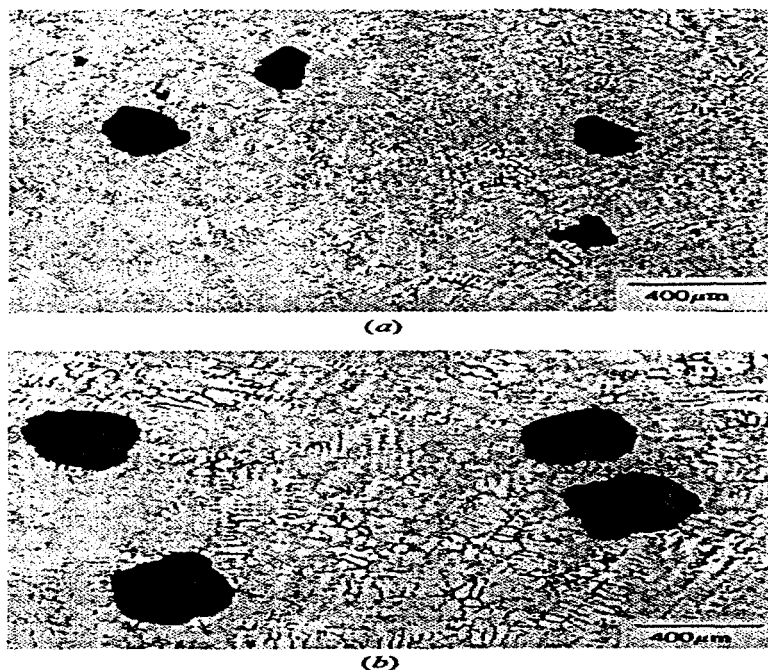


Figure 6. (a) Pore morphology in h3S alloy at 0.49 mL hydrogen/100g Al, $t_s \sim 12.5$ s
 (b) Pore morphology in h3L alloy at 0.49 mL hydrogen/100g Al, $t_s \sim 71$ s.³⁷

The effect of initial hydrogen content on the total amount of microporosity was studied using a total of 18 castings with varying hydrogen contents³⁸. As Figure 7(a) shows, there was a little porosity until 0.17 mL/100g Al hydrogen level, after which the percentage of porosity increased linearly with hydrogen content. This value, 0.17 mL/100g Al hydrogen level, is called the threshold hydrogen content $H_{o_{\text{thresh}}}$. Cluster analysis was performed on the samples to separately measure the gas and shrinkage pores. A limiting interpore distance of 150 μm was used. Each cluster of pores was assumed to represent a single shrinkage pore, while isolated pores were assumed to be gas pores. Figure 7(b) shows that there is virtually no gas porosity below $H_{o_{\text{thresh}}}$, but there is a small amount of shrinkage porosity. Above

$H_{0\text{thresh}}$, the amount of shrinkage and gas porosity increases, in a more or less linear manner, with the hydrogen content.³⁸

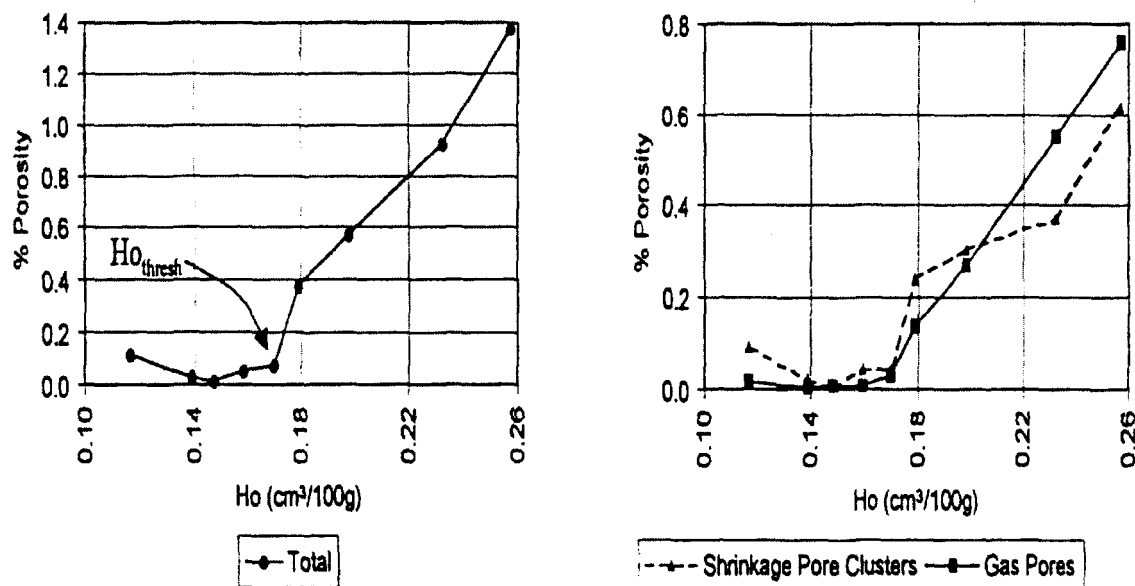


Figure 7. (a) Total amount of porosity and (b) Shrinkage and gas porosity, as a function of initial hydrogen content (H_0).³⁸

Melt Treatment

- Modification (S_r)

The influence of modification on porosity is a matter of considerable debate, stemming from the controversy over the behavior of S_r as a modifier. Argo and Gruzleski¹⁰ carried out a controlled study on porosity in modified and unmodified A365 alloy, using the Tatur test to identify differences in the distribution of porosity and shrinkage, Figure 8.

The Tatur test results showed three areas of significant difference between unmodified and modified castings. Modification increases the macroshrinkage as expressed

by differences in density, volume of microshrinkage and an increase in microshrinkage as percentage of the total shrinkage. The effects can be understood in terms of the changes to the Al-Si alloy phase diagram brought on by modification. It is well known that modification suppresses the eutectic transformation temperature without changing the liquidus temperature in hypoeutectic alloys. The result is an increase in the freezing range and the length of the mushy zone.

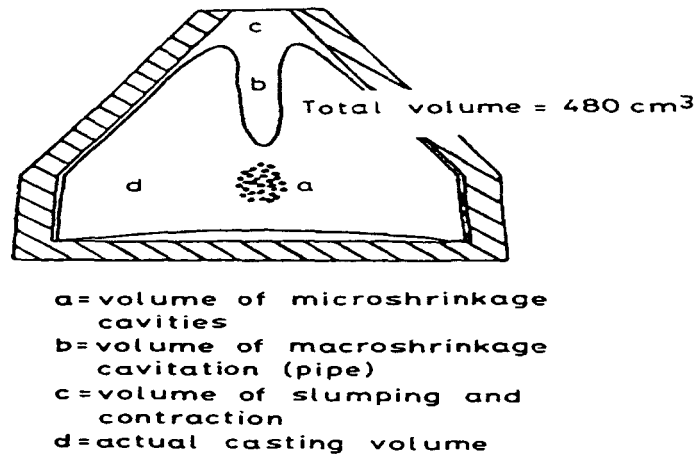


Figure 8. Schematic representation of the Tatur mold.¹⁰

The decrease of the pipe volume of approximately 44% on modification is due to interdendritic feeding difficulties caused by the increased volume of the mushy zone during solidification. In unmodified alloys, feeding is relatively easy, with liquid moving from the pipe, which acts as a riser to the solidifying regions. When modification is present, however, feeding is more difficult and the liquid cannot flow effectively into the mushy zone, resulting in a smaller pipe volume. Different mechanisms were suggested through which Sr can play a role in the formation of dispersed microporosity:^{39,32}

- Sr lowers the surface tension of liquid Al

As a reduced metal surface tension would make it possible for pores to form earlier during solidification, this would result in increased porosity.

- Sr forms a different oxide, which promotes pore formation

This will be due to the change in the composition of the oxide film caused by Sr at the surface of the melt. Perhaps, this new oxide film nucleates pores more easily, and it may not be as strong as alumina. Moreover, it may also be broken easily into smaller parts, thus providing nuclei for gas pores.⁴⁰

- Sr results in poor feeding from the riser

In modified bars, porosity increased along the length and was greatest near the riser.

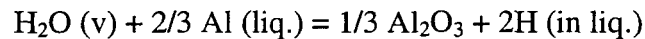
- Sr allows pores to increase to a larger size

A theoretical analysis was made of pore growth, which is controlled by the diffusion of dissolved hydrogen to the pore. It was concluded that most pores form in isolated pockets of liquid, thereby limiting the amount of gas that can diffuse to the pores. Consequently, increased porosity in Sr-modified castings may be related to the fact that pores have access to a larger pool of gas-containing liquid.⁴¹

- Sr allows gassing in the bulk of the casting

Another possibility is that the metal picks up additional dissolved gas during freezing, and this gas finds its way to the centre of the casting by convection. That is, the reaction at the mold surface may generate more internal porosity, in addition to pores just under the surface.

Argo and Gruzleski¹⁰ also studied the effect of Sr on the formation of subsurface porosity in an Al melt. It was found that the Sr promotes adsorption of gas from the moist atmosphere above the melt. This gas pickup occurs because aluminum is more chemically reactive than water vapor, resulting in the following chemical reaction:



In unmodified Al-Si alloys, the oxide is Al₂O₃ pure, which forms a stable and reasonable protective film. When Sr is present in the melt at levels normally used to produce modification, strontium aluminates (SrO. Al₂O₃) forms. The Sr-containing oxide film is less protective than pure aluminum, and is responsible for the more rapid gas pickup in modified alloys.

- Grain Refining (TiB₂)

It was also found that TiB₂ resulted in increasing nucleation sites as well as the number of grains, which lead to a marked reduction in pore size with an increase in pore density. The pore formed in the case of grain-refined material can be characterized from those in the Sr-modified samples by its quite spherical shape.⁴² In non-grain-refined alloys, pores were able to expand along the grain boundaries.

- Silicon Refining (P)

Phosphorous enters aluminum casting alloy melts through contact with tools, refractories, etc. In hypereutectic alloys, phosphorous is deliberately added because it reacts with the aluminum to form AlP particles, which nucleate primary silicon. This results in a fine dispersion of primary silicon. This effect is quite opposite to that observed in hypoeutectic alloys, where the silicon is coarsened by the addition of phosphorous.

- *Stirring Time*

An experimental technique to investigate the effect of stirring on oxide skins and porosity in aluminum A365 alloy was developed.⁴³ Oxide skins become submerged in the melt during pouring or stirring and serve as sites where one or more pores may form during solidification. There is evidence that they increase in numbers with stirring, strontium addition and pouring. In the work of Serratos *et al.*,⁴³ 1.4 kg of alloy A356 was melted in a clay-graphite crucible, using a resistance furnace. Twelve samples were prepared from the melt, the first six samples treated (degassed and fluxed) from which three samples were Sr-modified, and the other six samples were untreated with three of them also Sr-modified. The samples were studied and the results summarized as shown in Table 2. Two observations emerged from this table: in both treated and untreated melts that had not been stirred, there were more pores in the Sr-modified samples than in the unmodified samples. This is consistent with the usually accepted notion that Sr-modification results in more pores in Al-Si casting alloys. When untreated and modified melts are stirred, the number/density of the pores in the radiographs decreases with an increase in stirring time.

This suggests that the Sr-containing inclusions might have been centrifugally separated from the melt and were skimmed as dross before loading the sample into the vacuum chamber. On the other hand, the decrease could be attributed to an increase in the number of escaping gas bubbles prior to solidification. Generally, it is apparent that the greater the time of stirring before solidification, the greater will be the number of bubbles emerging from the top surface of the sample during solidification. Therefore, the number of inclusions increases with stirring.

Table 2 Volume percent porosity of treated and untreated samples ⁴³

Sample	Stirring Time (sec)	As-received Ingot condition	Melt treatment	Volume % porosity
1	0	unmodified	treated	0.28
2	15	unmodified	treated	2.45
3	30	unmodified	treated	9.32
4	0	modified	treated	0.56
5	15	modified	treated	3.00
6	30	modified	treated	3.37
7	0	unmodified	untreated	6.66
8	15	unmodified	untreated	8.35
9	30	unmodified	untreated	5.09
10	0	modified	untreated	7.70
11	15	modified	untreated	6.72
12	30	modified	untreated	6.70

Samuel *et al.*⁴⁴ showed the effect of stirring on pore formation. It was found that gentle stirring using a ladle did not affect the melt quality. Mechanical stirring at high speed, however, was very effective in contaminating the melt with surface oxides/dross, leading to complete clogging of the filter pores. Also, increasing stirring time (resulting from increasing the Sr level) would increase the possibility of introducing a greater amount of oxides into the melt, leading to a lower amount of filtered metal obtained.

Intermetallics

- β -Al₅FeSi

When the iron complex in Al-Si alloys exists as long needles of the β -Al₅FeSi phase, it makes the alloy brittle and weak in mechanical properties. An iron content up to 1.3-wt% has been found to be beneficial in terms of improved strength, hardness, and has a tendency toward hot cracking. Roy³⁷ showed that elongated and short pores characterize the pore distribution in f7 alloy (see Table 1). All pores are nucleated along the long sides of β

needles. Such a mechanism is expected to result in an increase in pore density, which is related to the metal feedability, or the ease with which the molten metal can flow into the different sections of the casting mold. In spite of the harmful effect of β needles as pore nucleation sites, their presence seems to limit pore growth.³⁷

- $\alpha\text{-Al}_{15}(\text{Fe},\text{Mn})_3\text{Si}_2$

The presence of iron in the $\alpha\text{-Al}_{15}(\text{Fe},\text{Mn})_3\text{Si}_2$ Chinese script form is known to be relatively less harmful. Roy³⁷ concluded from his experiments on alloy f8 (see Table 1) that α Chinese script phase particles are not suitable sites for pore nucleation. Also, they highlight the fact that these particles are effective in limiting pore growth.

Sludge

Manganese is always considered in relation to iron in foundry alloys. At low holding/casting temperatures, the manganese combines with iron and chromium (Cr always exists as impurities) to form sludge. Sludge is harmful as it is hard and abrasive. Sludge acts in a similar manner as α Chinese script particles in restricting pore expansion.

Al_2Cu

In materials containing a very low level of hydrogen *i.e.*, h1 alloy (hydrogen level ~0.06 mL/100g Al, ts~71s), shrinkage pores are seen to nucleate at the interface of the blocky Al_2Cu -phase particles.³⁷ It was found that strontium modifies Al_2Cu phase particles, resulting in more (Al+ Al_2Cu) eutectic pockets. It is seen that in the absence of β needles, these eutectic pockets can be considered as pore nucleation sites. They are, however, very much less active compared to β needles.

Alloying Elements

Magnesium

The pore size and distribution in s7 alloy (containing 0.67 wt pct Mg, hydrogen level ~0.21 mL/100g Al, t_s ~71 s, see Table 1) shows that the addition of magnesium reduces the percentage porosity without a noticeable change in pore size or shape. The role of magnesium in reducing percentage porosity is more pronounced when the hydrogen content is increased to ~0.5 mL/100g Al. This is obtained from h5 alloy (hydrogen level ~0.57 mL/g Al, t_s ~71 s, see Table 1) as compared to h3 alloy (hydrogen level ~0.49 mL/100g Al). It is interesting to note that the addition of strontium to a magnesium-containing alloy leads to a further decrease in percentage porosity.

Zinc

Zinc has a relatively high solubility in aluminum both at high and low temperatures. A zinc level up to 3-wt pct has been reported to improve high-temperature properties and alloy machinability. The role of zinc in porosity formation is not clear. It is believed that zinc may combine with phosphorus to form Zn_3P_2 , from alloy f5 (t_s ~71s). This combination enhances the pore size as compared to f1 and f2 alloys containing 0 and 19 ppm phosphorus, respectively, and obtained under similar solidification conditions.³⁷

Thermal parameters

Solidification Time (t_s)

For a given hydrogen level, increasing t_s will increase percent porosity, pore length and the pore area. This is due to the decrease in the cooling rate, which accordingly increases the pore volume fraction whether the alloy is modified, or not.

This effect of cooling rate on microporosity formation is affected to some degree by the melt treatment. Figure 9 compares the effect of the cooling rate on % porosity under different melt treatments, as obtained by Fuoco *et al.*⁴⁵ both unmodified and Sb-refined melts behave similarly with little effect in the freezing range. In Na- and Sr-modified alloys, however, the effect of the freezing range is more marked, although the increase in porosity due to an increased freezing range is always much less than that due to the addition of the modifier.

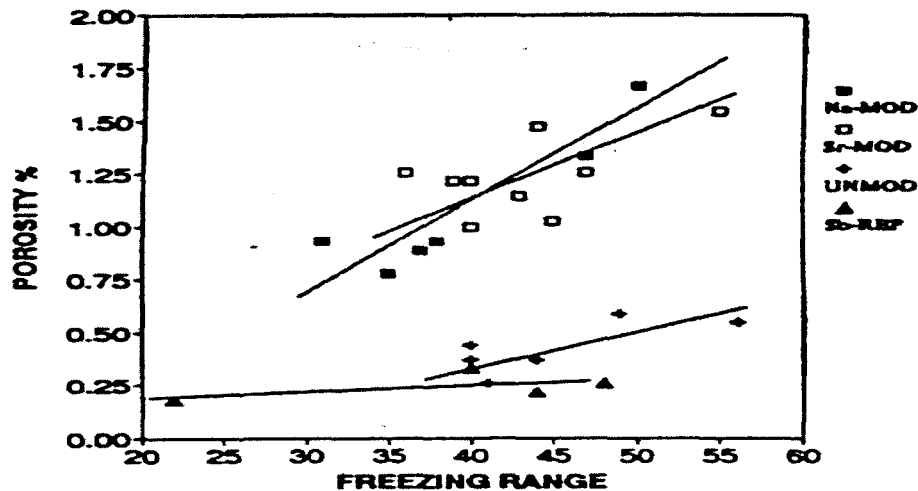


Figure 9. Summary of the variation of microporosity content with a freezing range for alloys with various melt treatments.⁴⁵

Solidus Velocity (V_s)

Solidus velocity is one of the strongest factors controlling hydrogen porosity formation, as the pore formation is a diffusion-controlled process.⁴⁶ All porosity parameters increase with solidus velocity, when the eutectic grows with equiaxed morphology as opposed to a planar front. This is explained as the effect of two nonexclusive phenomena; *viz.*

a reduced metal pressure when the permeability of the solid-liquid zone decreases, and an expansion of pores in isolated liquid pockets during the volumetric concentration of the last liquid to solidify. The isolated liquid pockets may be described as micro hot spots.

2.4 EFFECT OF TRAMP ELEMENTS

2.4.1 BISMUTH IN Al-Si ALLOYS

Bismuth solubility in Al is assumed to be almost negligible: it is less than 0.3 wt% at the monotonic temperature (658°C). The Al-Bi phase diagram is shown in Figure 10.

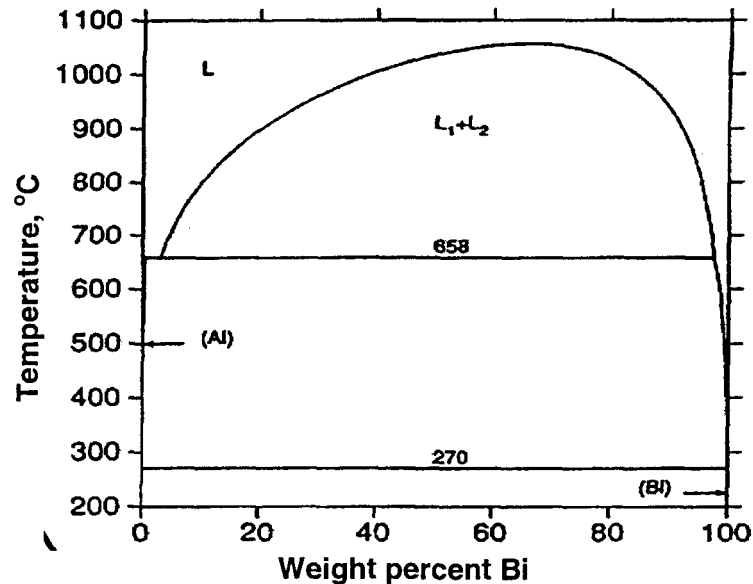


Figure 10. Al-Bi phase diagram.⁴⁷

Bismuth forms insoluble globules in a casting microstructure and acts as a chip breaker that reduces the lengths of chips during machining. If present in sufficient quantities (generally 0.5%) these globules increase machining speeds and reduce the need for cutting fluids.²

2.4.1.1 MICROSTRUCTURE EFFECTS

Sal'nikov and Zaigraikin⁴⁸ reported that Bi has a slight modification effect in an Al-11.7% Si alloy. The amount of modification increases with an increasing Bi concentration up to 0.3%. They also reported that Bi additions to a melt neutralize the modifying effect of Na. Some researchers found that Bi can produce a slight modification effect when it is added up to 3%, as it led to a slight improvement in the microstructure.⁴⁹

Kurdyumov *et al.*⁵⁰ reported that the modifying effect of Bi is reduced by the addition of Mg to Al-Si alloys. They also found that Bi neutralizes the effect of Na at 0.1% Bi and neutralizes the effect of Sr at 0.05%. Pillai *et al.*⁵¹ give the optimum amount of 0.2-0.25 wt pct for Bi as a modifier, Figure 11.

Cho *et al.*⁵² added bismuth to Sr-modified A356.2 alloy in the amounts of 0.005, 0.01, 0.02 and 0.1% Bi, using 99.99% pure Bi. As depicted in Figure 12, microstructure investigations showed that the Sr-modified samples started to show some indications of under-modification with only 0.005%Bi. A partially lamellar eutectic structure was observed with further Bi additions, up to 0.02%, and the microstructure was partially modified. It was also found that the amount of the lamellar structure was increased with an increased addition of bismuth. With as much as 0.1%Bi addition, the Sr modification effect was completely eliminated: acicular eutectic silicon was present and the structure was fully unmodified.

This influence of Bi on the microstructure of A356.2 alloy was similar with Sr additions of both 0.01 and 0.015 wt%. However, the modification treatment with higher amounts of Sr counteracted the detrimental effect of Bi. The microstructure obtained with 0.1% Bi also showed a developed acicular structure, Figure 12(d). By modification with

0.05% Sr, the eutectic silicon phase was well modified, Figure 13(a). The case is similar to Figure 13(b) when compared with Figure 12(d). This effect of bismuth contamination in A356.2 alloy was more severe at slower solidification rates, where more lamellar and coarser eutectic silicon appeared with the addition of 0.02%Bi.

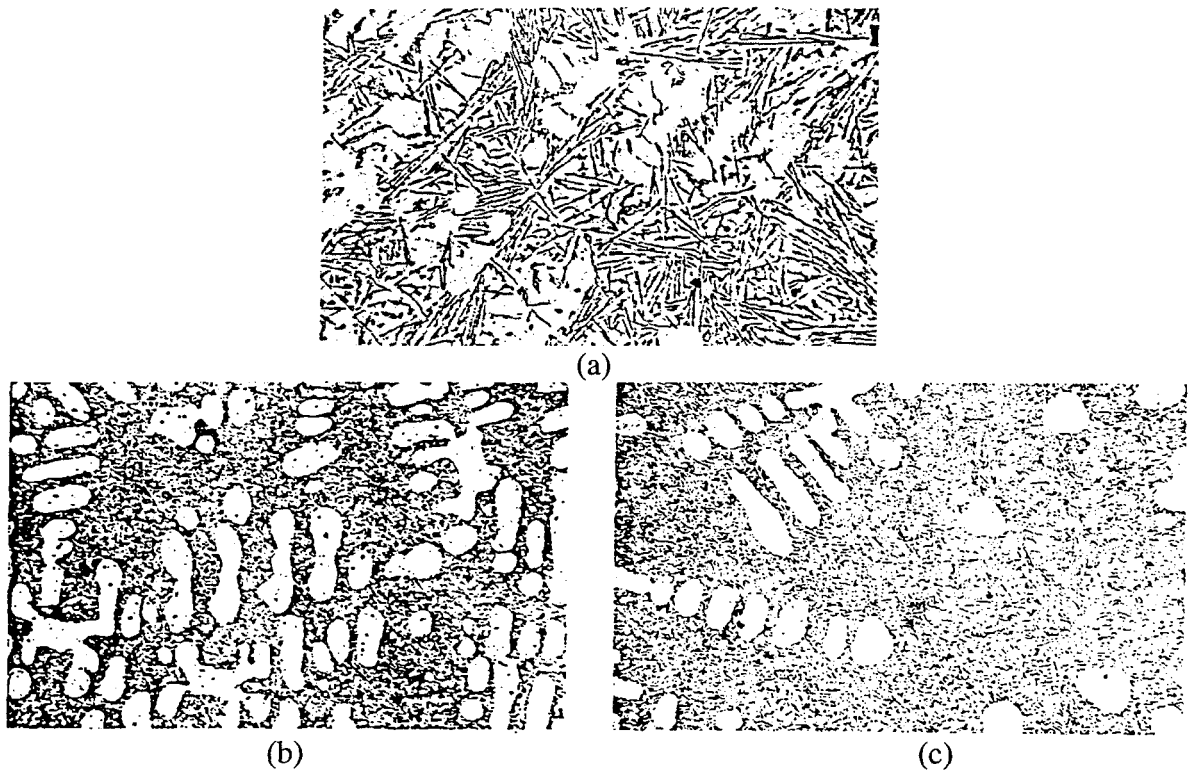


Figure 11. Photomicrographs of cast Al-Si eutectic alloys a) unmodified; b) treated with 0.2 wt pct Bi, c) treated with 0.25 wt pct Bi.⁵¹

The effect of Bi-Sr interactions on Si morphology was studied for 319-type aluminum alloy by Machovec *et al.*⁵³ They added various amounts of bismuth from 0.014 to 0.055 wt%, and Sr from less than 0.001 to 0.02 wt%. Based on the results of their

thermal analysis data, samples were chosen for metallographic inspection. The samples were sorted in order of apparent modification.

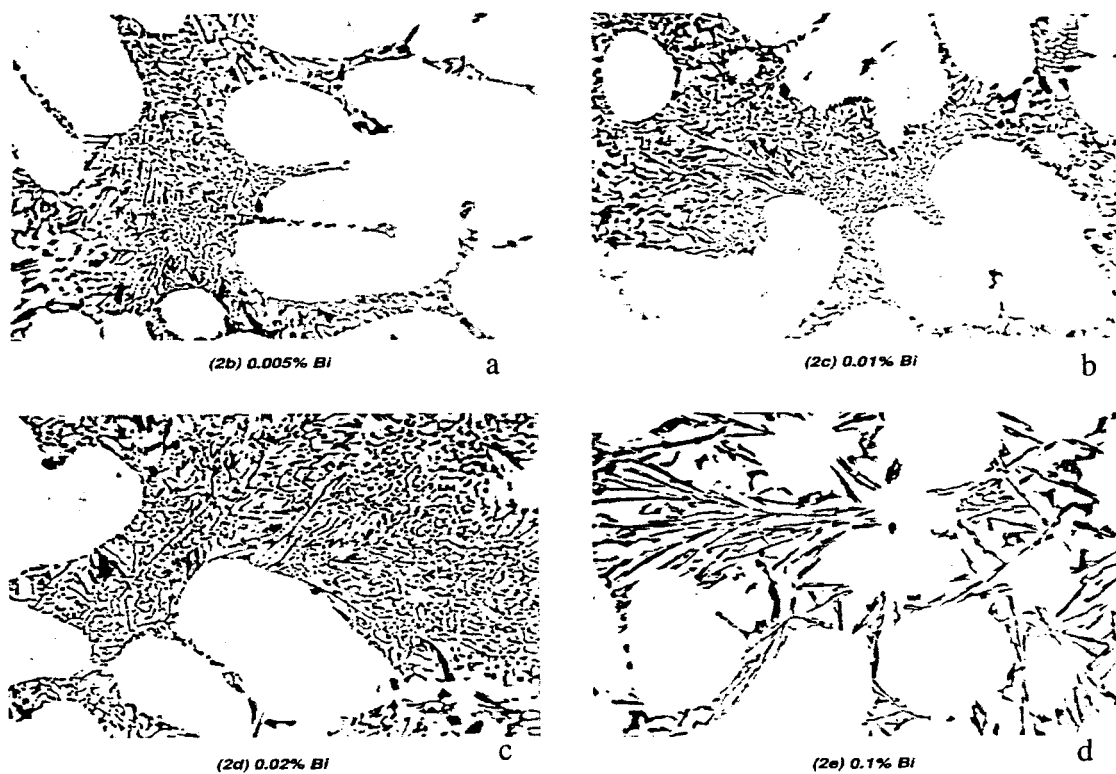


Figure 12. Microstructure of A356.2, cast in graphite mold, containing various percentages of Bi and modified with 0.015% Sr, 500X.⁵²

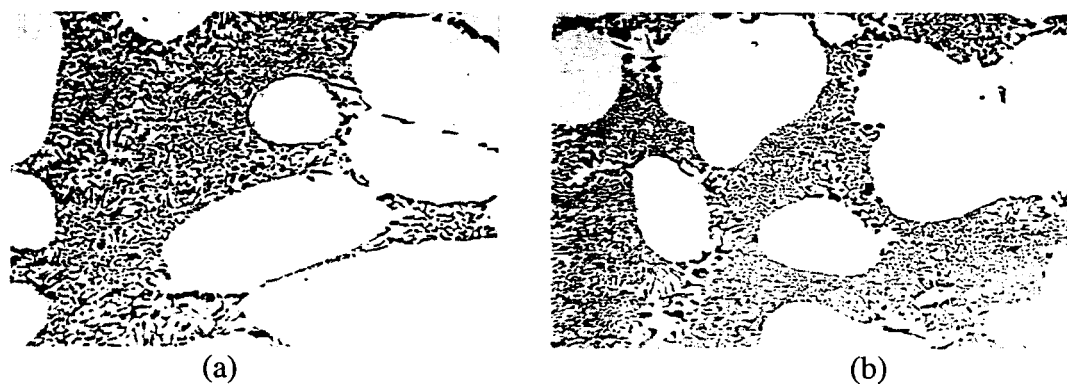


Figure 13. Eutectic Si structure in (a) 0.01% Bi, modified with 0.05% Sr, and (b) 0.02% Bi, modified with 0.02% Sr.⁵²

These visual results were then compared with the recorded eutectic temperature, the wt% Bi, the wt% Sr, and the Sr: Bi ratio for each sample. A description of the silicon morphology for each sample is listed in Table 3. It is remarked from this table that, at Sr:Bi ratios below 0.2, the Si structure was unmodified and the eutectic temperature was above 564 °C. At Sr: Bi ratios between 0.20 and 0.45, the eutectic temperature drops dramatically from around 566°C to 558°C and the modification level increases dramatically in this region with increasing Sr:Bi ratios. Above ratios of 0.45, the Si structure was modified and the eutectic temperatures remained consistent between 556°C and 558°C. According to previous results, it is recommended that, in alloys containing Bi, in order to modify the Si eutectic morphology, an Sr:Bi ratio of at least 0.45 must be maintained.

Table 3 Samples for the metallographic determination of the modification level⁵³

Sr/Bi Ratio	Wt% Sr	Wt% Bi	Eutectic Temperature	Si Morphology Description	AFS Level	Fig.
0.775	0.011	0.0142	556.4	fibrous and acicular	4	7a
1.449	0.020	0.0138	556.8	fibrous, lamellar, and acicular	4	7b
0.707	0.020	0.0283	558.3	fibrous, lamellar, and acicular	4	7c
0.307	0.017	0.0553	559.8	fibrous with some acicular and lamellar particles	4	7d
0.246	0.019	0.0772	558.6	lamellar and fibrous	3	7e
0.214	0.003	0.0140	559.8	lamellar and fibrous	3	7f
0.172	0.009	0.0524	562.1	lamellar plates	2	7g
0.000	0.000	0.0346	565.8	lamellar	2	7h
0.095	0.002	0.0210	566.0	lamellar and plate	2	7i
0.000	0.000	0.0543	567.9	plates	1	7j
0.000	0.000	0.0145	565.5	plates	1	7k

Kurdyumov *et al.*¹¹ found that the addition of Bi to hypoeutectic AL2 (Al-Si alloy) modified with Na counteracts the modification effect and leads to a marked coarsening of the eutectic Si crystals, Figure 14, curve 1.

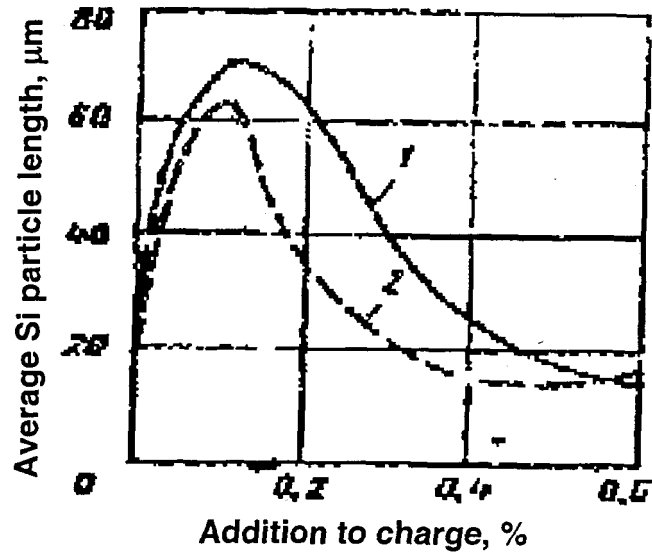


Figure 14. Addition of different modifiers to unmodified AL2 (Al-Si) alloy.¹¹

Other experiments showed the effect of various amounts of Na and Bi on the microstructure of AlSi9Cu3 alloy, Figure 15.⁵⁴ It is remarked that, the higher the residual bismuth content, the greater the amount of Na required for optimum modification.

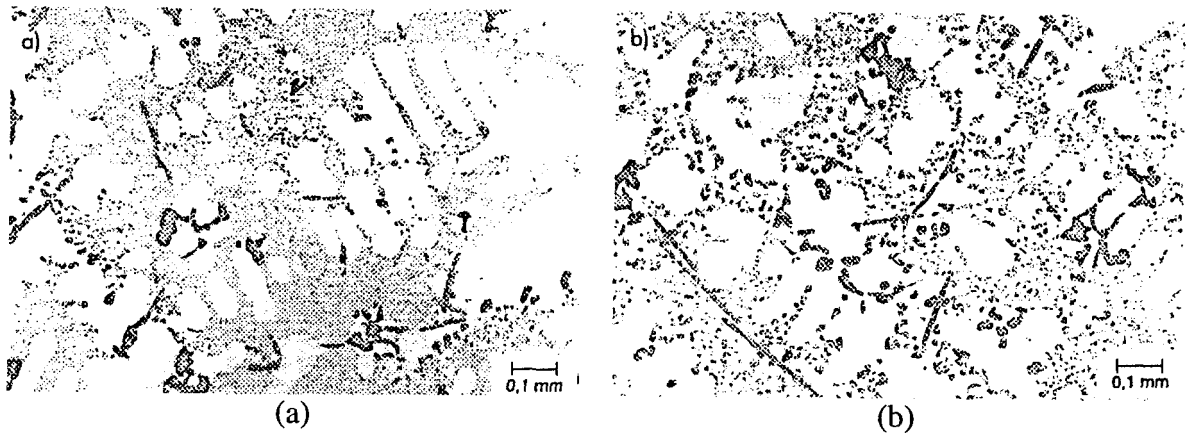


Figure 15. Effect of Bi and Na addition on the refining of eutectic silicon a) 136 ppm Na, 38 ppm Bi b) 76 ppm Na, 115 ppm Bi⁵⁴

Kurdyumov *et al.*⁵⁵ reported that Bi, Sb, Ga and Sn have an appreciable demodifying influence on alloy AL4 (Al-Si-Mg alloy) treated with sodium, Figure 16(b). The eutectic silicon structure becomes much larger on adding 0.05% Sb or Ga or 0.1% Bi. When larger amounts are added, the eutectic silicon is once more refined, since these elements have their own modifying action on the eutectic. Bi also has a coarsening effect on Sr modified AL4 alloy, Figure 16(c), and this effect appears around 0.05%, but larger amounts have no effect on eutectic silicon structure.

They also noted that the modifying effects of Bi and Sb are much weaker in alloy AL4 than in alloy AL2. This difference is probably explained by the formation of the intermetallides Mg_3Bi and Mg_3Sb , which significantly reduce the activity of Bi and Sb in the melts. They also concluded that, the differing effects of the various tramp elements on the modified alloy structure must be taken into account in selecting the best additive. In the cases of AL4 melts contaminated with Bi, Cd, Sn, and/or Ga, consistent modification effects can only be ensured by treatment with Sr.

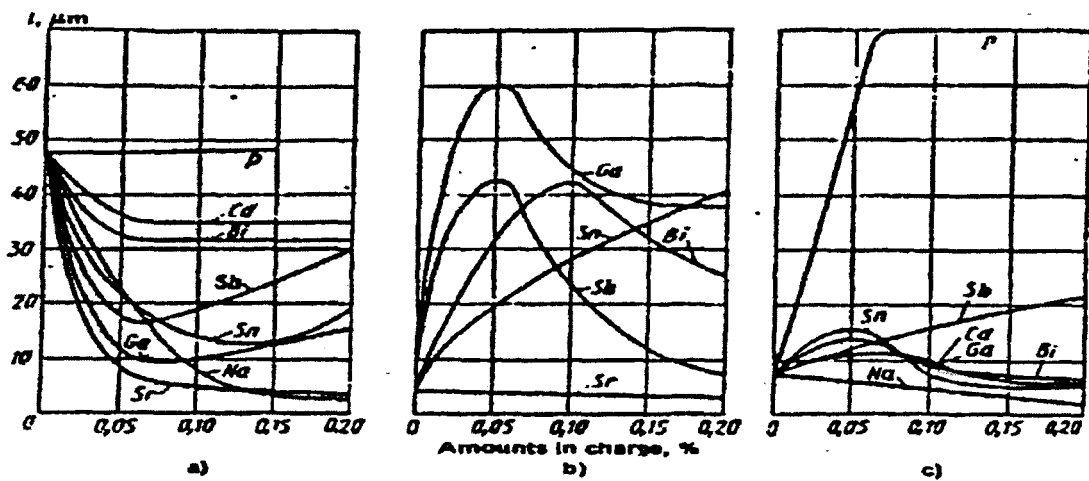


Figure 16. a) Original, b) Na treated, and c) Sr treated AL4(Al-Si-Mg) alloy.⁵⁵

2.4.1.2 THERMAL ANALYSIS

Interactions between Bi and Sr can be elucidated using thermal analysis experiments. Figure 17 represents the relation between the wt% Bi and eutectic temperature at various Sr contents, for 319 alloys. At Sr levels of 0.002-0.004-wt% Sr, increasing the Bi from 0.014 to 0.02 wt% results in an increase in eutectic temperature. Further Bi additions at the 0.002-0.004-wt% Sr level do not cause a further increase in the eutectic temperature. At 0.007-0.011-wt% Sr, increasing the Bi level up to 0.04 wt% does not increase the eutectic temperature. Further Bi additions at the 0.002-0.004-wt% Sr level result in a rise in the eutectic temperature.⁵³

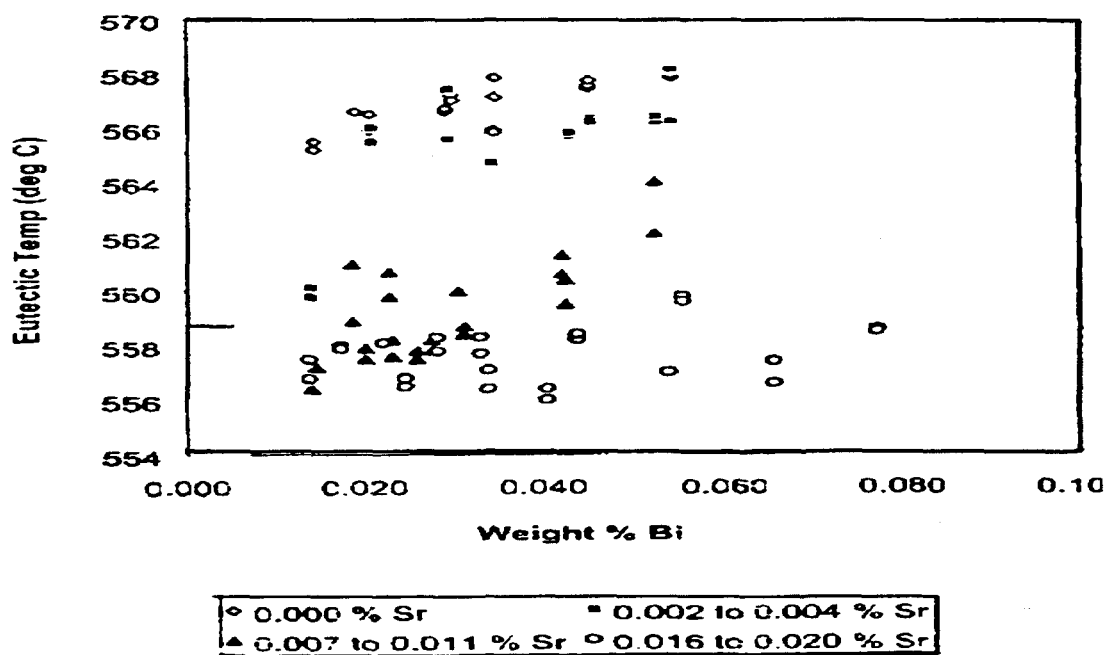


Figure 17. Al-Si eutectic temperatures versus %wt Bi in a melt separated by wt% Sr.⁵³

The influence of bismuth additions on the temperature of the eutectic in A356.2 alloy is illustrated by Cho *et al.*⁵² in Figure 18. Without bismuth, the Sr-modified alloy exhibits a eutectic temperature of 566.14°C, but the eutectic temperature continuously increases with bismuth content, up to 574.09°C (0.1%Bi added), strongly suggesting a reduction in eutectic modification and confirming the microstructural effects documented previously.

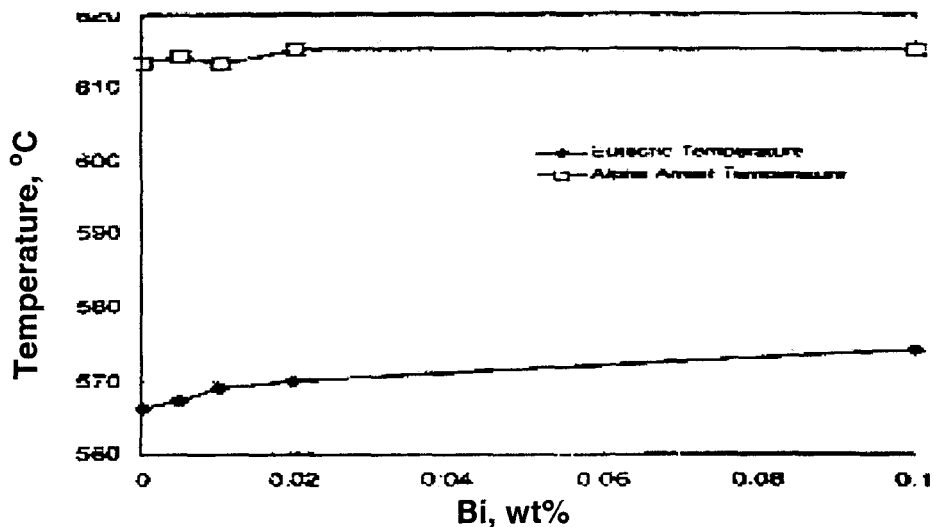


Figure 18. The alpha-aluminum-arrest and eutectic-arrest temperature of A356.2 alloy, modified with 0.015%Sr, obtained in conventional silica thermal analysis cups.⁵²

2.1.4.3 POROSITY

The effect of Bi addition on %porosity for unmodified and Na-modified AlSi9Cu3 alloy reported by Kube *et al.*⁵⁴ is shown in Figure 19. It is seen that, with an increase in the bismuth content of the alloy (A365.2), the pipe depth decreases, while the microshrinkage

tends to increase. It was proposed that this change in shrinkage characteristics with increased bismuth content is more significant when the solidification rate is slow, leading to leakage in commercial castings, such as intake manifolds. However, test molds produced in this study, from the Sr-modified A365.2 alloy, showed an increase in pipe depth with increasing bismuth, up to 0.02% (200 ppm), and then a marked decrease in pipe depth as the bismuth addition was further increased to 0.1% (1000 ppm).⁵²

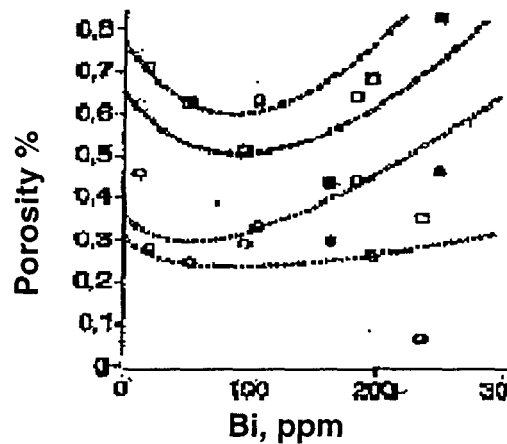


Figure 19. Amount of Bi, ppm vs. percentage porosity.⁵⁴

2.4.1.4 MECHANICAL PROPERTIES

The influence of bismuth in amounts up to 0.05% (500 ppm) on the hardness and tensile properties of both sand cast and chill cast aluminum having a modified A413 composition is demonstrated in Table 4. Both the unmodified as well as Na- or Sr-modified conditions were also investigated. Over this range of bismuth content no significant deterioration in hardness or in tensile properties could be identified, Figure 20, even though

there was a marked influence of bismuth on microstructure, as previously discussed in section 2.4.1.1.

Table 4 Chemical composition of G-AlSi12 (Cu) (modified A413) (wt%)⁵²

Si	Fe	Cu	Mn	Mg
12.8	0.81	0.74	0.23	0.35
Cr	Zn	Ti	Ni	Pb
0.031	0.31	0.041	0.033	0.041

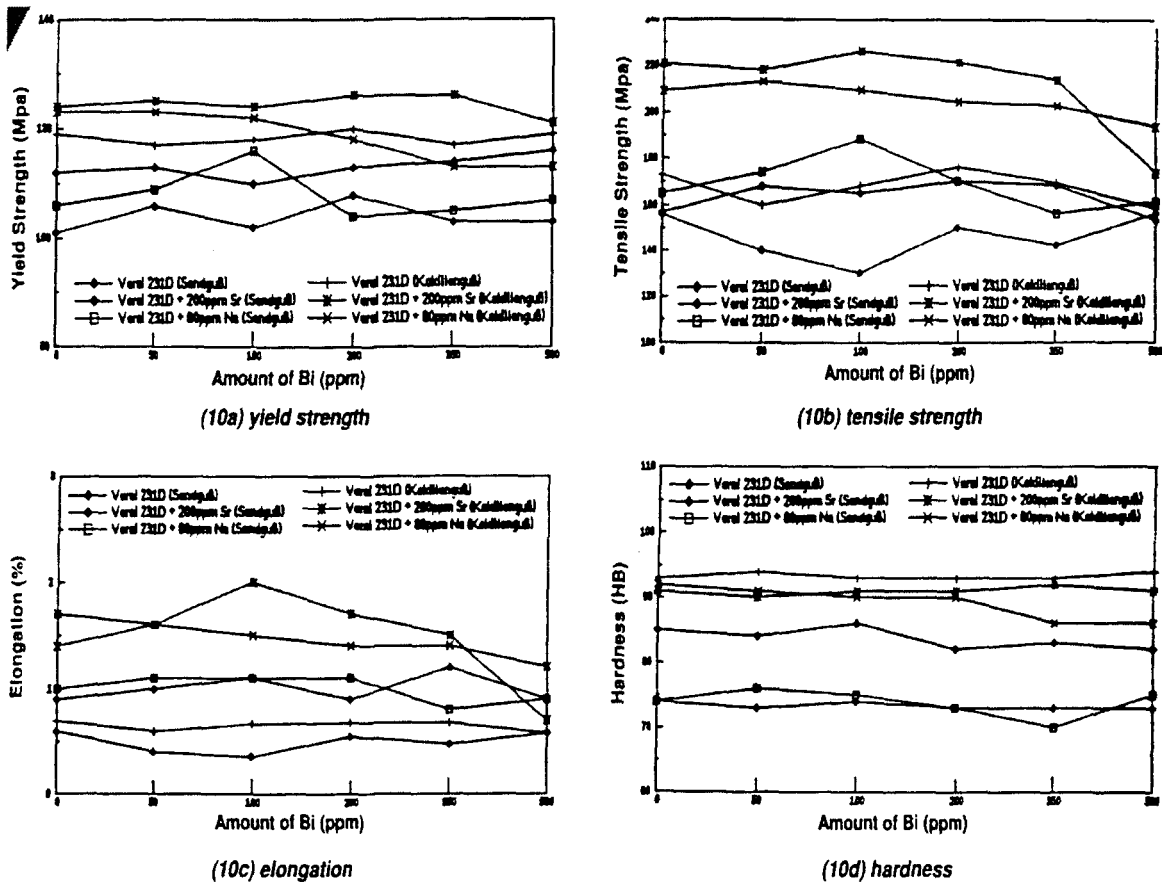


Figure 20. Effect of Bi on the mechanical properties of unmodified, Na-modified and Sr-modified Al casting alloy, A413.8.⁵²

The beneficial effect of modification, of both sodium and strontium, on tensile properties was evident, however. Note that hardness was significantly decreased with both forms of modification, and more noticeably in the sand cast material.⁵²

The effect of Bi as a modifier on mechanical properties of the Al-Si alloys was studied by Inoyama *et al.*,⁴⁹ Figure 21. It is clear that, the Bi addition caused a slight increase in both tensile strength and hardness. This is expected to be due to the modifying action of Bi on the structure of the eutectic Si in these kinds of alloys.

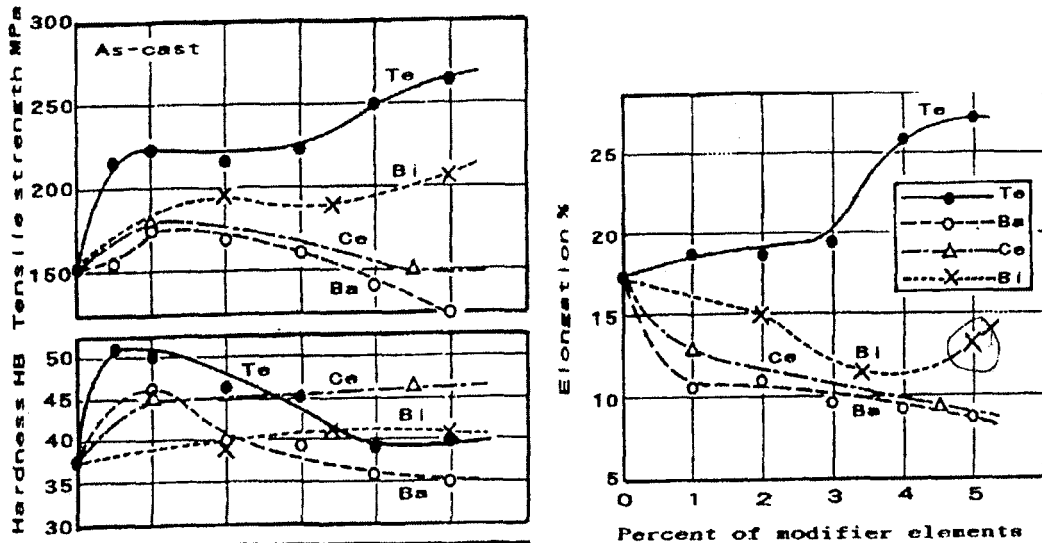


Figure 21. Effect of the addition of modifier elements on mechanical properties in as-cast specimens.⁴⁹

2.4.2 CALCIUM IN Al-Si ALLOYS

2.4.2.1 CA AS IMPURITY

Impurity calcium is usually attributed to low-purity commercial silicon used in the production of Al-Si alloys. The recommended maximum amount of calcium tolerable in aluminum alloys varies according to individual research. It was reported that calcium gives

rise to porosity and microcavitation, so the tolerable amount of calcium content would be 0.002% (20 ppm) in Al-Si alloys. It was proposed that 0.003% (30 ppm) Ca would be a tolerable amount in Al-Si alloys, since it has deleterious effects on fluidity and shrinkage properties. Others have suggested 0.004% as a maximum tolerable amount in an Al-Si-Mg type alloy.⁵⁶

The phase diagram of the Al-Ca system shows that calcium has very low solubility in aluminum: less than 0.05% at (0.08 wt%) at the eutectic temperature, 616°C, and less than 0.03 at (0.05 wt%) at 600°C, Figure 22. At equilibrium, it would be expected that calcium in excess of 0.03% would be present as the compound Al_4Ca , with a lesser amount typically present. A range of Ca-Si compounds is possible, although their formation within the phase diagram has not been well defined.

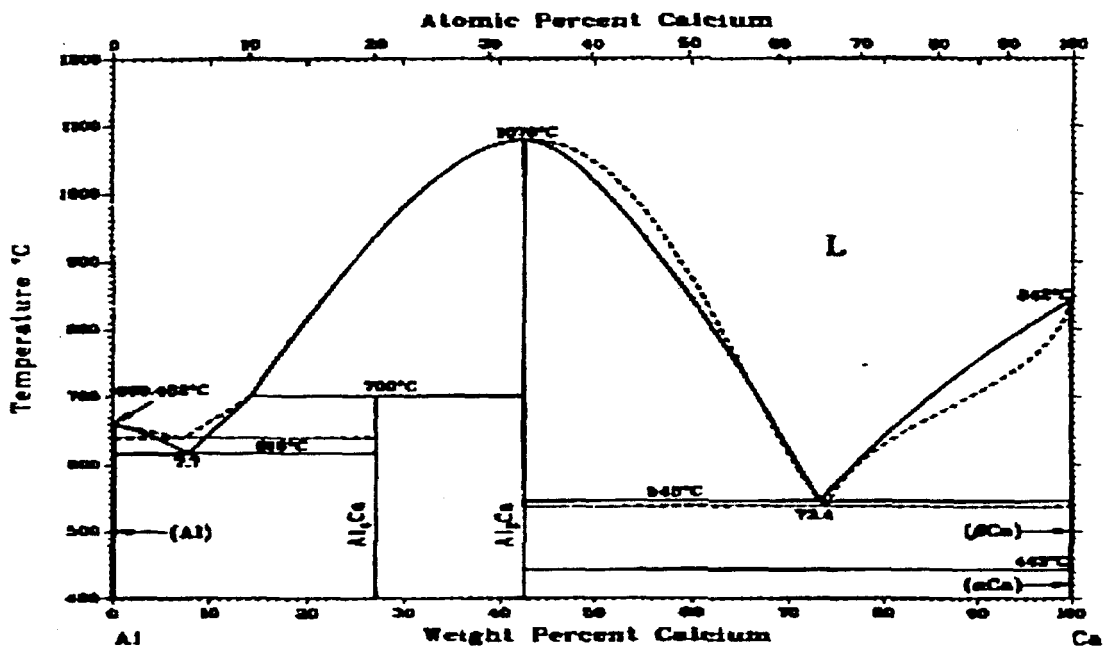


Figure 22. Al-Ca phase diagram.⁴⁷

2.4.2.2 CA COMPOUNDS

Calcium forms a variety of compounds with aluminum, alloying elements and impurities. It has been reported⁵⁶ that calcium combines with aluminum and forms the intermetallic compounds Al_4Ca and Al_2Ca . It would be expected that the addition of commercial silicon to a bath of molten aluminum alloy would result in the formation of the higher calcium-containing compound, Al_2Ca , around the added particles, with the lower calcium-containing compound forming subsequently as equilibrium is approached.

Calcium also combines with silicon to form intermetallic compounds of $CaSi_2$, Ca_3Si_4 , $CaSi$, Ca_5Si_3 and Ca_2Si . In Al-Si casting alloys, the $CaSi_2$ intermetallic compound is insoluble in aluminum and has been seen to have a deleterious effect on the mechanical and corrosion properties of the alloy.⁵⁶

Calcium, by means of compound formation, has been used to remove impurity silicon and bismuth from aluminum melts introduced through the use of aluminum scrap in the charge. Calcium reportedly⁵⁶ combined with impurity silicon to form intermetallic compounds, $CaSi_2$ and $CaSi_2Al_2$ in the aluminum melt, which was successfully removed by filtering. It was reported that when 3% of calcium was added to an Al-5%Si alloy, at least $CaSi_2$ and $CaSi_2Al_2$ intermetallic compounds were formed and the concentration of silicon in the alloy was reduced up to 50%, after holding the melt at the temperature of 700° C, Figure 23.

Calcium also reduced the impurity bismuth in the aluminum alloy melt by the reported formation of the compound Bi_3Ca_5 in an Al-5%Cu alloy, Figure 24.⁵⁷

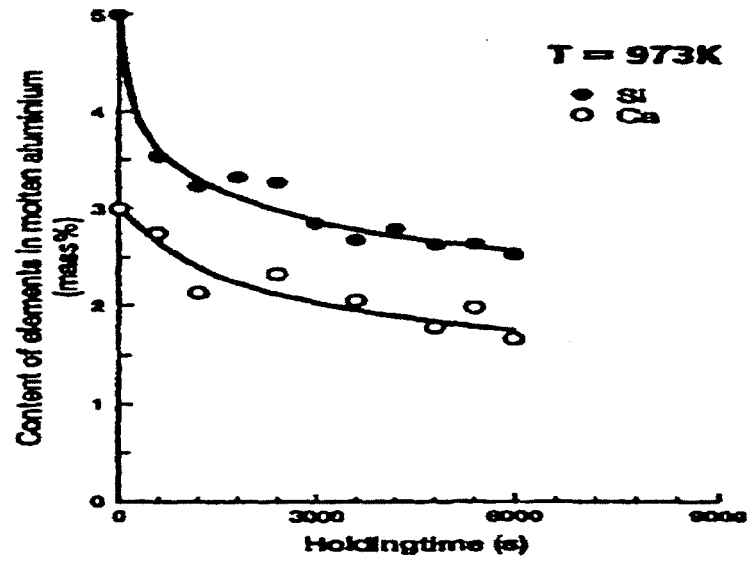


Figure 23. Calcium and silicon interactions in Al-5%Si alloys at 700 °C.⁵⁶

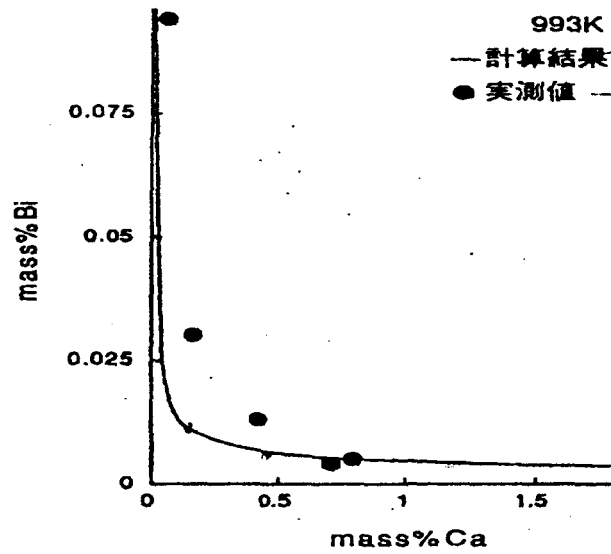


Figure 24. Effect of Ca addition on % Bi.⁵⁷

2.4.2.3 *REMOVAL OF IMPURITY CALCIUM*

Removal of calcium from an aluminum alloy melt has reportedly been accomplished by using a sufficiently high melting temperature, but this method deleteriously affects mechanical properties by influencing the composition and the amount of hydrogen in the melt. Also, chlorine can be used to remove calcium from an aluminum alloy melt, if it is used as part of a gas mixture; gas bubbling usually contributes to the removal of alkali elements, such as calcium, lithium and sodium, as well as other inclusions. Furthermore, a mixture of C_2Cl_6 and red phosphor has been successfully used for eliminating calcium in aluminum alloys.⁵⁶

However, it has been found that calcium in the melt reacts with chlorine to produce a stable chloride salt, which is normally present in the solid form at the melt temperature, so that it becomes difficult to remove. Calcium is also removed by adding red phosphorus, in amounts approaching twice the calcium content, in an Al-Si alloy.

2.4.2.4 *EFFECT OF Ca AS A MODIFIER*

Calcium is well recognized as a modifier of the eutectic in Al-Si alloys.⁵⁶ While modification of the eutectic with calcium is less effective than sodium or strontium, it is considerably more durable than other major modifiers, Figure 25.

2.4.2.5 *INTERACTION OF CALCIUM WITH MODIFIERS*

It has been reported that calcium reacts with and poisons antimony modification, as does sodium and strontium. Calcium appears to be an effective scavenger for antimony in

the A356 alloy, with a weight ratio greater than 4:1 Ca to Sb, probably by forming the intermetallic compounds CaSb , Ca_3Sb_2 and/or CaSb_3 . The interaction between calcium and antimony is generally well known, but the interactions between calcium and strontium and/or sodium are not as well understood.

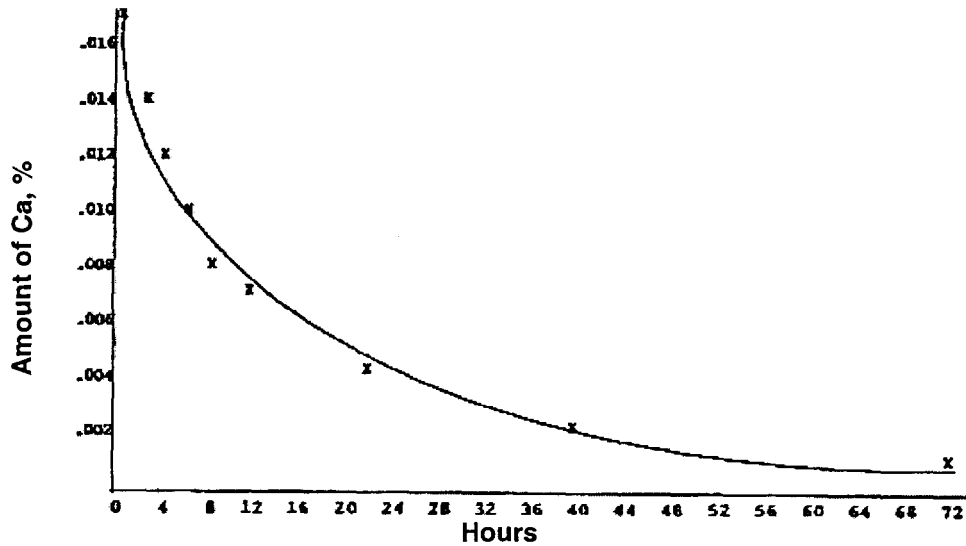


Figure 25. Calcium loss vs. holding time of SAE332 (Al-Si-Cu-Mg alloy) at 665.6 °C.⁵⁶

2.4.2.6 EFFECT OF CALCIUM ON IRON IMPURITIES

It is well known that iron is often considered one of the most harmful impurities in aluminum alloys. It has quite a high solubility in molten aluminum, but the solubility of iron in the solid state is very low, only 0.05% at 660 °C. Iron also forms several undesirable intermetallic compounds in aluminum alloys, which are responsible for the reduction of the mechanical properties of the alloys. However, it has been found that calcium refines and

spheroidizes iron intermetallic compounds, as well as eutectic silicon in Al-Si alloys, therefore resulting in improved mechanical properties.

The effects of calcium and iron additions on the eutectic silicon size are shown in Figure 26. A dramatic increase or decrease in the area and maximum length of the eutectic silicon phase was not observed, but 0.003% (30 ppm) of calcium additions reduced the area and the maximum length of eutectic silicon by about 20-40%, in comparison with the alloy produced without calcium.⁵⁶ It was also reported that calcium deactivated the impurity particles, which would otherwise act as crystallization centres for eutectic silicon in unmodified Al-Si eutectic alloys.

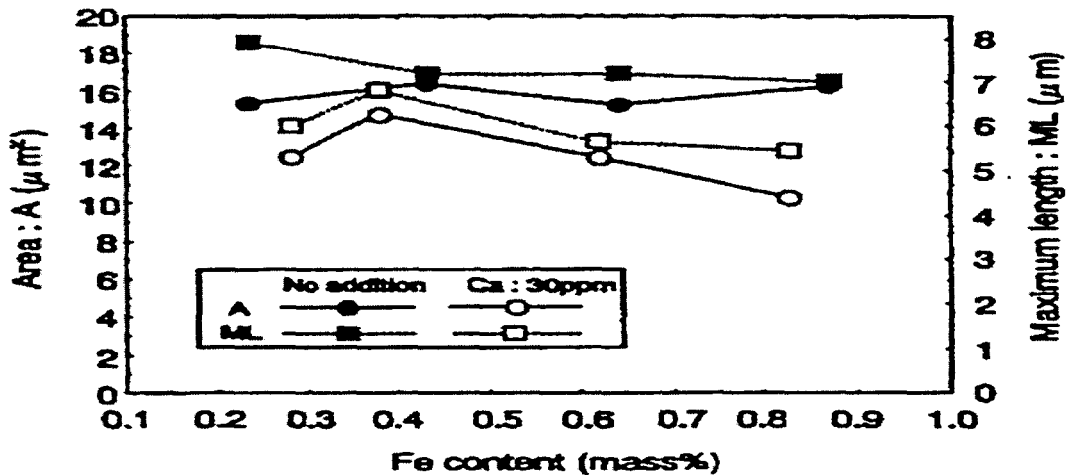


Figure 26. Effect of calcium and iron additions on the eutectic silicon size.⁵⁶

2.4.2.7 EFFECT OF CALCIUM ON MECHANICAL PROPERTIES

The effect of Ca was observed in hypoeutectic Al-Si alloys.⁵⁶ As Figure 27 shows, in the case of AC2A (Al-4%Cu-4.5%Si) alloy, it is apparent that a calcium addition of

0.05% (500 ppm) can achieve maximum tensile strength and elongation for the treated alloy. However, calcium levels in excess of 0.05% (500 ppm) are detrimental to both tensile strength and elongation, because of the formation of undesirable compound CaSi_2 .

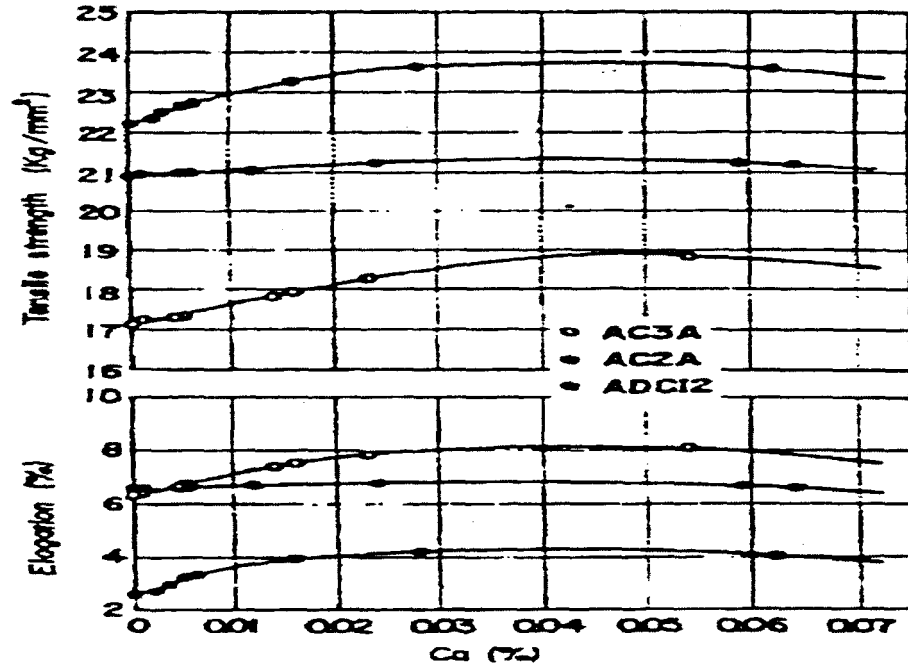


Figure 27. Effect of Ca on tensile strength and elongation of AC3A (Al-Si), AC2A (Al-Si-Cu), ADC12 (Al-Si-Cu) alloys.⁵⁶

The role of calcium was also studied in another hypoeutectic alloy, AC2B-T6 (Al-6.5%Si-Cu-Mg). In this investigation, 0.003% (30 ppm) calcium was introduced in a series of melts containing increasing amounts of iron, (0.2, 0.4 and 0.8% Fe). It is evident that tensile strength and elongation were detrimentally affected by increasing the iron level, but the yield strength was not significantly affected. However, at all iron contents, the addition

of 30 ppm calcium had a beneficial effect on these properties. This was attributed to a spheroidizing of the intermetallic iron compounds.

For impact and fatigue properties, it is found that in the AC2B-T6 aluminum-casting alloy with different iron contents (ranging from 0.2% to 0.8%), both properties were improved by a 0.004% (40 ppm) addition of calcium. The influence of calcium was more apparent in conventional fatigue properties. This has been attributed to the refining and spheroidizing of the eutectic silicon and the iron intermetallic compound.

Hardness was not significantly affected by the addition of calcium. Additions of up to 0.07% (700 ppm) of calcium were made in AC3A, AC2A and ADC12 alloys, but there was no marked influence of calcium on the hardness values, Figure 28.

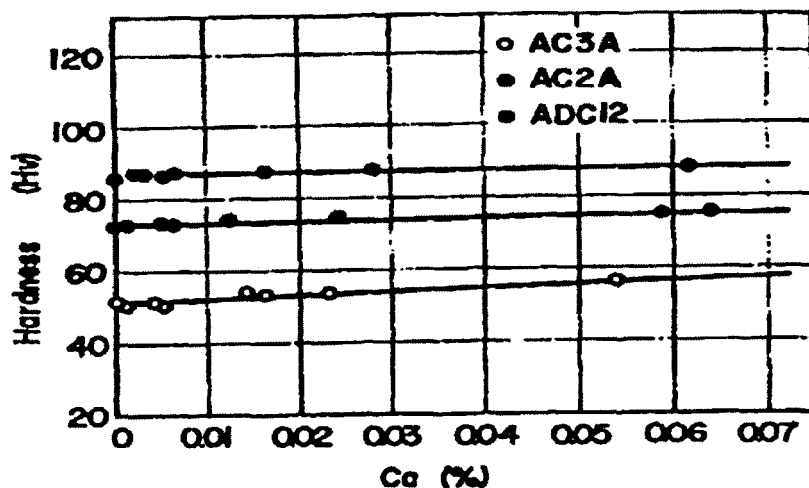


Figure 28. Effect of Ca on Vickers hardness of AC3A (Al-Si), AC2A (Al-Si-Cu), ADC12 (Al-Si-Cu) alloys.⁵⁶

2.4.2.8 EFFECT OF CALCIUM ON CASTING CHARACTERISTICS

It was found that calcium additions increased the viscosity of an aluminum melt very rapidly up to 0.4% (4000 ppm) calcium, then increased slowly above this value. Due to the increased viscosity and surface tension of aluminum alloys by the addition of calcium, decreased fluidity and feedability were observed.

Fillability of the AC3A (Al-Si), AC2A (Al-Si-Cu), ADC12 (Al-Si-Cu) alloys was significantly reduced with calcium additions up to about 0.01% (100 ppm) when a riser was used, while there was no change in fillability without a riser. Also, it was observed that the feedability of the three alloys was notably reduced by additions of calcium.⁵⁸

2.4.2.9 EFFECT OF CALCIUM ON POROSITY FORMATION

It was reported that the porosity and shrinkage in cast Al-Si alloys were influenced by the formation of the intermetallic compounds, CaSi_2 , CaSi_2Al_2 . Calcium increases the hydrogen solubility of the aluminum melt only at the trace concentration levels which are the result of the reaction of calcium with moisture in the atmosphere, and is often responsible for casting porosity. Even with very small amounts of calcium about 0.001% (10 ppm) molten aluminum alloys had a tendency to pickup hydrogen from the atmosphere.

The effect of calcium on hydrogen absorption of molten Al-Si alloys was studied by Hiroshi *et al.*⁵⁹ for AC2B (Al-Si-Cu) alloy ingots. They concluded that:

- At a constant temperature, increasing holding time will increase hydrogen content.
- At a certain humidity level, alloys containing a high amount of calcium (0.002-0.004) achieve higher porosity levels.

- At a constant holding time and temperature, increasing calcium content will increase the porosity level.

An increased porosity level with Ca content is mainly due to the increased amount of hydrogen absorption even during a very short holding time. The oxide formed on the melt surface sinks. It is considered that this happens because Ca improves wettability between the oxide and the molten metal. This accordingly promotes the oxidation of the melt, causing considerable hydrogen absorption.⁵⁹

When titanium content in the AC2B (Al-Si-Cu) alloy is maintained at 0.1%, the number of pores reduces accordingly with the increasing Ca content because of a reduction in the surface tension of the liquid alloy, which results in easier formation and escape of gas bubbles.⁶⁰

Calcium also influenced the tendency of eutectic alloys to form shrinkage cracks. While a hot tearing tendency was little affected by calcium content in Al-Si alloys, the calcium effect on shrinkage cavity formation was considerable, Figure 29.⁶¹

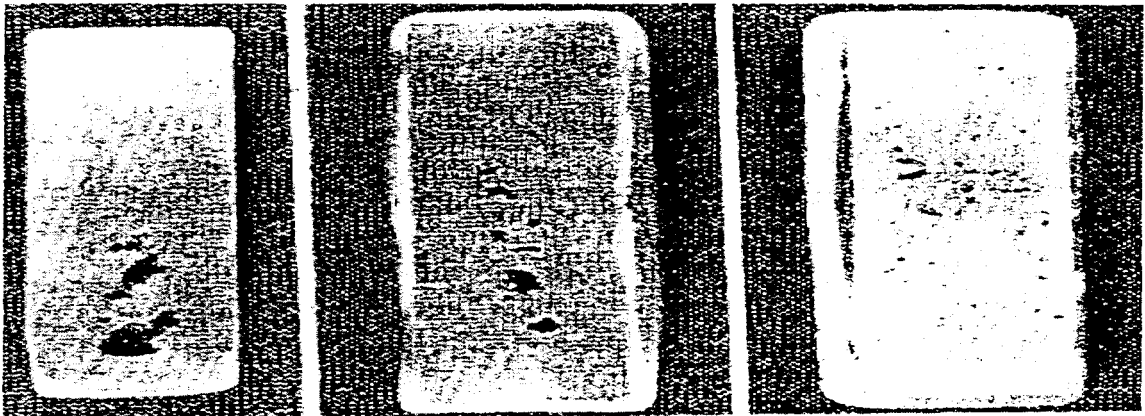


Figure 29. Effect of Ca on shrinkage cavity formation in Al-Si alloy: a) 0.0005% Ca, b) 0.014% Ca, c) 0.026% Ca.⁶¹

CHAPTER 3

EFFECT OF Bi AND Ca ADDITIONS ON THE EUTECTIC Si PARTICLE CHARACTERISTICS IN Sr-MODIFIED 319 ALLOYS

CHAPTER 3

EFFECT OF Bi AND Ca ADDITIONS ON THE EUTECTIC Si PARTICLE CHARACTERISTICS IN Sr-MODIFIED 319 ALLOYS

3.1 INTRODUCTION

In this part of the work, the Sr-modified 319 alloys with Bi/Ca addition were melted and poured into a graphite mold. The effect of Bi and Ca addition on the eutectic silicon was studied through thermal analysis, microstructure examination, silicon particle measurements and electron probe microanalysis (EPMA) to clarify the different phases.

3.2 EXPERIMENTAL PROCEDURE

3.2.1 ALLOY AND MELT PREPARATION

The as-received 319 alloy ingots were cut into small pieces, cleaned, dried, and melted in a 30-kg capacity SiC crucible, heated in an electric resistance furnace. The melting temperature was kept at $735 \pm 5^\circ\text{C}$. The melt was degassed with argon for twenty minutes using a rotary impeller degassing system (150 rpm). Strontium was added in the form of Al-10% Sr master alloy, whereas magnesium was added as pure metal. The Sr-modified alloy was coded B, while the one containing Mg and Sr was coded C. The chemical compositions of the as-received alloy (coded A), and alloys B and C are listed in Table 5.

Table 5 Chemical composition (wt %) of the alloys used in the present work

Alloy code	Si	Cu	Fe	Mg	Ti	Zn	Sr	P
319 base, A	6.08	3.56	0.1	0.04	0.147	0.003		0.0015
(319 + Sr), B	6.03	3.55	0.11	.0425	.1366	.0028	0.008	0.0015
(319+Sr+Mg), C	6.16	3.67	0.1	0.386	0.13	.0017	0.008	0.0015

Trace additions of Bi and Ca were made using Al-5% Bi and Al-10% Ca master alloys. Tables 6 and 7 list the various Bi and Ca additions and the respective alloy codes. The initial P concentration in these alloys was ~15 ppm. In some cases, particularly in the Ca-containing alloys, phosphorous was added intentionally, up to 60 ppm, to study its role on Ca compound precipitation.

Table 6 Alloy codes for Bi-containing alloys

Alloy Code	Alloy + addition (ppm)	Alloy Code	Alloy + addition (ppm)
BBA	B+ 25 ppm Bi	CBA	C+ 145 ppm Bi
BBB	B+ 145 ppm Bi	CBB	C+ 228 ppm Bi
BBC	B+ 287 ppm Bi	CBC	C+ 306 ppm Bi
BBD	B+ 753 ppm Bi	CBD	C+ 637 ppm Bi
BBE	B+ 1151 ppm Bi	CBE	C+ 1152 ppm Bi
BBF	B+ 2250 ppm Bi	CBF	C+ 2799 ppm Bi
BBG	B+ 4543 ppm Bi	CBG	C+ 4683 ppm Bi
BBH	B+ 4945 ppm Bi	CBH	C+ 5470 ppm Bi
BBI	B+ 6640 ppm Bi	CBI	C+ 6640 ppm Bi
BBJ	B+ 7170 ppm Bi	CBJ	C+ 9600 ppm Bi

Table 7 Alloy codes for Ca-containing alloys

Alloy Code	Alloy + addition (ppm)	Alloy Code	Alloy + addition (ppm)
BCA	B+ 017 ppm Ca	CCA	C+ 50 ppm Ca
BCB	B+ 070 ppm Ca	CCB	C+ 91 ppm Ca
BCC	B+ 089 ppm Ca	CCC	C+ 138 ppm Ca
BCD	B+ 129 ppm Ca	CCD	C+ 221 ppm Ca

3.2.2 THERMAL ANALYSIS

The alloys were cut into small pieces, dried, and melted in a 1-kg capacity SiC crucible, and heated by means of an electric resistance furnace. The melting temperature was kept at $750^{\circ}\text{C} \pm 5^{\circ}\text{C}$. At this temperature, measured Bi and Ca additions were made using a perforated graphite bell. The melt was stirred for about 15 minutes to ensure the homogeneous mixing of the additions. The molten metal was poured into a 600°C preheated cylindrical graphite mold to obtain near-equilibrium cooling conditions.

Thermal analysis was performed by attaching a highly sensitive chromel-alumel (type K) thermocouple through the bottom of the mold, halfway up into the mold cavity along the mold centerline. The part of the thermocouple within the mold was protected by double-walled ceramic tubing, as shown in Figure 30.

The temperature-time data was obtained using a high-speed data acquisition system linked to a computer (at a rate of 0.2 sec). Samples for chemical analysis were taken simultaneously for each melt condition. From the thermal analysis data, the cooling curves and their first derivatives were plotted.

In order to ensure the sensitivity of the employed thermocouples, a series of four experiments was carried out using the B alloy under identical conditions. The results are listed in Table 8 for Al-Si eutectic undercooling. It is evident from the table that the fluctuation in the measurements is about $\pm 0.1^{\circ}\text{C}$.

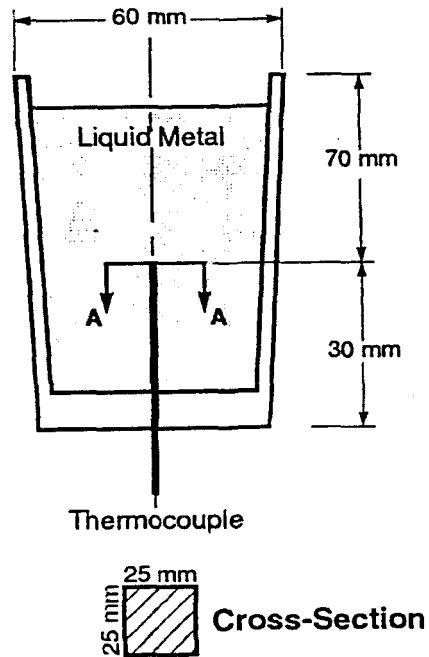


Figure 30. Graphite mold.

Table 8 The undercooling values obtained for alloy B from 4 identical experimental conditions

Experiment	Undercooling, °C
1	1.2
2	1.3
3	1.2
4	1.1

3.2.3 METALLOGRAPHY

Samples for metallography were sectioned from the graphite mold castings (from the central part containing the thermocouple tip), mounted, and polished. The microstructures were examined using optical and scanning electron microscopy and correlated with the cooling curves obtained from thermal analysis.

The Si particle characteristics (length, area, aspect ratio, and density) were measured using a Leco 2001 image analyzer in conjunction with the optical microscope. The various phases observed were identified using electron probe microanalysis, using a Jeol JXA-8900L WD/ED combined microanalyzer operating at 20 kV and 30 nA, where the size of the spot examined was $\sim 2 \mu\text{m}$.

3.3 RESULTS AND DISCUSSION

3.3.1 THERMAL ANALYSIS

From the thermal analysis data, the cooling curves were plotted for each alloy condition. Figure 31 shows a comparison of the cooling curves obtained for the Sr-modified 319 alloy (B) with various Bi additions. The cooling curve marked 1 corresponds to the base 319 alloy. The addition of Sr (80 ppm, curve 2) causes depression in the Al-Si eutectic temperature, T_{eut} , (from 565°C to 555°C), indicating full modification of the Si. When Bi is added to B alloy, T_{eut} begins to increase gradually, reaching a value of 562°C at 2250 ppm Bi. This observation signifies the “demodification” effect of Bi on the Sr-modified alloy.⁸ When the Bi concentration is of the order of 5000 ppm or above, T_{eut} starts to decrease once again, indicating that the Bi is now acting as a modifier.⁶

Figure 32 shows the cooling curves obtained from 319 alloy containing 0.4 wt% Mg and 0.008 wt% Sr (C). As can be seen, T_{eut} decreases to its minimum of $\sim 547^{\circ}\text{C}$ (*cf.* curves 1 and 2).⁶² Introduction of Bi continuously raises T_{eut} , up to an addition of ~ 5000 ppm Bi. Beyond this concentration, T_{eut} begins to decrease, but at a much slower rate compared to that observed in the B alloys. This may partly account for the interaction between Mg and

Bi to form a complex oxide and thus, retard the modification effect of Sr. This will be discussed later, in section 3.

In the case of Ca addition to the B alloy, Figure 33, it was observed that at ~17 ppm Ca, the T_{eut} increased by about 5 degrees (*cf.* curves 2 and 3) due to its “demodification” effect.¹³ In C alloy, however, the eutectic temperature remained constant, with Ca additions up to 50 ppm, Figure 34. This observation can be attributed to the formation of Mg- and Ca-containing intermetallics restricting the “demodification” effect of Ca in these alloys.

The change in the eutectic undercooling associated with Bi addition is a significant indicator of its influence on the cast microstructure. Similar to the case of sodium and strontium modification, this undercooling can also be considered as a thermal indication of the progress of eutectic modification.^{8,45}

From Figure 35, it can be seen that the amount of undercooling in the Sr-treated 319 alloy (B alloy) is associated with a fairly large undercooling of ~1.2°C (*cf.* curve 2 with curve 1 for the base 319 alloy). The addition of Bi results in a slow decrease of the undercooling, as evident from curves 6 and 7, corresponding to 1150 and 2250 ppm additions, respectively. It should be noted that curve 7 is more or less similar to curve 1, produced from the base 319 alloy with zero undercooling. A further increase in Bi concentrations led to the gradual reappearance of the undercooling, indicating that Bi begins to act as a modifier, with a significant undercooling of ~0.7°C at 7170 ppm Bi. In the case of the (Sr+Mg)-containing C alloys, no undercooling was observed at any Bi-level, due to the interaction of the Bi with the Sr and Mg.

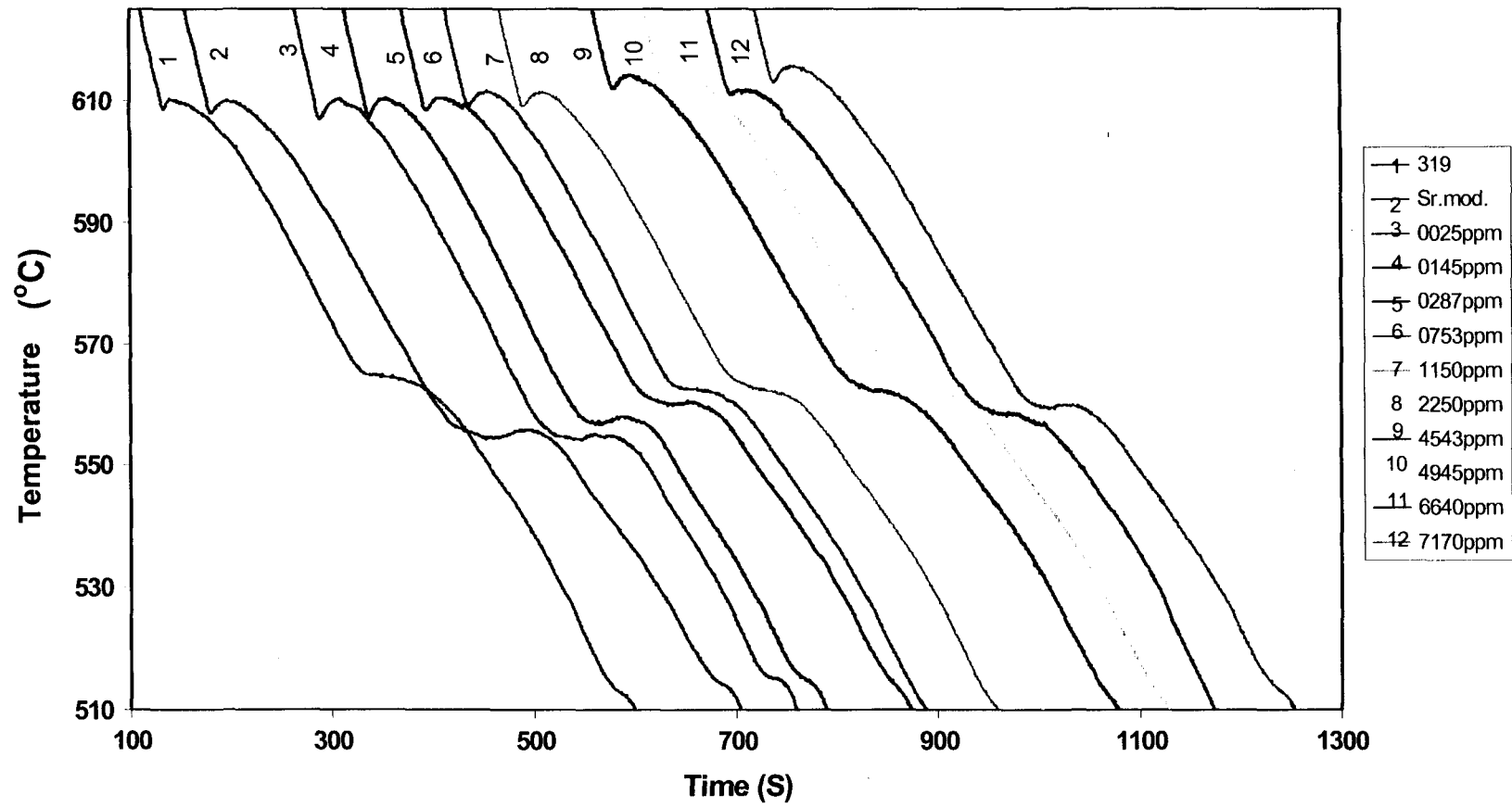


Figure 31. Cooling curves obtained for B alloys containing various amounts of Bi.

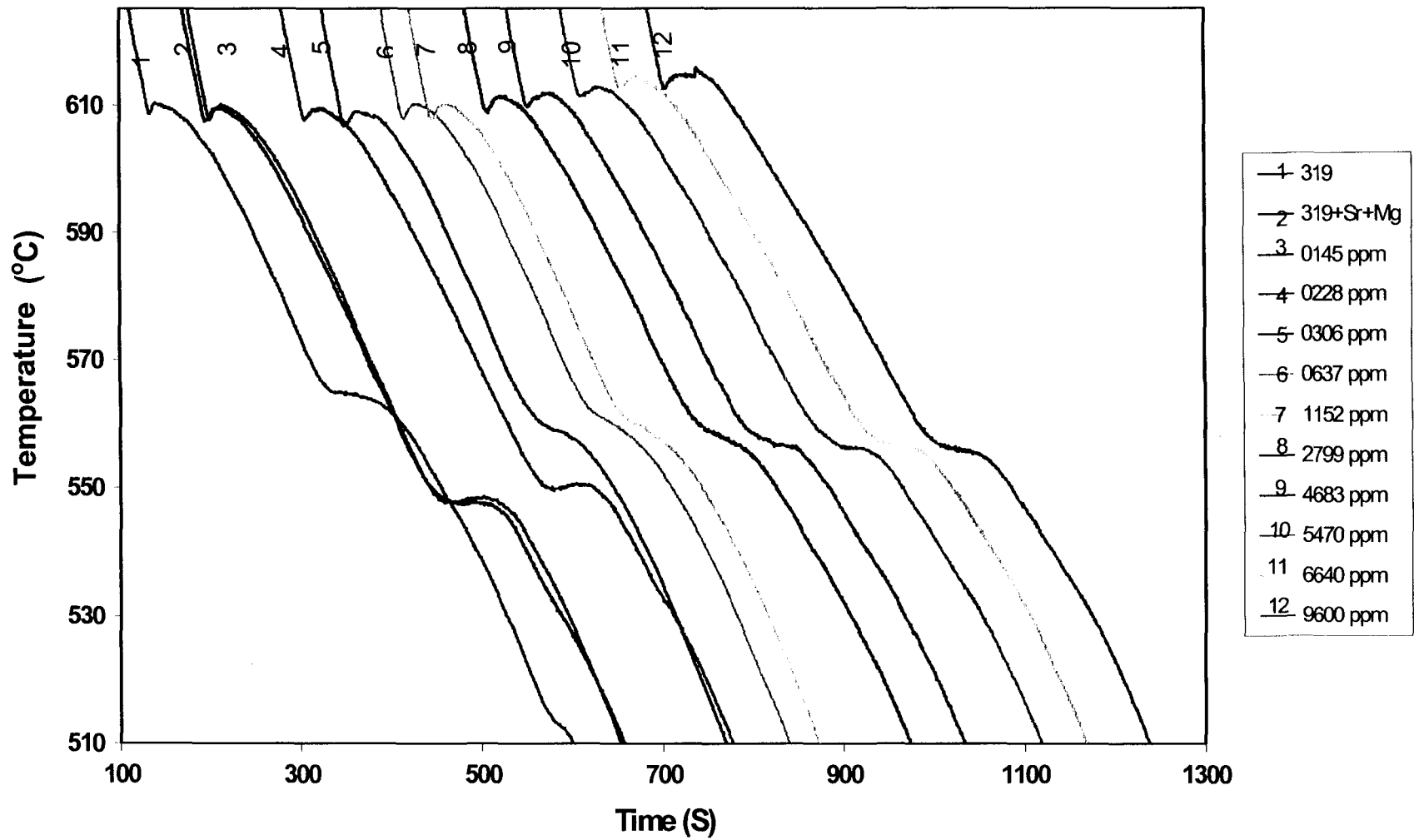


Figure 32. Cooling curves obtained for C alloys containing various amounts of Bi.

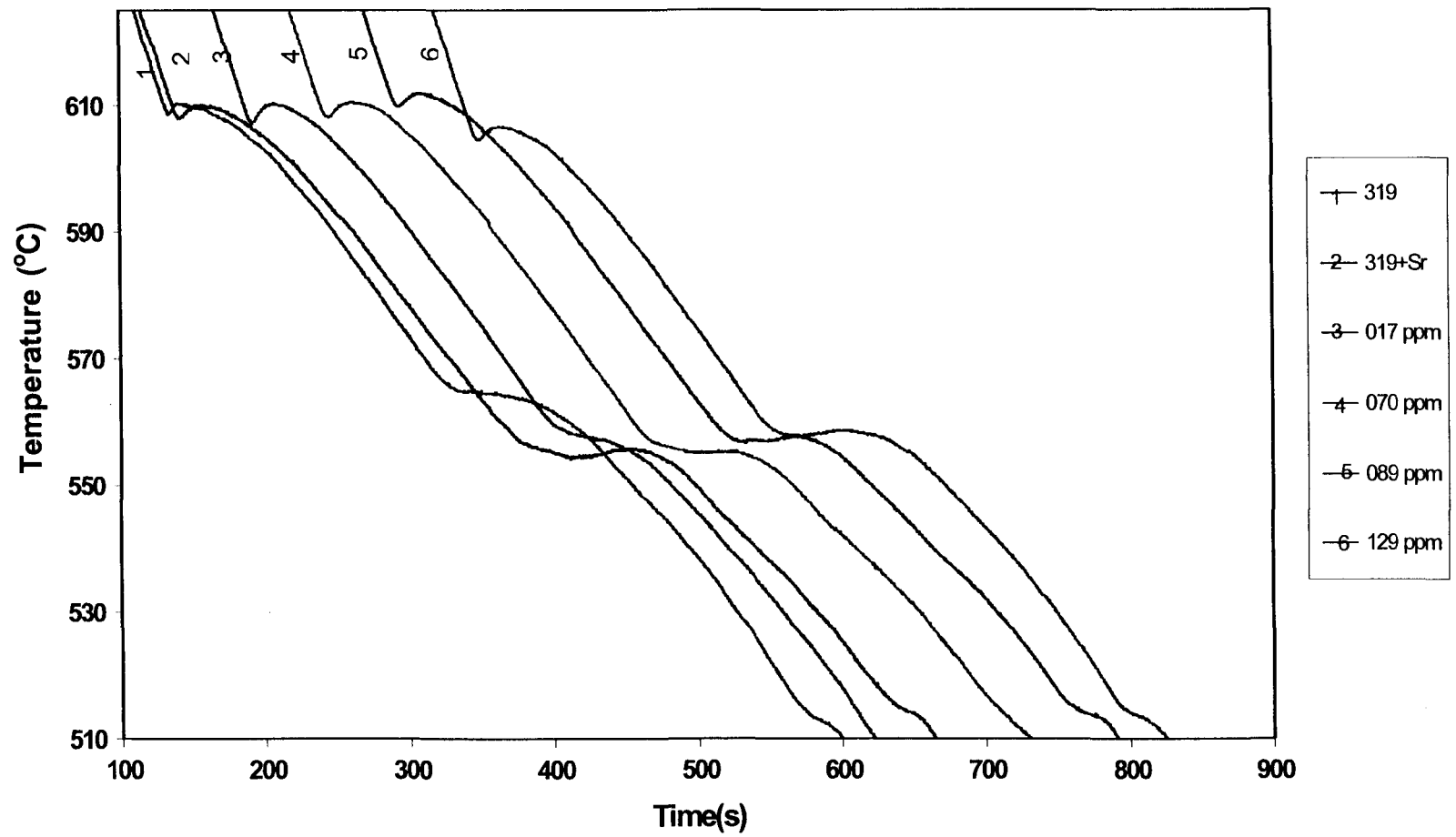


Figure 33. Cooling curves obtained for B alloys containing various amounts of Ca.

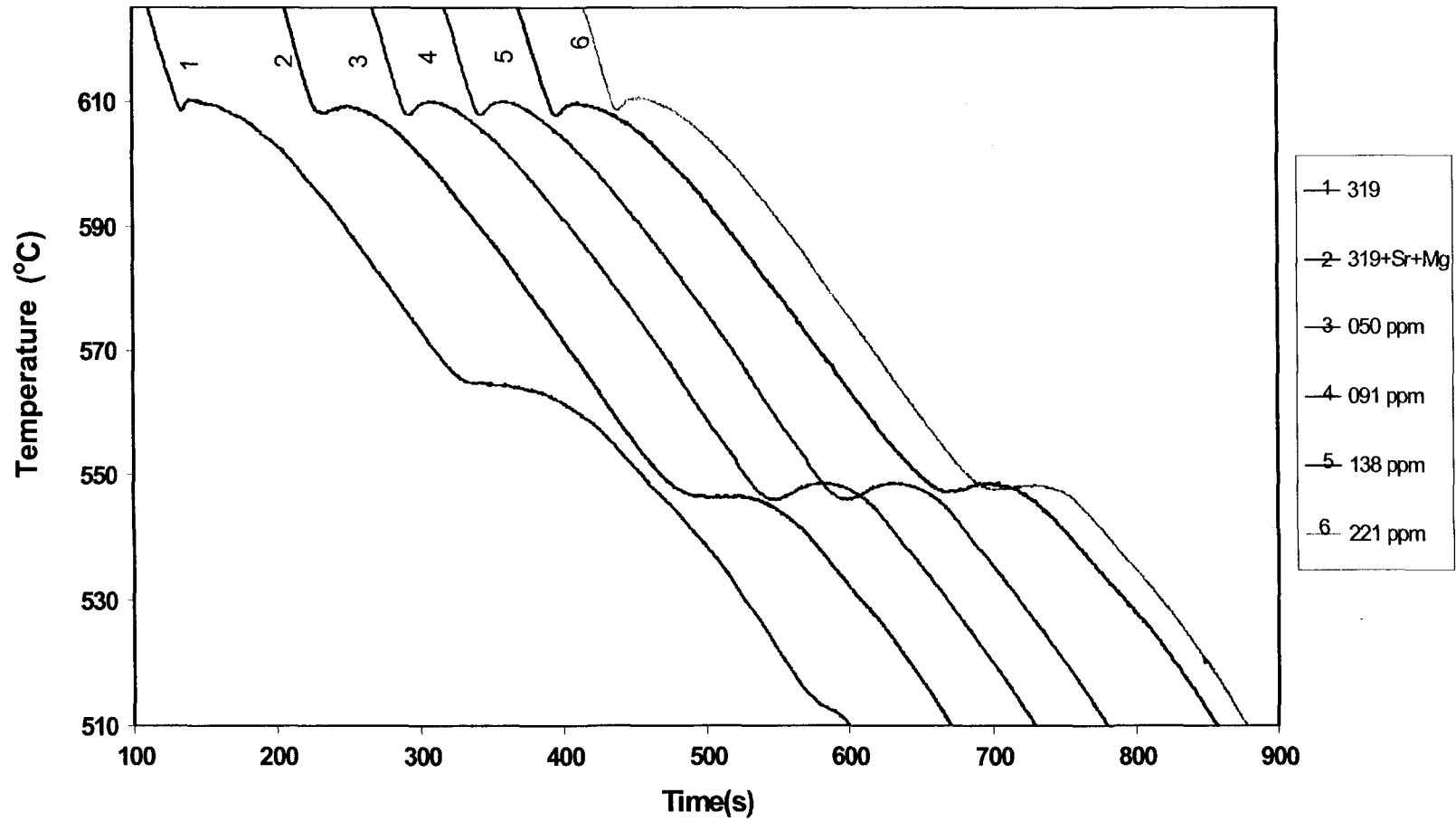


Figure 34. Cooling curves obtained for C alloys containing various amounts of Ca.

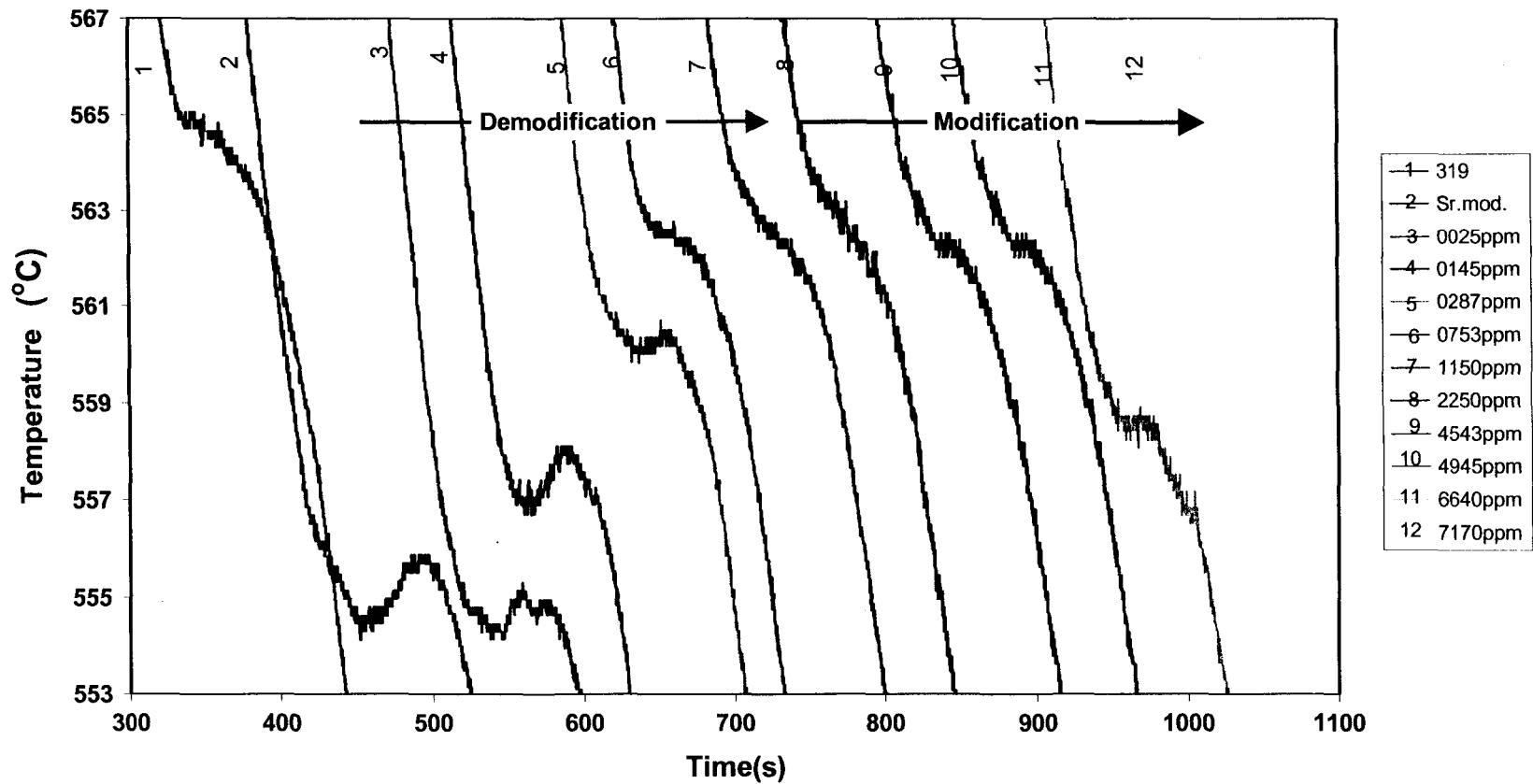


Figure 35. The effect of Bi addition on eutectic undercooling in B alloys.

3.3.2 IMAGE ANALYSIS: Si PARTICLE CHARACTERISTICS

The effect of trace additions of Bi and Ca on the Si particle characteristics was evaluated by examining the corresponding metallography samples using an image analyzer in conjunction with an optical microscope. Figure 36 through 39 show the variations in the Si particle characteristics (*viz.*, average particle length, area, roundness and density) as a function of the added amounts of Bi. As can be seen, the addition of Bi to the Sr-modified 319 alloy (group B) counteracts the modification effect of Sr, leading to a noticeable coarsening of the Si crystals. The Si particle size increases gradually with an increase in Bi addition up to 3000 ppm. At this level, the Si particle parameters are approximately comparable to those of the base 319 alloys. At higher Bi concentrations, the modification effect of Bi appears in the partial refinement of the Si particles, which can be seen from the decrease in the Si particle length and area, with a corresponding increase in the particle roundness and density.

For the Mg-added alloys (C alloy), the Si particle measurements followed more or less the same trend observed in the Sr-modified B alloys, Figures 36 to 39. The Si average particle area and length values of the base C alloy are relatively higher than those reported for the B alloy, due to the interaction between Mg and Sr.

It was reported by Joenoes and Gruzleski⁶³ that Mg reacts with Sr to form the complex $Mg_2Sr(Si_3Al_4)$ intermetallic, resulting in a significant reduction in the amount of Sr available for Si modification. With the addition of Bi, the Si particle area and length increase gradually up to ~5500 ppm Bi, and then decrease with further Bi addition. These

results are in good agreement with those of Kurdyumov *et al.*¹¹ on the effect of trace elements on Na- and Sr-modified Al-Si-Mn alloy.

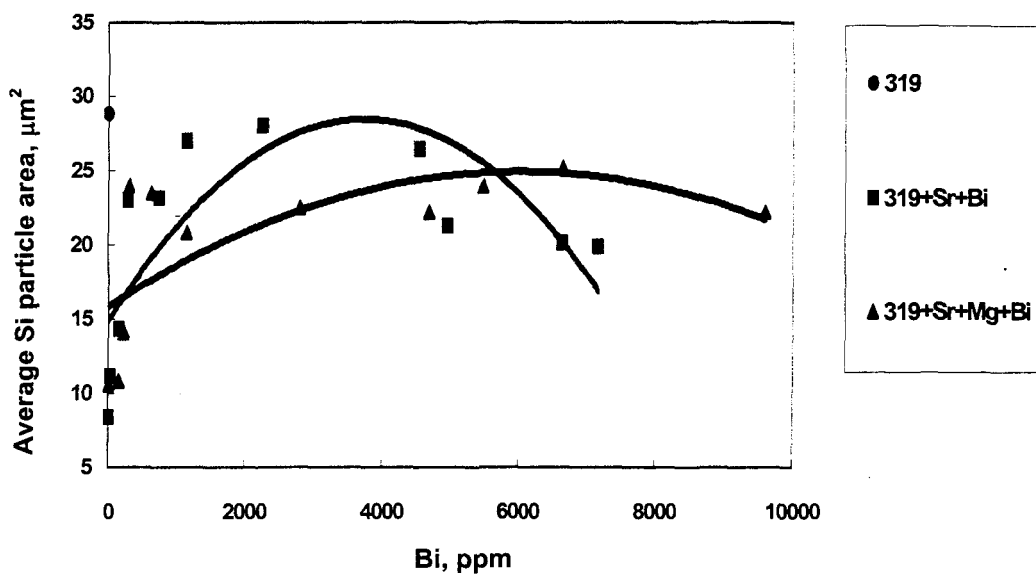


Figure 36. Average Si particle area as a function of Bi content in B and C alloys.

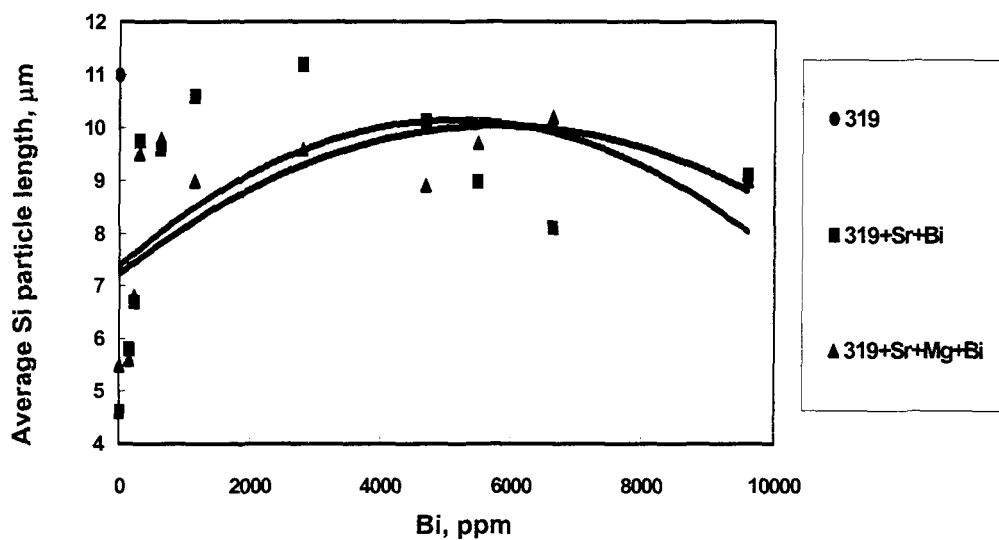


Figure 37. Average Si particle length as a function of Bi content in B and C alloys.

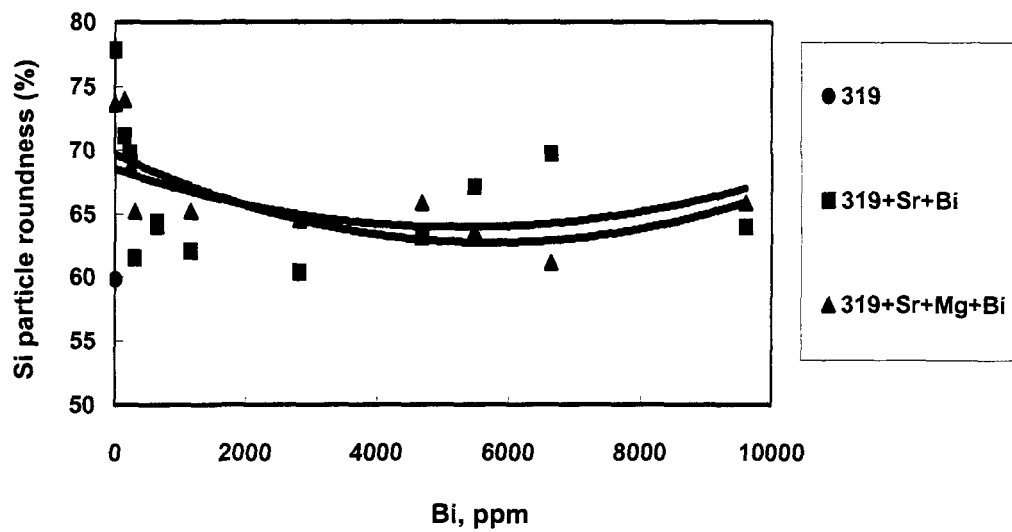


Figure 38. Average Si particle roundness as a function of Bi content in B and C alloys.

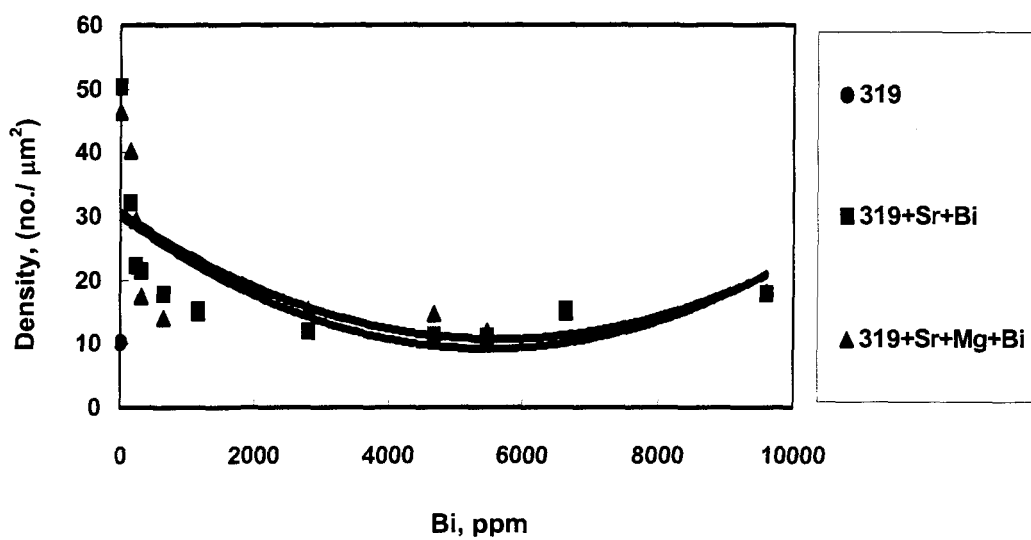


Figure 39. Average Si particle density as a function of Bi content.

Figures 40 to 43 reveal that Ca has a slight effect on the Si particle characteristics. The average Si particle area and length increase almost linearly with the increase in Ca concentration, with a corresponding decrease in the particle roundness and density. This behavior is independent of the alloy composition, *i.e.* B or C alloy. The trend, however, is more pronounced in the B, than in the C alloy due to the formation of Al-Ca-Sr intermetallics in the former. As Mg is not part of this intermetallic, its presence in the C alloy will enhance the modification of the Si particles, in spite of the formation of $Mg_2Sr(Si_3Al_4)$. Thus, the net amount of modification will depend on the amount of free Sr available in the alloy matrix.

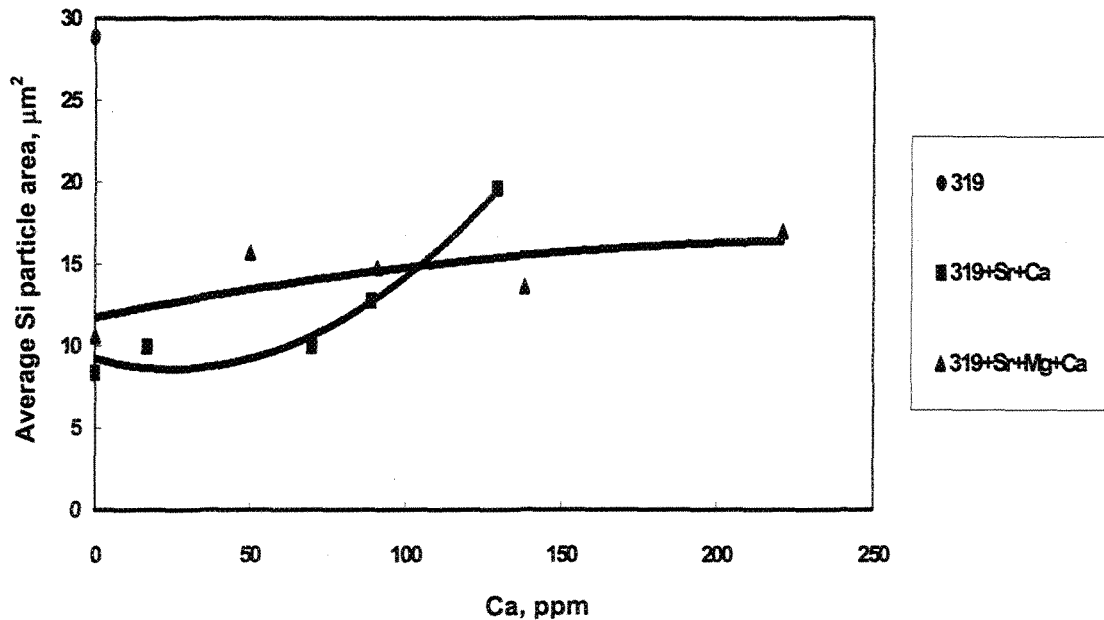


Figure 40. Average Si particle area as a function of Ca content in B and C alloys.

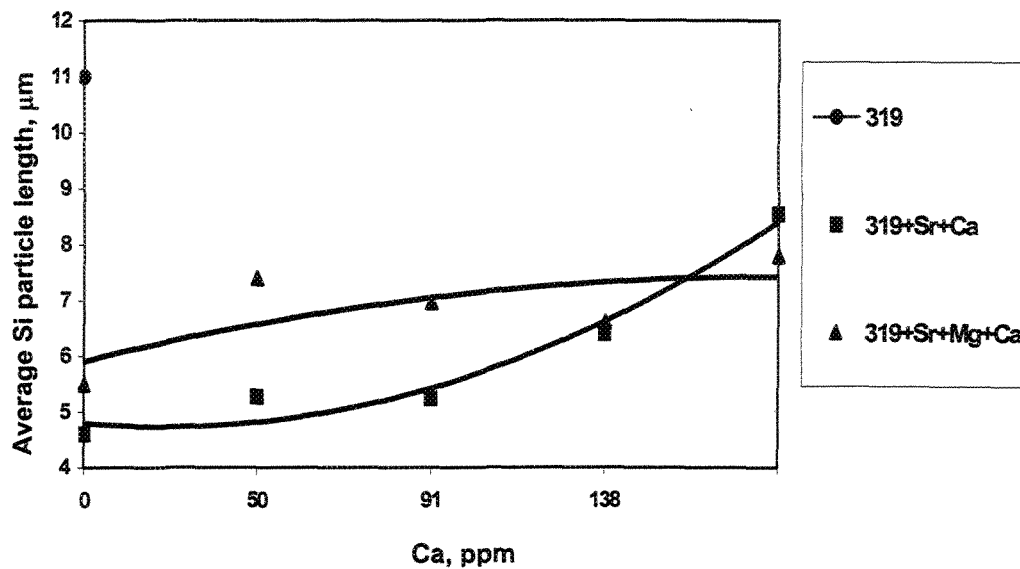


Figure 41. Average Si particle length as a function of Ca content in B and C alloys.

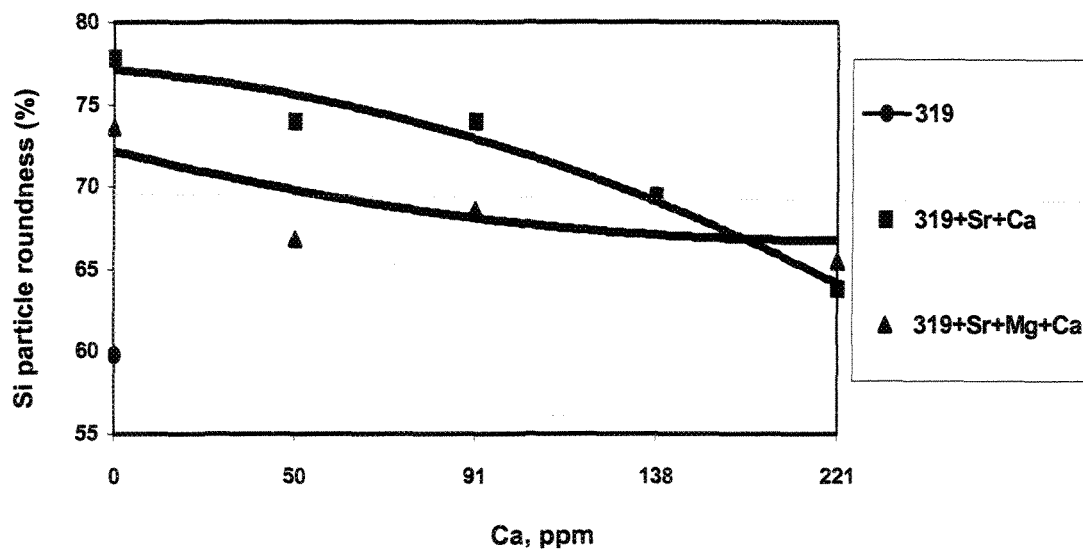


Figure 42. Average Si particle roundness as a function of Ca content in B and C alloys.

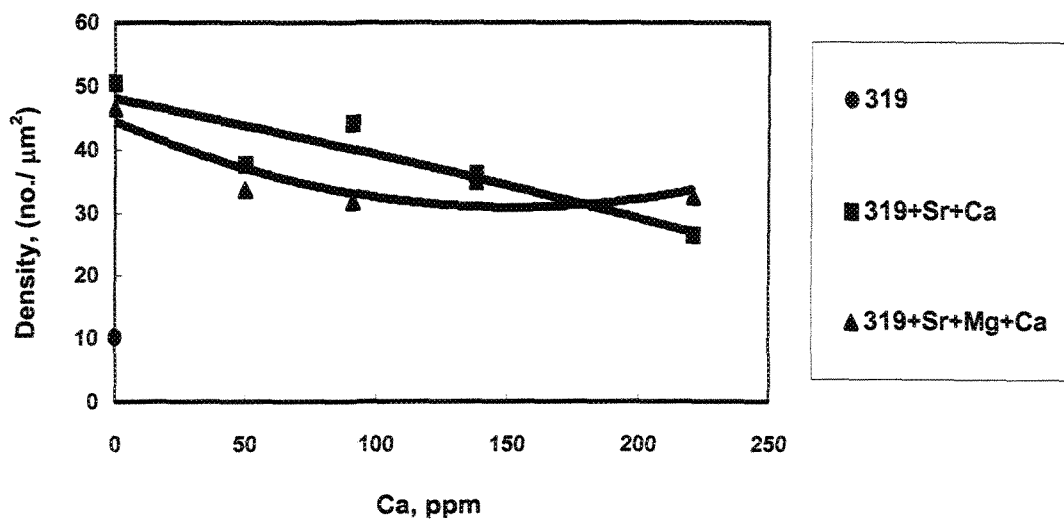


Figure 43. Average Si particle density as a function of Ca content in B and C alloys.

3.3.3 MICROSTRUCTURAL ANALYSIS

3.3.3.1 OPTICAL MICROSCOPY

Figure 44(a) shows the microstructure obtained for base 319 alloys (A alloy) in the as-cast condition, displaying a eutectic structure typical of an unmodified alloy. With the addition of 80 ppm Sr, to the B alloy, the morphology of the Si particles changed into fibrous form, indicating full modification of the eutectic structure, Figure 44(b). The C alloy (containing ~0.4 wt % Mg) exhibited lamellar and Chinese script-like Si particles, Figure 44(c) compared to the fibrous form obtained for the B alloy.

The addition of Bi in amounts up to 287 ppm to the B alloy resulted in the coarsening of the Si particles, *i.e.*, in a partially modified structure. When the amount of Bi exceeded 1150 ppm, the Sr modification was completely annulled, Figure 45(a) which is in

good agreement with the results obtained by Chow *et al.*⁸ Similar results were obtained for the C alloy also, in that the structure appeared unmodified for Bi levels up to ~1152 ppm, Figure 45(b).

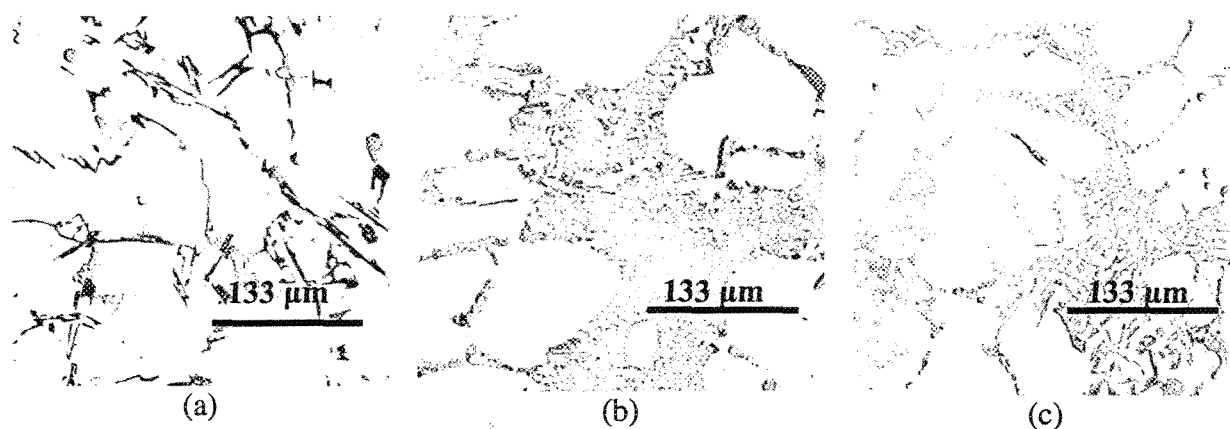


Figure 44. Eutectic Si structure obtained in (a) A, and (b) B, and (c) C alloys.

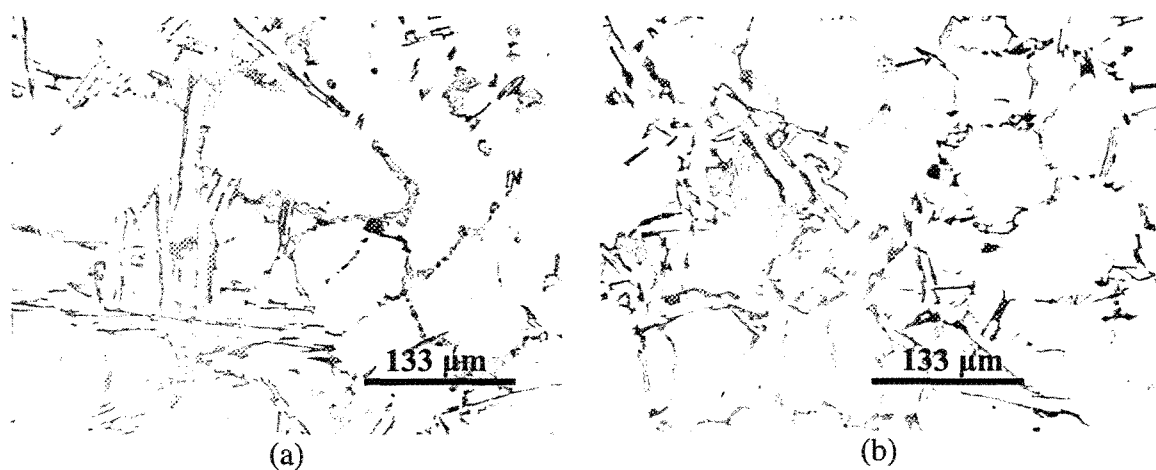


Figure 45. Eutectic Si structure obtained in (a) BBE alloy (B + 1151 ppm Bi), and (b) CBE alloy (C + 1152 ppm Bi).

The degradation of Sr modification in the presence of Bi may be interpreted in terms of a Bi-Sr interaction in the B alloy or a Bi-Mg-Sr interaction in the C alloy. As mentioned previously, the addition of an excessive amount of Bi for the same level of Sr (~80 ppm) leads to partial modification by Bi, regardless of the alloy composition.

Similar to the case of Bi addition to B alloy, Ca (~129 ppm) is found to markedly reduce the modification effect of Sr, resulting in coarse acicular Si particles, as exemplified in Figure 46(a). The higher magnification micrograph of Figure 46(b) corresponding to the Mg-containing C alloy, clearly shows the presence of a large plate-like Ca containing particle (arrowed). At its centre, a black spot can be observed, analyzed as being an AlP particle, which acts as a nucleation site for the Ca-containing phase. As can be seen, the eutectic Si particles surrounding the Ca-containing particle are acicular due to the concentration of Sr in the latter, and thus a depletion of Sr in the vicinity.

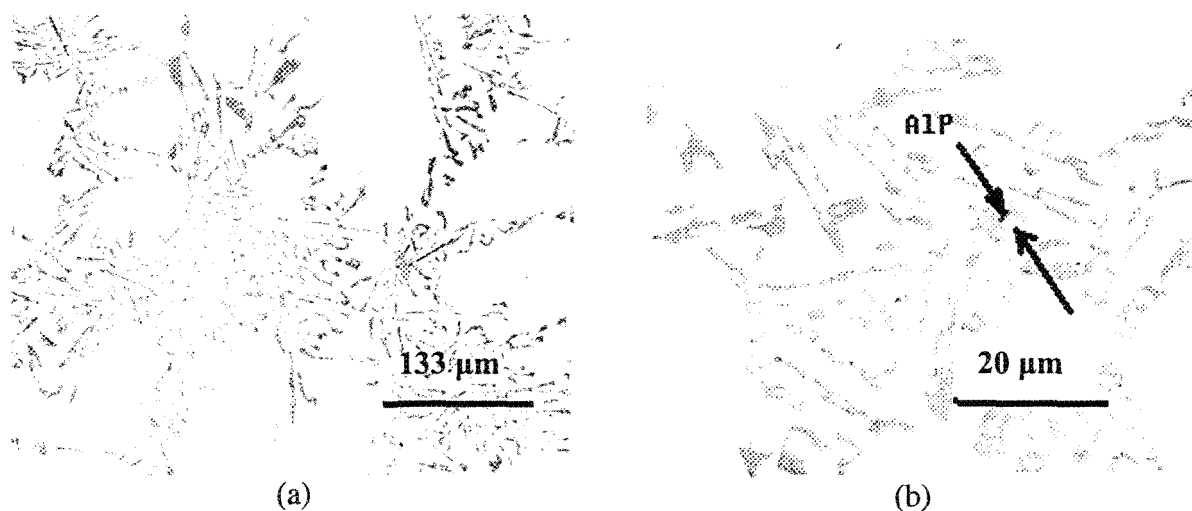


Figure 46. Eutectic Si structure obtained in (a) BCD alloy (B + 129 ppm Ca), and (b) CCD alloy (C + 221 ppm Ca).

3.3.4 ELECTRON PROBE MICROANALYSIS

3.3.4.1 EFFECT OF BI ADDITION

Figure 47 shows the distribution of the Bi containing phase, precipitated in the form of fine dispersed particles throughout the matrix taken from the 319 alloy (containing ~0.4 wt% Mg + 300 ppm Sr + 9000 ppm Bi) sample. Due to the high atomic weight of Bi, it is detected easily.

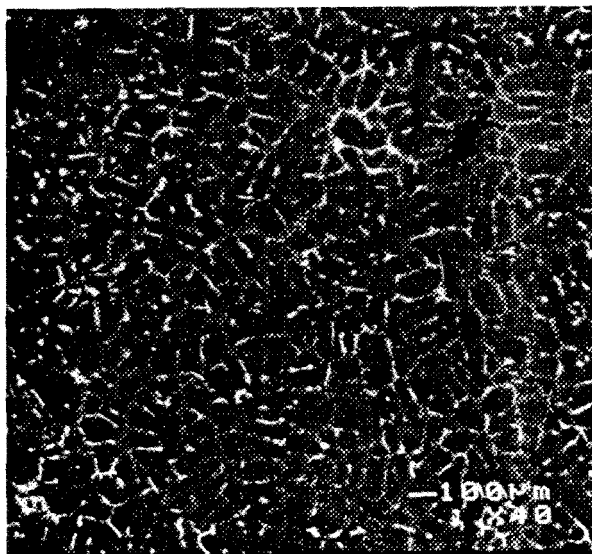


Figure 47. Bi distribution in (319+300 Sr+9000 ppm Bi) alloy.

Figure 48(a) is a high magnification back-scattered image for the CBJ alloy (C alloy + 9600 ppm Bi) showing the morphology of the Bi-containing particle. It was found that Bi precipitated in the form of oxide particles with irregular form. Due to its high oxygen content, Figure 48(d), it was difficult to establish the stoichiometric composition of this oxide phase. Table 4 lists the approximate concentrations of the main elements that were

detected in the bismuth oxide. It is interesting to note that in the C alloy (containing ~0.4 wt% Mg), Mg represents a major constituent of the Bi phase, as evident from Figure 48(c). These results were confirmed by the associated EDX analysis, Figure 49, displaying strong Bi and Mg reflections accompanied by an oxygen profile across the Bi-containing particle.

In the CBE (C alloy + 1152 ppm Bi) sample, the Sr was revealed to be more concentrated in the Bi-containing particle than in the surrounding matrix, as shown in Figure 50 and Table 9.

The EDX spectrum for the 319 alloy (containing ~0.4 wt% Mg + 300 ppm Sr + 9000 ppm Bi) sample, Figure 51, exhibited a clear Sr peak that overlapped with the Si reflection, due to the proximity of their $L\alpha$ and $K\alpha$ lines, respectively⁶⁴.

It should be pointed out here that, although images of the Ca-Bi interaction have been presented in the literature, no mention of the presence of oxygen was made.⁶⁵ The oxygen observed in the present work can be explained in terms of the high oxygen affinity of Bi, especially at high temperatures such as 750°C. It should be borne in mind that ΔH (the enthalpy of formation) for Bi_2O_3 is about -137.9 kcal compared to -143.84 kcal for the formation of MgO.⁶⁶

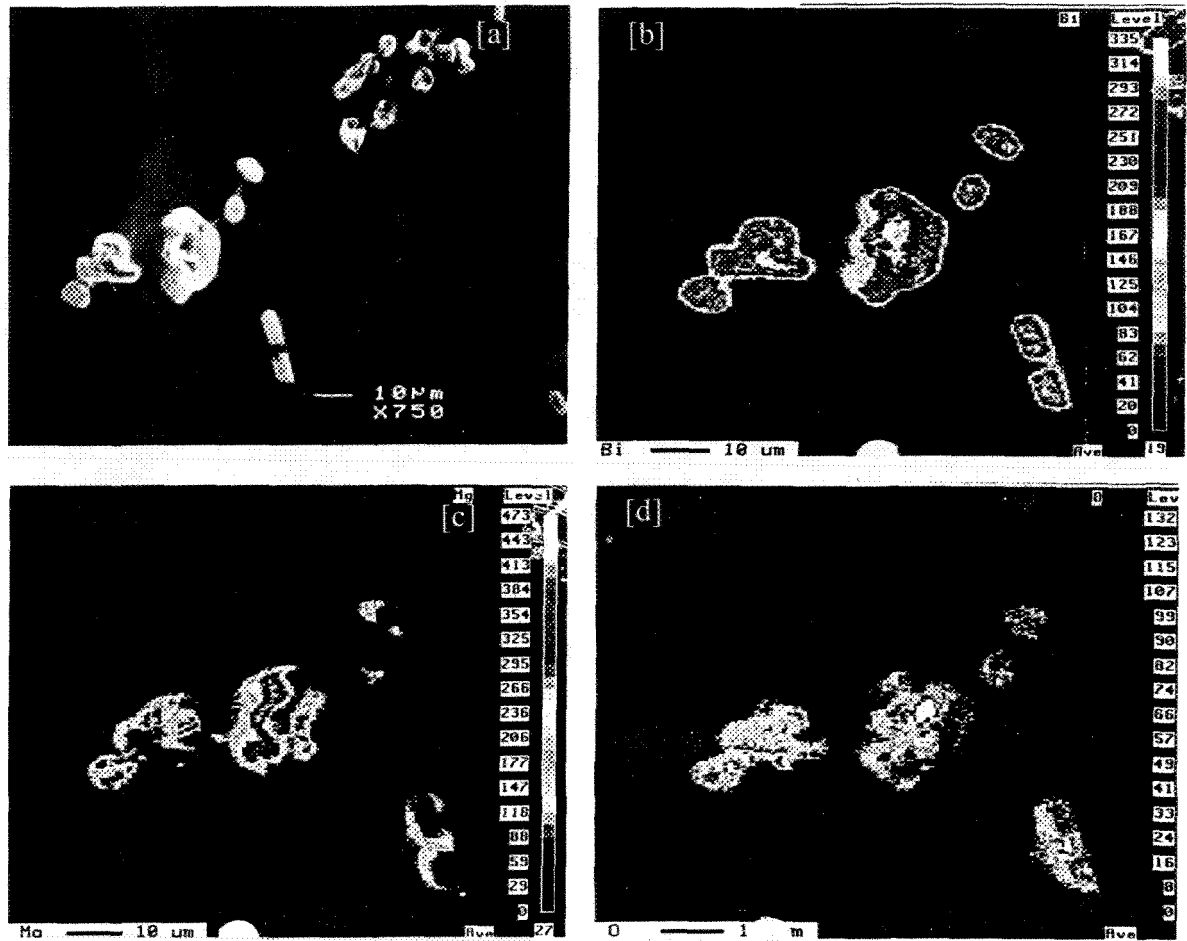


Figure 48. SEM micrographs obtained from CBJ alloy (C + 9600 ppm Bi)
 a) SEM micrograph;
 b) Bi image of (Mg,Bi) oxide particles;
 c) Mg image of (Mg,Bi) oxide particles;
 d) O image of (Mg,Bi) oxide particles.

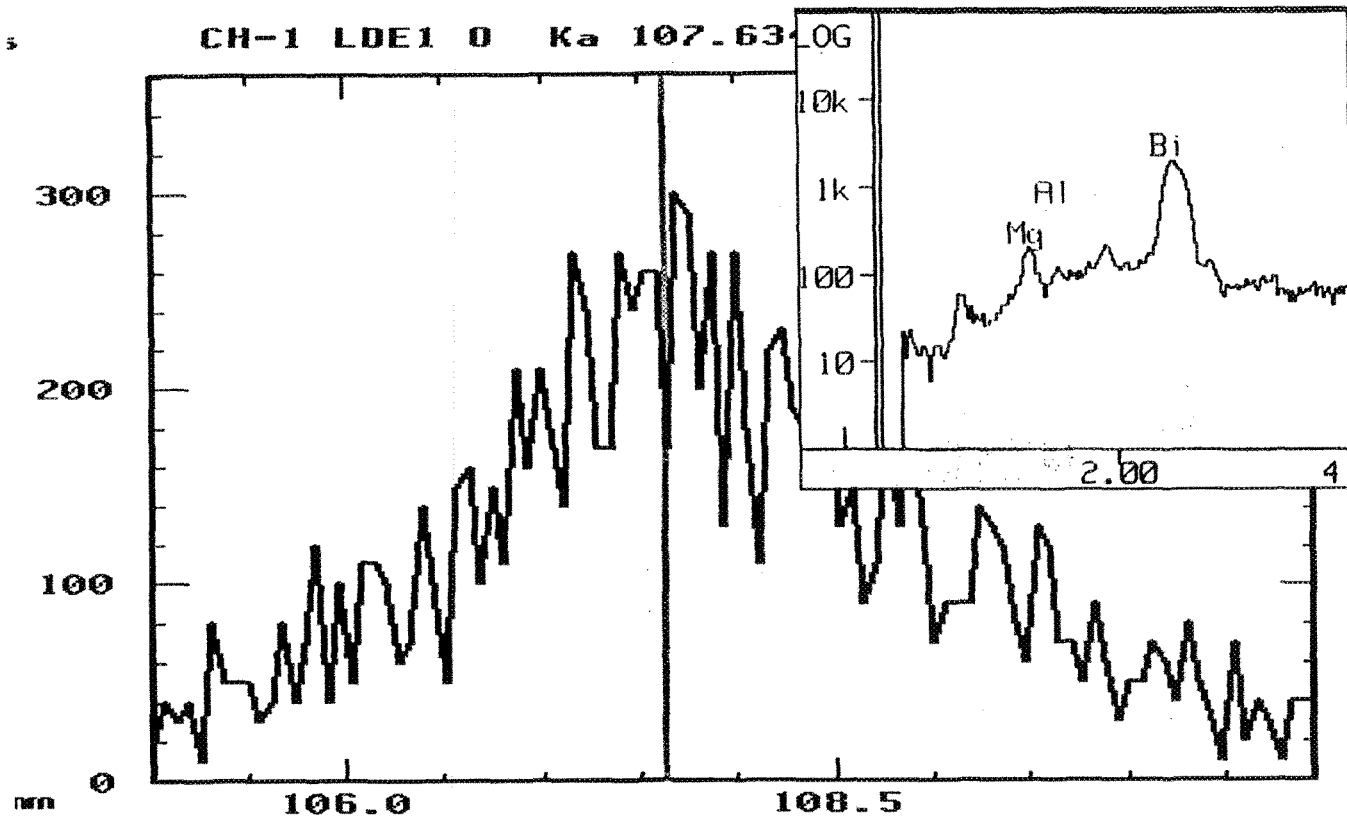


Figure 49. EDX spectrum and oxygen scan corresponding to Mg-Bi-O particles observed in the CBJ alloy samples (C alloy + 9600 ppm Bi).

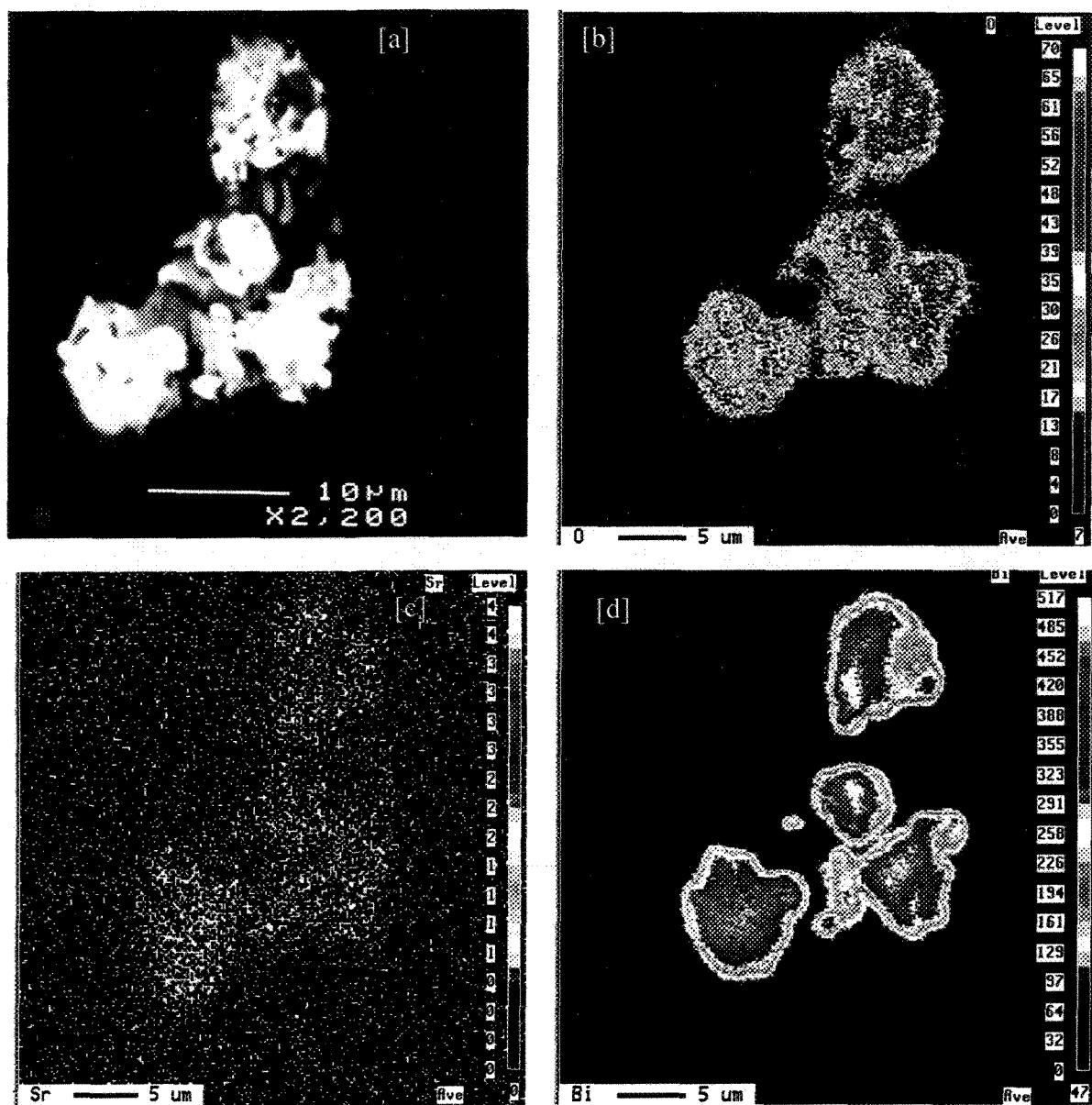


Figure 50. a) Backscattered image, and X-ray images of b) O, c) Sr, and d) Bi taken from CBE alloy sample (C alloy + 1152 ppm Bi).

Table 9 Approximate composition (at%) of bismuth oxide particles observed in CBE alloy sample (C alloy + 1152 ppm Bi)

Alloy Code	Element	At%	Suggested oxides
CBJ (C alloy + 9600 ppm Bi) Spot taken from the particle	Al	3.0	(Mg,Bi,Sr) oxides
	Si	0.27	
	Mg	13	
	Bi	29.2	
	Sr	0.016	
	O	53.3	
CBE (C alloy +1152 ppm Bi) Spot taken from the particle	Al	4.58	(Mg,Bi,Sr) oxides
	Si	2.7	
	Mg	15.16	
	Bi	20.2	
	Sr	0.16	
	O	55.45	

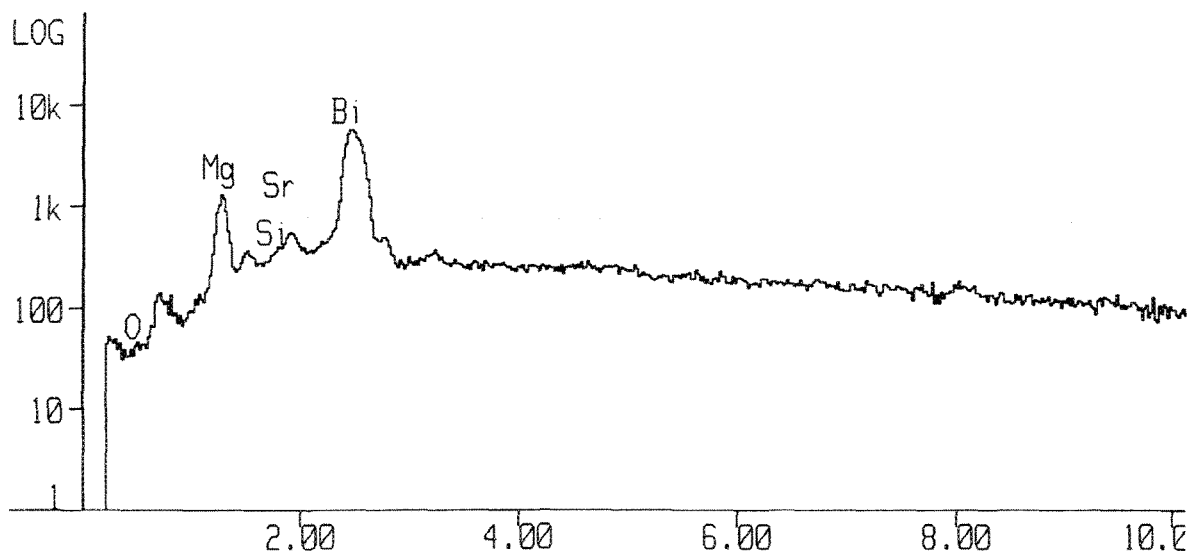


Figure 51. EDX spectrum corresponding to a Mg-Sr-Bi-O particle observed in 319 alloy containing (0.4 % Mg + 300 ppm Sr + 9000 ppm Bi).

3.3.4.2 EFFECT OF CA ADDITION

Figure 52(a) displays the morphology of the Ca-containing phase precipitated in B alloy containing 129 ppm Ca. It was found that the Ca precipitated in the form of short, gray rods, as inferred from Figure 52(b), which was taken from a pore observed on the sample surface. The distribution of elements within the rods is given in Figure 53, it can be seen that Sr constitutes a major element of these rod-like particles. The exact chemical analysis of this phase is provided in Table 10, suggesting an approximate composition of $\text{Al}_7(\text{Ca}, \text{Sr})\text{Si}_7$.

The corresponding EDX spectrum, Figure 54, reveals strong Al, Si, and Ca reflections. For Al, Si, and Ca, as mentioned previously, the lines for Si and Sr always appear overlapped. The presence of the small Cu peak in Figure 54 is probably due to the precipitation of Al_2Cu on the edge of the Ca-containing rod-like particle.

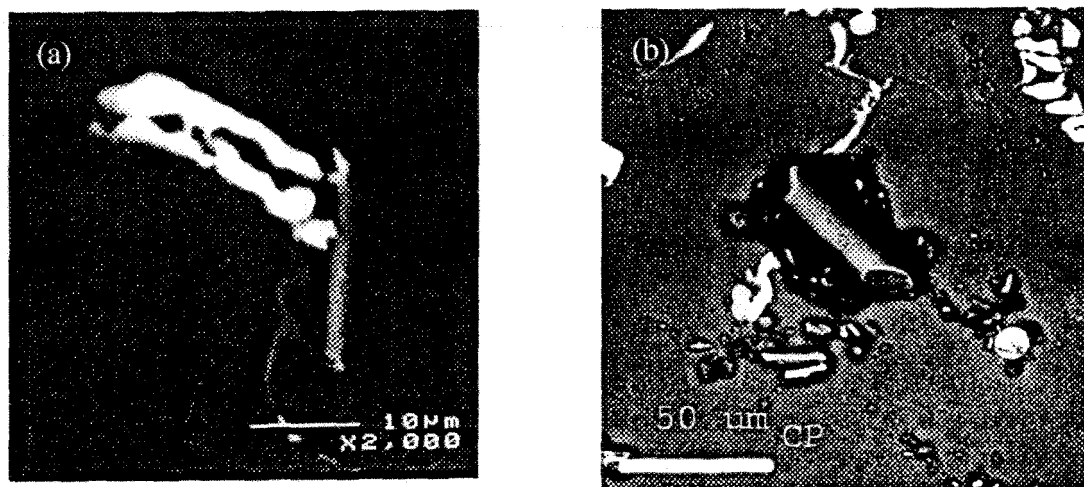


Figure 52. Backscattered images taken from BCD alloy (B + 129 ppm Ca) showing the morphology of the rod-type Ca-containing particle a) plane view, and b) inside a pore

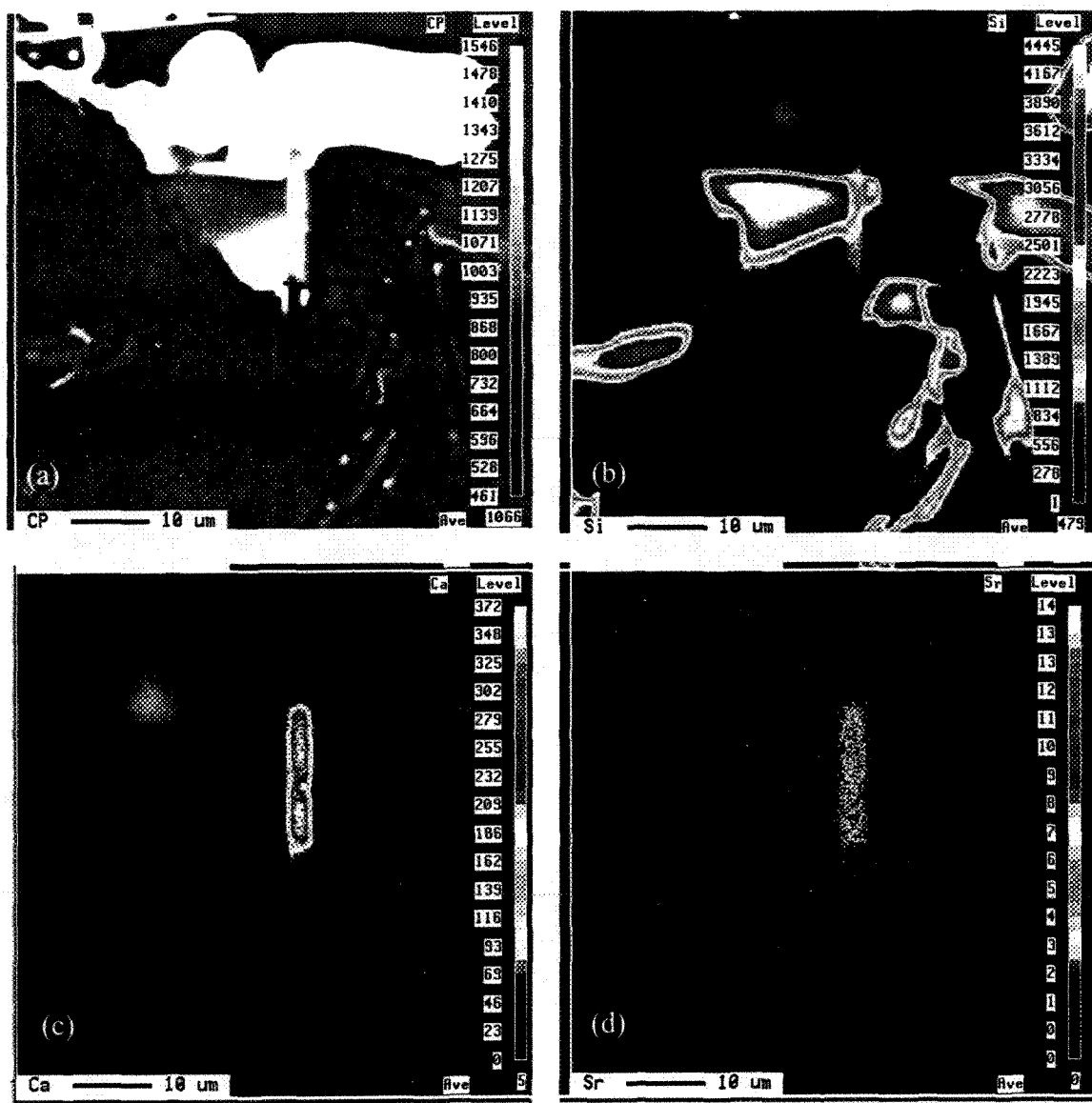


Figure 53. (a) Backscattered image, and X-ray images of (b) Si, (c) Ca, and (d) Sr in the rod-type Ca-containing particle observed in BCD alloy (B + 129 ppm Ca).

Table 10 Chemical composition of the examined Ca-containing phase particles obtained from WDS analysis

Alloy Code	Element	Wt%	At%	Shape	Suggested Composition
BCD (B + 129 ppm Ca).	Al	40.5	44.9	Rod type	$Al_7(Ca, Sr) Si_7$
	Si	38.6	41.2		
	Ca	14.95	11.174		
	Sr	4.71	1.61		
CCD (C+ 221 ppm Ca) (Analysed area-spot 1*)	Al	33.6	39.8	Plate type	$Al_2(Ca, Sr) Si_2$
	Si	34.9	39.7		
	Ca	21.83	17.417		
	Sr	6.46	2.35		
CCD (C+ 221 ppm Ca) (Analysed area-spot 2*)	Al	30.22	22.24		AIP Al_2O_3 Al_2MgO_4
	Si	23.47	16.6		
	Ca	17.17	8.5		
	Sr	4.47	1.01		
	Mg	4.07	3.33		
	P	3.23	2.07		
O	37.16	46.122			

*Spot positions are shown in Figure 55; ** Low value of Al due to the high O

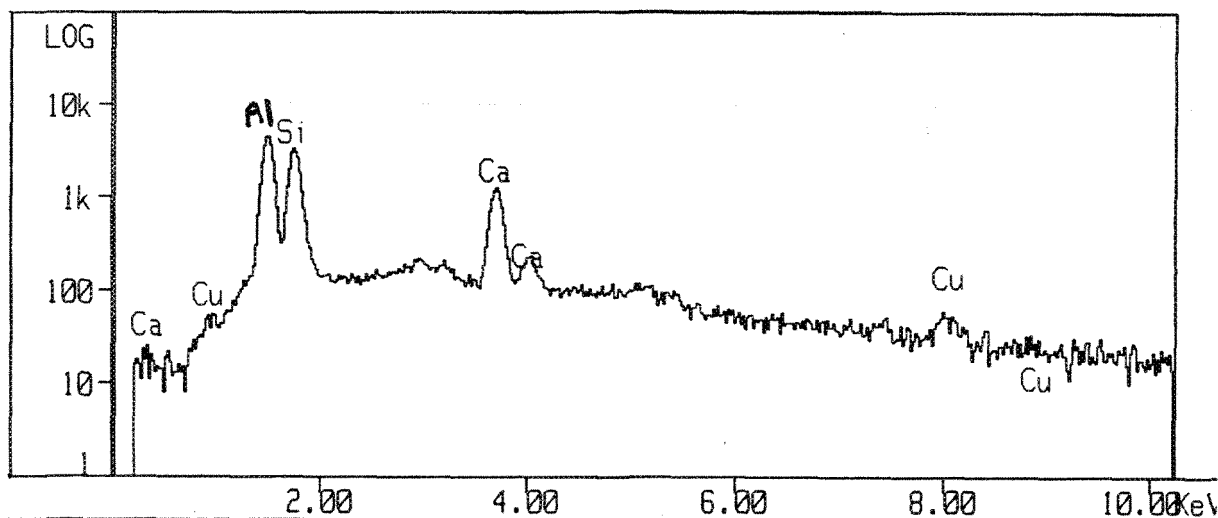


Figure 54. EDX spectrum showing the elements observed in the rod-type, BCD alloy (B alloy + 129 ppm Ca).

Figure 55 is the backscattered micrograph corresponding to the optical micrograph shown in Figure 46, taken from the CCD alloy (C alloy + 221 ppm Ca), and shows the morphology of the Ca-containing particle precipitated in the alloy. The particle is characterized by the presence of twinning surfaces²¹, as indicated by the black arrows.

At the particle centre, a mixture of AlP, Al₂O₃, and Al₂O₄Mg particles were observed (arrow-head, Figure 55). Thus, it could be reasonably presumed, based upon this, that these oxide particles and/or AlP would act as a nucleation site for the precipitation of the Ca-containing particle, followed by its growth through the formation of twinning planes.⁹ From the WDS analysis shown in Table 10, the chemical composition of this phase is suggested to be Al₂(Ca, Sr)Si₂.

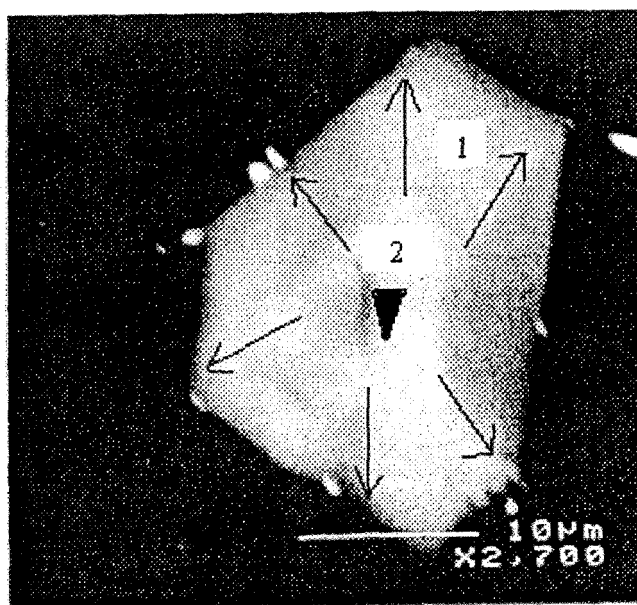


Figure 55. Backscattered image taken from the CCD alloy (C + 221 ppm Ca) showing growth through twinning in a plate-like Ca-containing phase particle, spot analysis of points 1 and 2 are given in Table 10.

The change in the morphology of the Ca-containing phase from rod type in the B alloy, to plate type in the C alloy, may be interpreted in terms of the depression in the Al-Si eutectic temperature of the alloy with the addition of Mg (*i.e.*, the C alloy). It is reasonable to assume that in the Al-Ca-Si system, the presence of Mg would displace the ternary eutectic temperature towards a lower Ca concentration. In this case, the Ca phase would precipitate in the form of primary crystals (*i.e.*, plate type) instead of rods. The confirmation of this hypothesis, however, is beyond the scope of the present work.

Figure 56 shows an example of the presence of magnesium oxide (MgO or Al_2O_4Mg) and AIP at the centre of a Ca plate-type particle. It should be noted that, although the second particle in Figure 56(a) does not reveal the presence of any impurities at its centre, the WDS analysis found traces of these oxides, suggesting that heterogeneous nucleation is the main nucleation mechanism for the precipitation of this phase. The element distribution within the Ca plate particle is best illustrated in Figure 57.

The line scans reveal the concentration gradients of Ca and Sr across the particle surface. In this case, the main nucleation impurity is the AIP. The corresponding EDX spectrum, Figure 58, displays strong reflections due to Al, Si, Sr, P, Mg, and Ca, which is consistent with the WDS analysis.

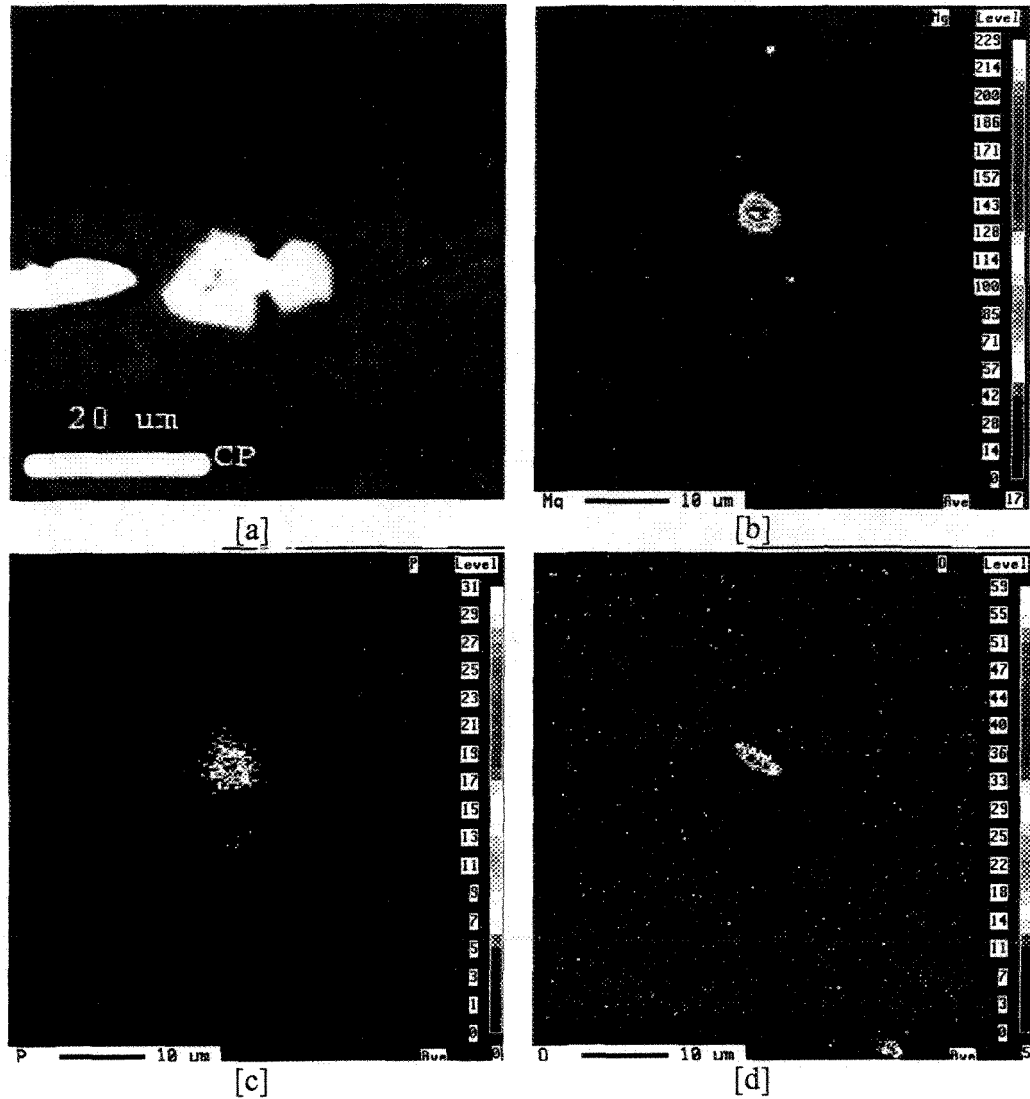


Figure 56 a) Backscattered image, and X-ray images of b) Mg, c) P, and d) O elements in the plate-type Ca-containing phase particle observed in CCD alloy (C alloy containing 221 ppm Ca).

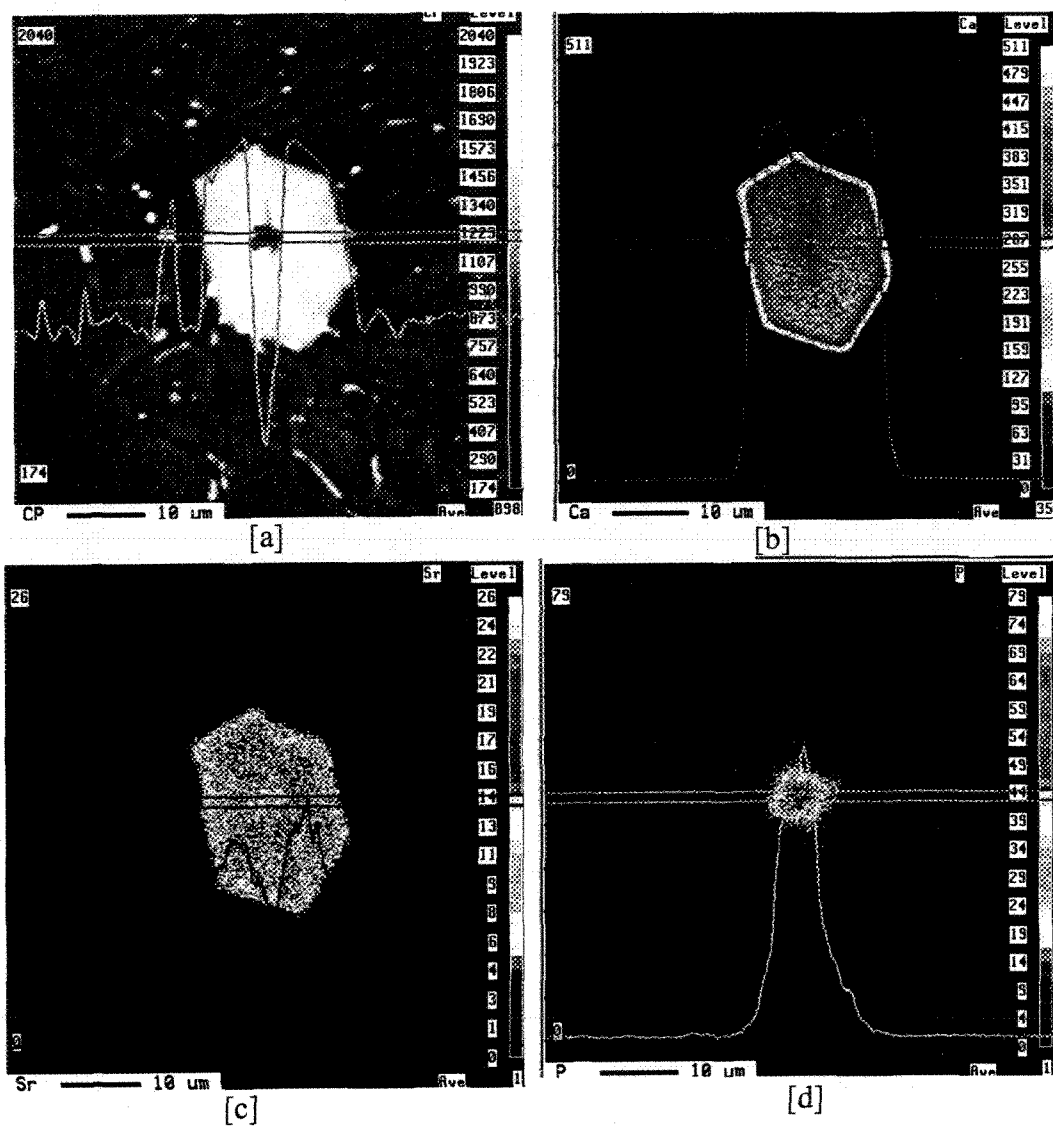


Figure 57. a) Backscattered image showing a plate type Ca-containing phase particle in CCD alloy, and images of b) Ca, c) Sr, and d) P elements across the particle. Line scans taken across the image are superimposed in each case.

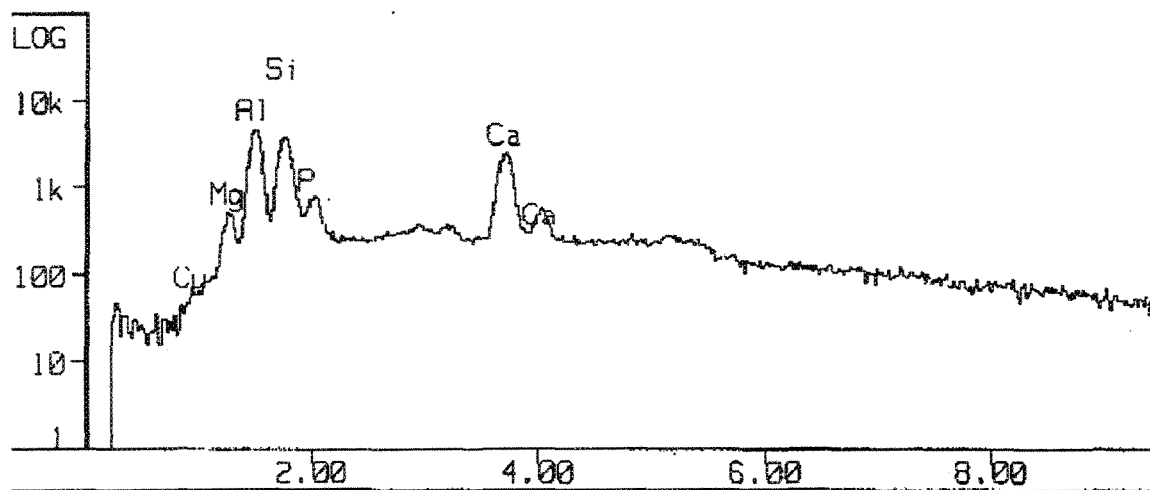


Figure 58. EDX spectrum taken from the plate-type Ca-containing phase particle in CCD alloy showing Al, Si, Sr, P, and Mg reflections.

CHAPTER 4

EFFECT OF Bi AND Ca ADDITIONS ON POROSITY AND EUTECTIC Si PARTICLE CHARACTERISTICS IN Sr-MODIFIED 319 ALLOYS UNDER VARIABLE COOLING CONDITIONS

CHAPTER 4

EFFECT OF Bi AND Ca ADDITIONS ON POROSITY AND EUTECTIC Si PARTICLE CHARACTERISTICS IN Sr-MODIFIED 319 ALLOYS UNDER VARIABLE COOLING CONDITIONS

4.1 INTRODUCTION

Microporosity is invariably found in most aluminum alloy castings. This kind of porosity is a consequence of the influence of several strongly interacting alloy and process parameters that determine the amount and nature of porosity that will occur in a casting.^{67,68}

As such porosity is known to significantly influence the mechanical properties, it becomes essential to quantify microporosity formation as a function of these parameters, particularly in the case of castings used in critical structure applications, where it is important to be able to predict the occurrence of porosity with reasonable accuracy.⁶⁹

In the present study, one of the parameters to consider would obviously be the effect of the bismuth and calcium additions on the porosity formed in the alloy casting. As the solidification conditions also affect the resultant porosity, a variable angle wedge mold was used in this part of the study where, by using thermocouples attached at different positions in the mold, solidification parameters could also be determined by conducting thermal analysis experiments.

In addition to studying porosity formation, the wedge mold used was also a good tool to investigate the effect of Bi and Ca additions on the formation of hot spots. The formation of such casting defects was frequently observed in the small wedge mold castings, on account of the thin sections produced with the 0° angle mold configuration.

Certain shapes, because of their influence on heat extraction during solidification, are likely to cause shrinkage cavities. Whenever solidification is delayed at a particular location, that section will exhibit such defects unless adequate feeding from the riser is ensured. Hot spots can occur in many different places, for example in bosses, pads and flanges - generally at locations where a thick section is joined to a thinner one. As thin sections are heated rapidly, they cannot extract as much heat as the surrounding areas. This effect of delaying freezing gives rise to the formation of shrinkage cavities.⁷⁰

In addition to porosity formation, the effect of the Bi and Ca additions on the eutectic Si particle characteristics under the variable cooling conditions provided by the wedge mold could also be investigated. Both aspects are covered in this chapter. The alloys, additives and melt treatment procedures used in this part of the study were the same as those described in Chapter 3.

4.2 EXPERIMENTAL PROCEDURE

The alloys were melted in a 7-kg capacity silicon carbide crucible using an electrical resistance furnace. The melting temperature was kept at $750 \pm 5^\circ\text{C}$. The melts were modified using strontium (~150 ppm), the Bi and Ca additions made similar to those

described in section 3.2.1. Table 11 gives the chemical compositions of the B and C alloys that were used to prepare the various Bi- and Ca-containing alloys listed in Table 12.

Table 11 Chemical compositions (wt%) of the two main alloys used

Alloy	Si	Cu	Fe	Mg	Mn	Ti	Zn	Sr
B	6.14	3.63	0.11	0.048	<0.0005	0.14	<0.0017	0.0152
C	6.16	3.48	0.10	0.635	<0.0015	0.15	<0.0017	0.0118

Table 12 Alloy codes for Bi- and Ca-containing alloys

Alloy code	Alloy used + addition
BB	B+ 0621 ppm Bi
BB1	B+ 1555 ppm Bi
BB2	B+ 2186 ppm Bi
BB4	B+ 3785 ppm Bi
BB6	B+ 6060 ppm Bi
CB	C+ 0464 ppm Bi
CB1	C+ 0874 ppm Bi
CB2	C+ 1034 ppm Bi
CB4	C+ 2264 ppm Bi
CB6	C+ 3020 ppm Bi
BC	B+ 0052 ppm Ca
BC2	B+ 0103 ppm Ca
BC5	B+ 0465 ppm Ca
CC	C+ 0063 ppm Ca
CC2	C+ 0094 ppm Ca
CC5	C+ 0486 ppm Ca

The melts were poured into a variable angle wedge mold (see section 4.2.1). The mold was variously adjusted to angles of 0, 5, 15 degrees, in order to incorporate the effect of different cooling conditions. Before pouring, the mold was inclined at 35° with respect to the vertical position and then tilted up during pouring to minimize turbulence effects.

Three pairs of thermocouples (chromel-alumel, type K) were each placed at positions corresponding to those from which samples from the casting were later sectioned for metallographic examination. The temperature-time data was obtained using a high-speed data acquisition system linked to a computer (at a rate of 0.02 sec). Samples for chemical analysis were taken simultaneously for each melt condition.

For metallographic examination, three samples were sectioned from each mold casting, corresponding to the three positions at which the thermocouple pairs were used to record the thermal data. The surface containing the thermocouple tip was polished in each case (1 μm diamond paste).

Porosity and eutectic Si particle measurements were carried out using an Olympus optical microscope, where a Leco 2001 image analyzer was used in conjunction with the microscope for quantification purposes. The measurements were carried out at 100X, over an appropriate number of fields such that the entire sample surface was traversed in a regular, systematic manner, and the corresponding measurements noted. Care was taken to avoid the outer edges of the sample to minimize cooling rate discrepancies between the sample edges and centre. For porosity measurements, the percentage porosity and the average pore length parameters were measured. In the case of the eutectic Si particle characteristics, the average Si particle area, length, and roundness, and the Si particle density were measured.

4.2.1 VARIABLE ANGLE WEDGE MOLD

An adjustable taper wedge mold⁶⁸ manufactured from mild steel was used in this part of our study. Figure 59 shows a schematic diagram of the mold. The inside of the mold was spray-coated with a thin layer of vermiculite. The mold is designed with tapered sidewalls, which increase in thickness towards the bottom. Such a design provides the mold with a higher heat extraction capability at the bottom and ensures directionality in the solidification of the casting. The mold can be opened at one end. One of the sidewalls can be rotated around its bottom axis to adjust the pitch. Angles of 0° , 5° and 15° were used in our experiments, which provided a wide range of solidification conditions. The casting molds corresponding to these three angles are termed *small*, *medium* and *large*, respectively. Thermocouples were positioned along the vertical centerline of the casting using holes drilled through the face of the mold. In our experiments, the thermocouples were located at 2.5, 4, 6.5, 7.5, 11.5 and 17.5 cm from the bottom of the mold (and not as shown in Figure 59). Temperature gradient and interface velocities were measured only in the vertical direction, though the wedge mold also exhibited temperature gradients in the horizontal direction. Due to the lack of directional solidification in the latter case, the horizontal interface velocity was not measured. Thus it should be kept in mind that the interface velocity discussed in subsequent sections always refers to that in the vertical direction.

4.2.2 THERMAL ANALYSIS

4.2.2.1 THERMAL GRADIENT

The thermal or temperature gradient was calculated at a particular thermocouple location as the temperature difference between that thermocouple and the thermocouple located above it in the casting, divided by the distance between them. The unit of the thermal gradient is $^{\circ}\text{K}/\text{cm}$ or $^{\circ}\text{C}/\text{cm}$. A positive thermal gradient is taken to mean that the uppermost thermocouple (of the six thermocouples used) is at a higher temperature than the lowest one. The temperature gradients at the liquid, eutectic or solid temperatures were thus the gradients ahead of the respective interface (into the liquid or partially liquid metal). Thermocouple failure resulted in the lack of data at certain positions for some samples. From successful runs, therefore, an average gradient corresponding to each thermocouple (sample) position was calculated and used in the data analysis.

4.2.2.2 INTERFACE VELOCITY

The velocity of the solid interface could be determined through a knowledge of the time t_1 at which the thermocouple in a location reached the solidus temperature. The time t_2 it took for the thermocouple immediately above to reach this temperature was also recorded. The distance between the two thermocouples divided by the $(t_2 - t_1)$ time interval gave the interface velocity in cm/s . An average solidus velocity was calculated for each sample in the same way the average temperature gradient was calculated. The effect of additions on the velocity of the interface was also studied.

4.3 RESULTS AND DISCUSSION

The techniques of thermal-, image-, and electron probe microanalysis were used in this part of our study. Cooling curves were plotted and the thermal gradients and interface velocities calculated from the thermal analysis experiments. Si particle characteristics and porosity measurement data were obtained using image analysis. Electron probe microanalysis was used to identify the morphologies and chemical compositions of the different phases. The data obtained from these various measurements is discussed in the following sections.

4.3.1 THERMAL ANALYSIS

4.3.1.1 EUTECTIC TEMPERATURE

Figure 60 shows the temperature-time cooling curves obtained for the large mold (mold angle 15°) for (a) B (Sr-modified), and (b) C (Mg-added) alloys at the different thermocouple positions denoted 1 through 6.

The effect of Bi addition on the Al-Si eutectic temperature is clearly evidenced in the remarkable increase in the eutectic temperature in the Sr-modified alloy at about 2000 ppm Bi addition, as shown in Figure 61, compared with that observed in Figure 60(a) for the B alloy. These results confirm those obtained in the first part of the study carried out with the graphite mold.

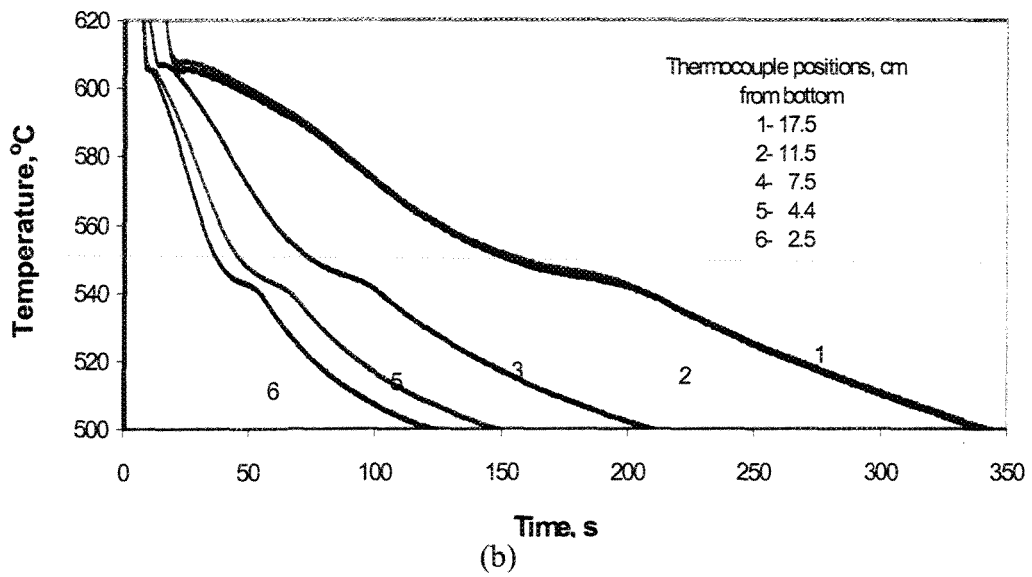
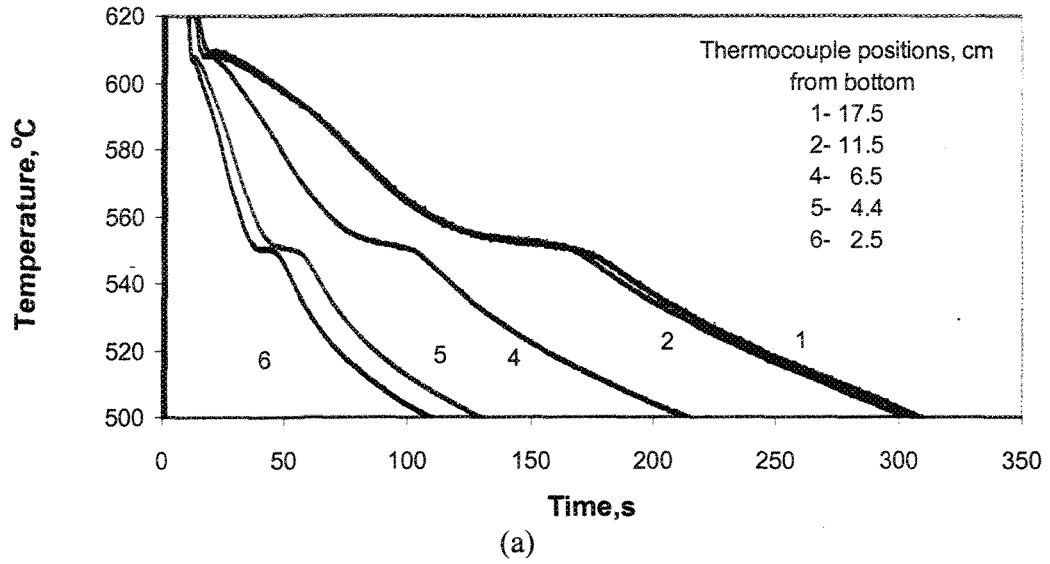


Figure 60. Cooling curves obtained for (a) B alloy, (b) C alloy, large mold (15° angle).

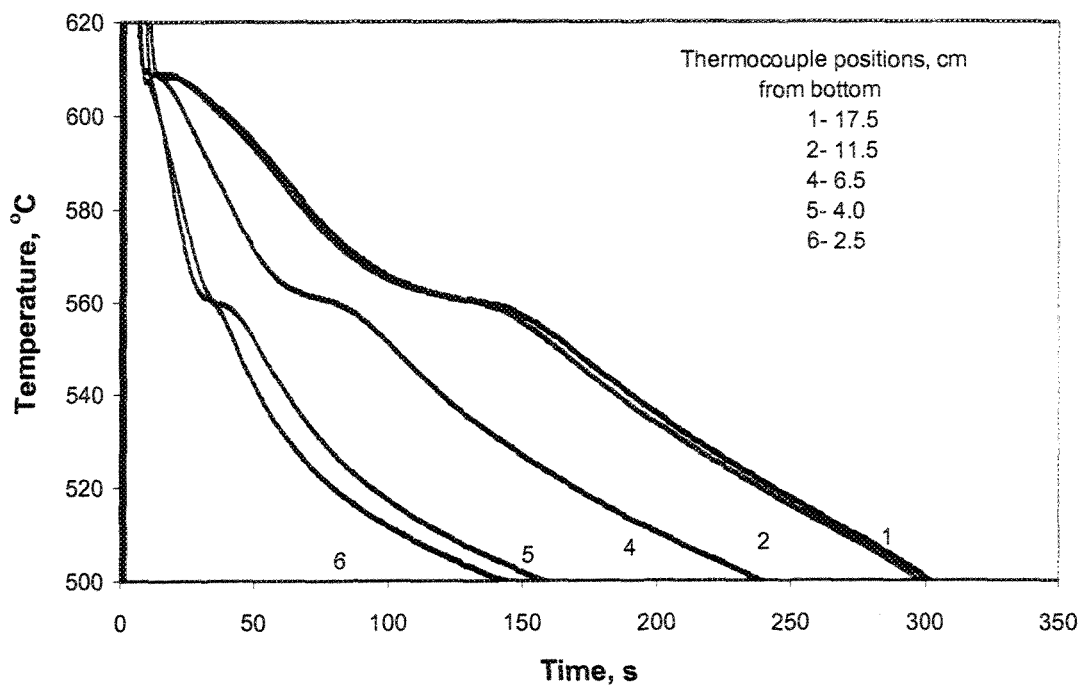


Figure 61. Cooling curves obtained for BB2 alloy (B alloy + 2186 ppm Bi, large mold).

An example of the effect of Ca addition on the Al-Si eutectic temperature of C alloy is shown by the cooling curves of Figure 62 for CC2 alloy (C alloy + 94 ppm Ca). Comparing Figure 62 with Figure 60(b) for C alloy reveals that Ca does not noticeably affect the eutectic temperature of the C alloy, as discussed previously in section 3.3.1 in the case of the graphite mold castings.

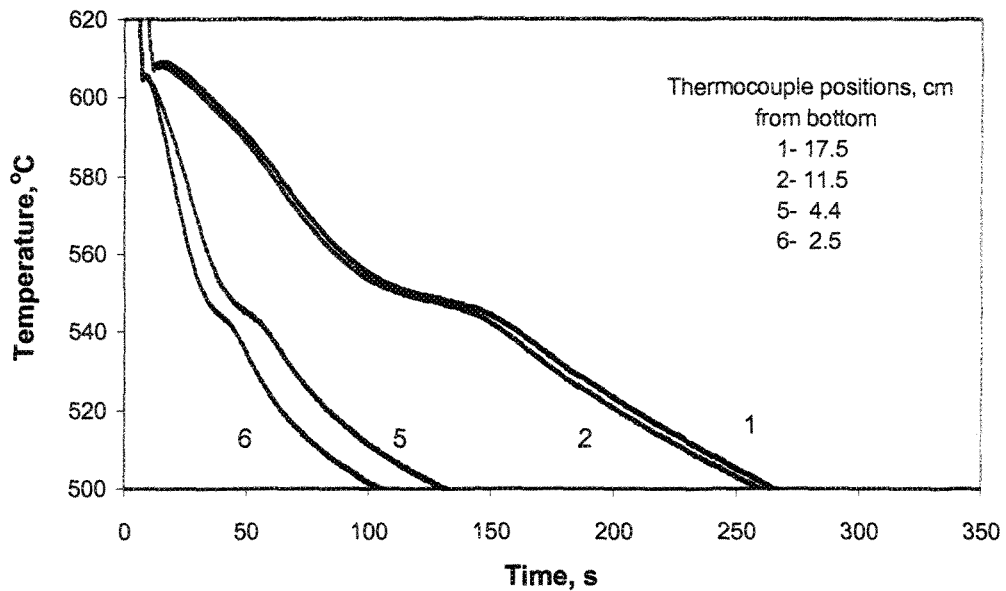


Figure 62. Cooling curves obtained for CC2 alloy (C alloy + 94 ppm Ca, large mold).

4.3.1.2 TEMPERATURE GRADIENTS AND INTERFACE VELOCITIES

The average vertical temperature gradients at solidus temperature, as a function of the distance from the bottom of the mold were plotted for the different alloy compositions. The simultaneous comparison of temperature, local temperature gradient and cooling rate, using graphs of the type shown in Figure 63, facilitated the recognition of specific temperatures. As described previously in section 4.2.2.1, a positive thermal gradient corresponded to the case when the uppermost thermocouple (T1) of the six thermocouples used registered a higher temperature than the lowest one (T6), with respect to the bottom of the mold.

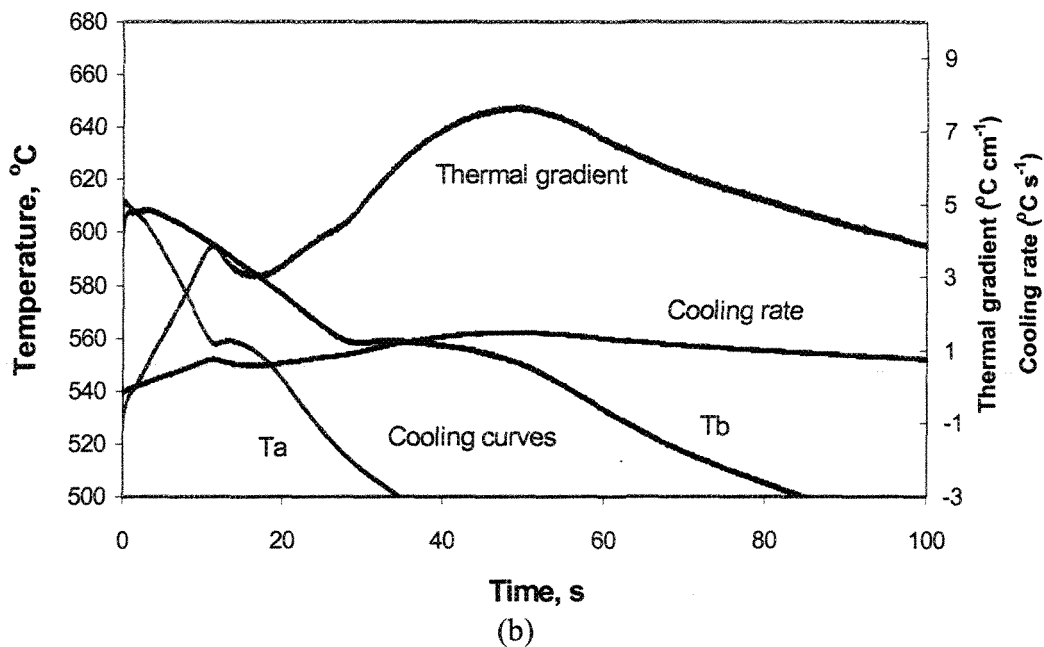
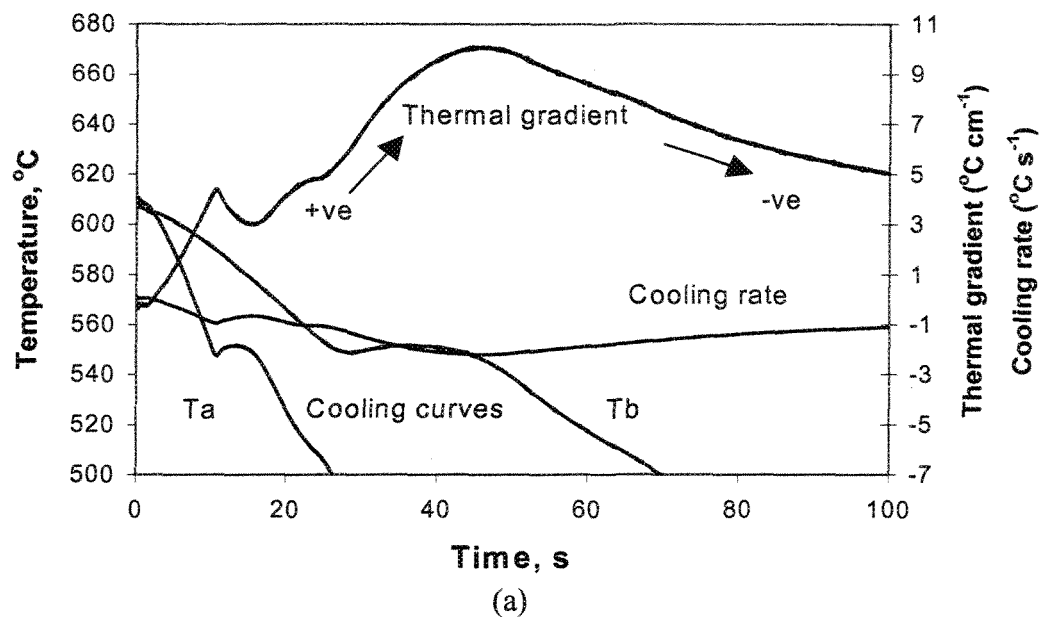


Figure 63. Comparison of temperature, thermal gradient and cooling rates versus time for (a) B (Sr-modified 319), (b) BB2 (B+2186 ppm Bi), and (c) BC2 (B+103 ppm Ca) alloys (small mold).

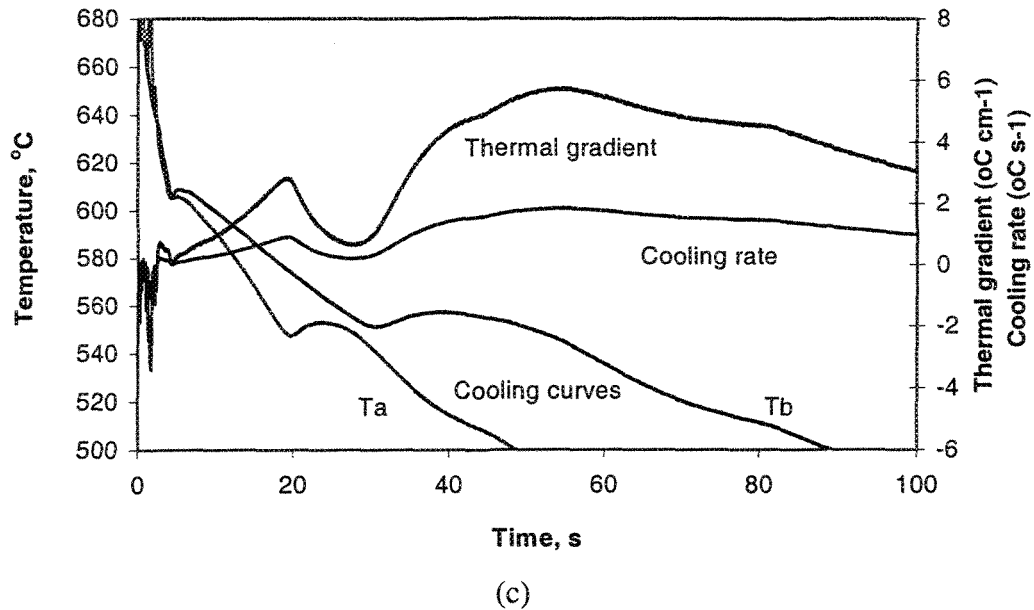
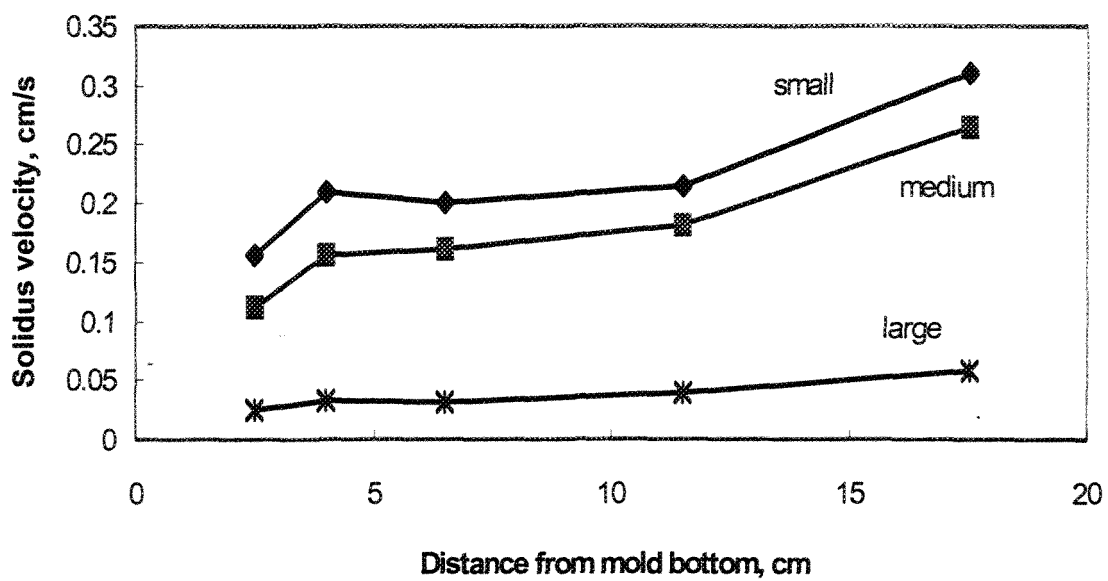
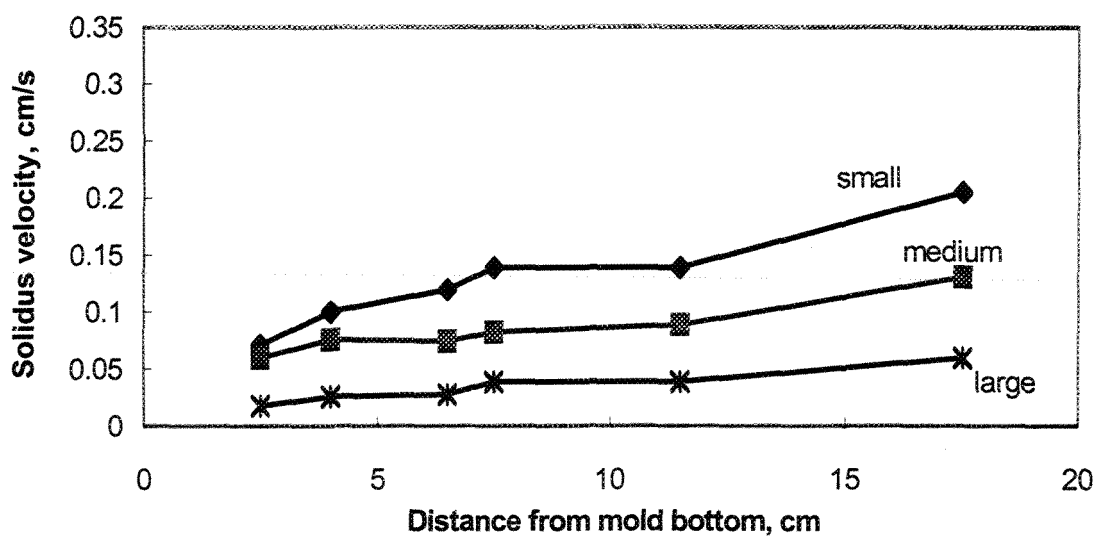


Figure 63. Comparison of temperature, thermal gradient and cooling rates versus time for (a) B (Sr-modified 319), (b) BB2 (B+2186 ppm Bi), and (c) BC2 (B+103 ppm Ca) alloys (small mold).

The average vertical solidus velocity was also measured for the different castings. Figures 64(a) and (b) illustrate plots of the average vertical solidus interface velocities obtained as a function of the distance from the bottom of the mold for (a) B (Sr-modified 319), and (b) BB2 (B + 2186 ppm Bi) alloys, respectively, as measured in the small, medium and large molds. By comparing the two figures, we can observe that the interface velocities are lowered with Bi addition to the B alloy. Similar observations were made in the case of the C alloy with Bi addition, Figure 65.

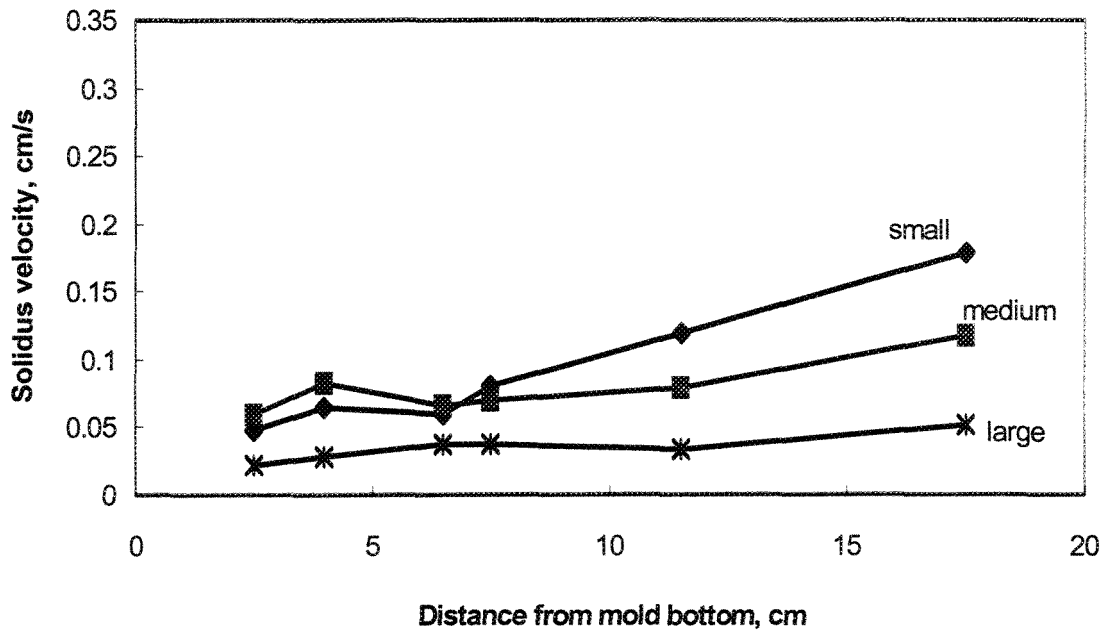


(a)

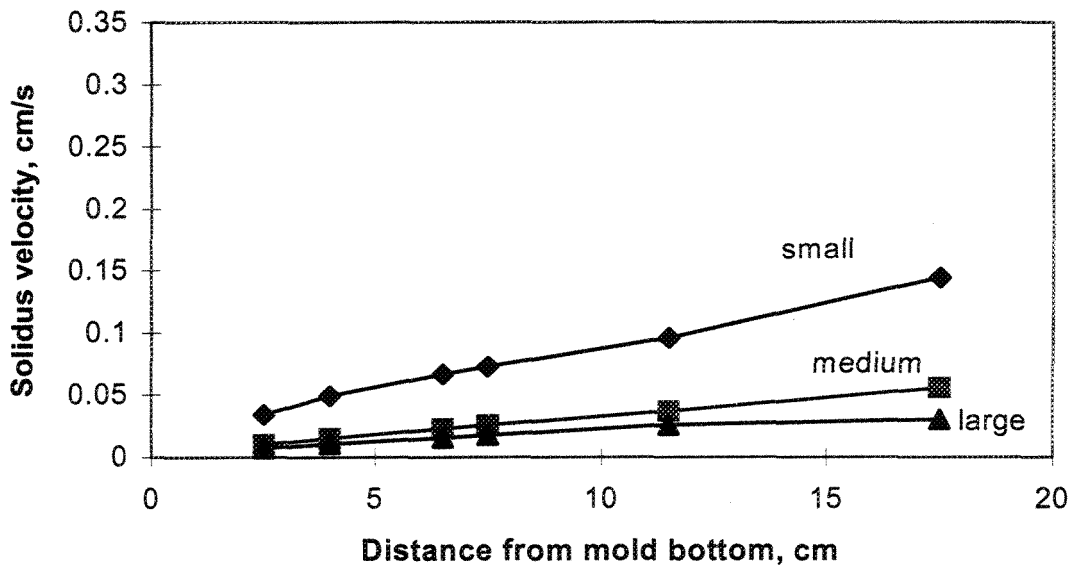


(b)

Figure 64. Average vertical solidus interface velocities in the wedge mold as a function of the distance from the bottom of the mold for (a) B alloy, (b) BB2 alloy (B + 2186 ppm Bi) for small, medium and large molds.



(a)



(b)

Figure 65. Average vertical solidus interface velocities in the wedge mold as a function of the distance from the bottom of the mold for (a) C alloy, (b) CB6 alloy (C + 3020 ppm Bi) for small, medium and large molds.

Figure 66 attempts to explain these observations, through a schematic representation of the growth of an α -Al dendrite in the B (Sr-modified 319) and Bi-containing B alloys. In (a), only Si and Sr atoms are rejected in front of the growing dendrite. Consequently, there is more room for the dendrites to grow compared to case (b), where the addition of Bi introduces further solute rejection into the surrounding liquid (*i.e.*, $\Delta C_2 > \Delta C_1$).

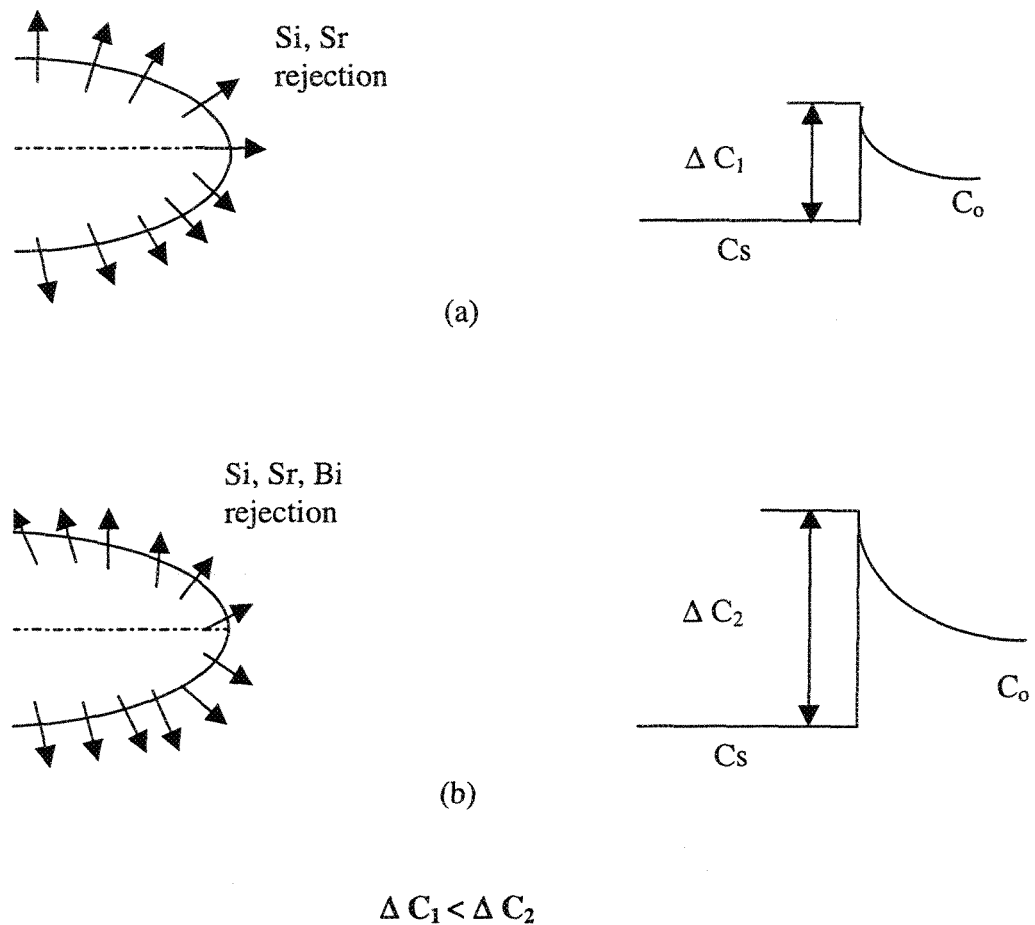
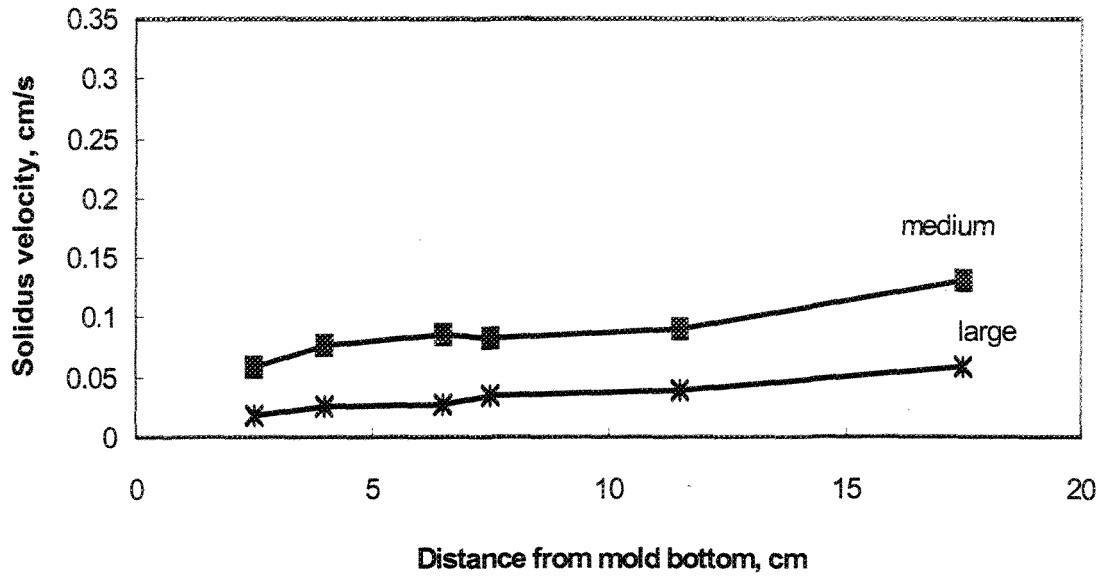


Figure 66. Schematic diagram showing rejection of solute atoms in front of a growing α -Al dendrite in (a) B (Sr-modified 319 alloy), (b) Bi-containing B alloy.

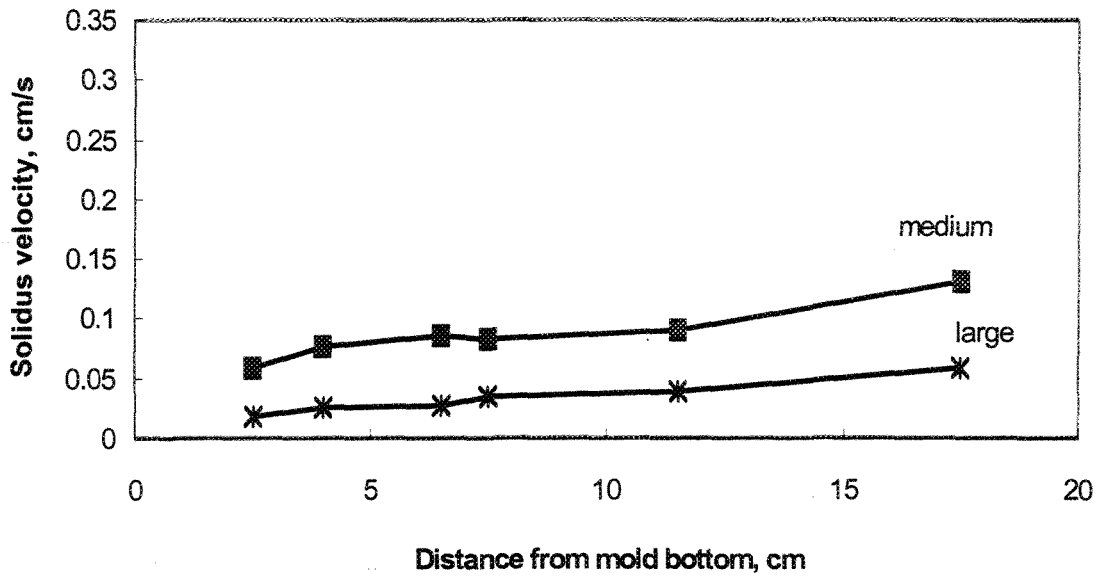
The same explanation can be extended to the case of Ca addition, where the Ca affects the interface velocity in a similar fashion, as can be seen from Figure 67. Due to difficulties associated with the measurements made for the small mold configuration (*i.e.*, thermocouple failure), only the plots for the medium and large molds are shown in the figure.

The effect of Bi and Ca addition on the interface velocity can be further understood by referring to the Al-Bi and Al-Ca phase diagrams shown in Figures 10 and 22, respectively. As can be seen, the concentrations of both Bi and Ca in aluminum are almost negligible at room temperature. Thus, no solid solution will be formed and all the Bi and Ca will be rejected. It is interesting to compare the differences in Figures 64 and 67 between B and C alloys, where, due to the presence of Mg in the latter,⁷¹ the curves in Figures 67(a) and (b) show a closer similarity to each other and to those of Figure 64(b), than those displayed in 64(a).

Figure 68 provides an indication of how the dendrite arm spacing (DAS) varies as a function of the distance from the mold bottom for the Sr-modified B alloy with the three mold configurations.



(a)



(b)

Figure 67. Average vertical solidus interface velocities in the wedge mold as a function of the distance from the bottom of the mold for (a) BC2 alloy (B + 103 ppm Ca), and (b) CC2 alloy (C + 94 ppm Ca), for medium and large molds.

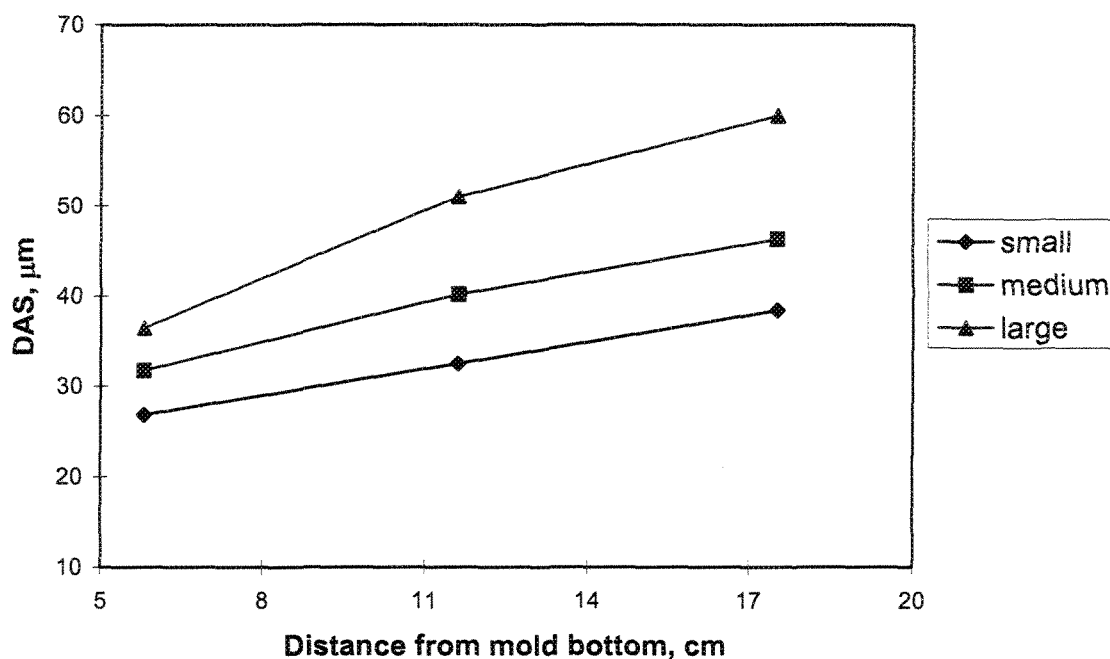


Figure 68. Dendrite arm spacing versus distance from mold bottom for B alloy for different mold configurations.

4.3.2 IMAGE ANALYSIS

Porosity and eutectic Si particle measurements were carried out as described in section 4.2, on samples obtained from B and C alloys containing various Bi and Ca additions cast in the small and large molds.

4.3.2.1 Si PARTICLE MEASUREMENTS

The effect of Bi addition on the eutectic silicon particle characteristics followed the same trend as that observed in the case of the graphite mold samples discussed in section 3.3.2. Figures 69 and 70 show the effect of Bi addition on the average Si particle area in B

and C alloys, respectively. The figures show that there is no effect due to the difference in cooling rate between the two molds.

The regions marked modification and demodification in Figures 69 and 70 are further illustrated by the microstructures of Figures 71 and 72, where the changes in the eutectic Si particle characteristics can be clearly seen. Starting from the well-modified eutectic Si regions observed in Figure 71(a), addition of Bi “demodifies” the Si particles so that they appear in coarse, acicular form in Figure 71(b), until, at an increased Bi addition of ~ 6060 ppm the refinement of the Si particles is again observed, indicating that the Bi now acts as a modifier.

Essentially the same observations are noted in the case of the C alloy, Figure 72. It is interesting to compare the morphology of the well-modified eutectic structure in Figure 72(a) with that of 71(a). The presence of 0.4 wt% Mg in the C alloy results in the appearance of the Si particles in a more script-like form compared to the extremely fine particles observed in the B alloy. Such a structure is typical of the higher Mg-containing 319.2 alloys.⁷²

With respect to the effect of Ca addition on the Si particle characteristics, it was found that, although the Si particle area increased with Ca addition to the B and C alloys, the standard deviation also increased, indicating the non-homogeneity of the Si particle size within the microstructure.

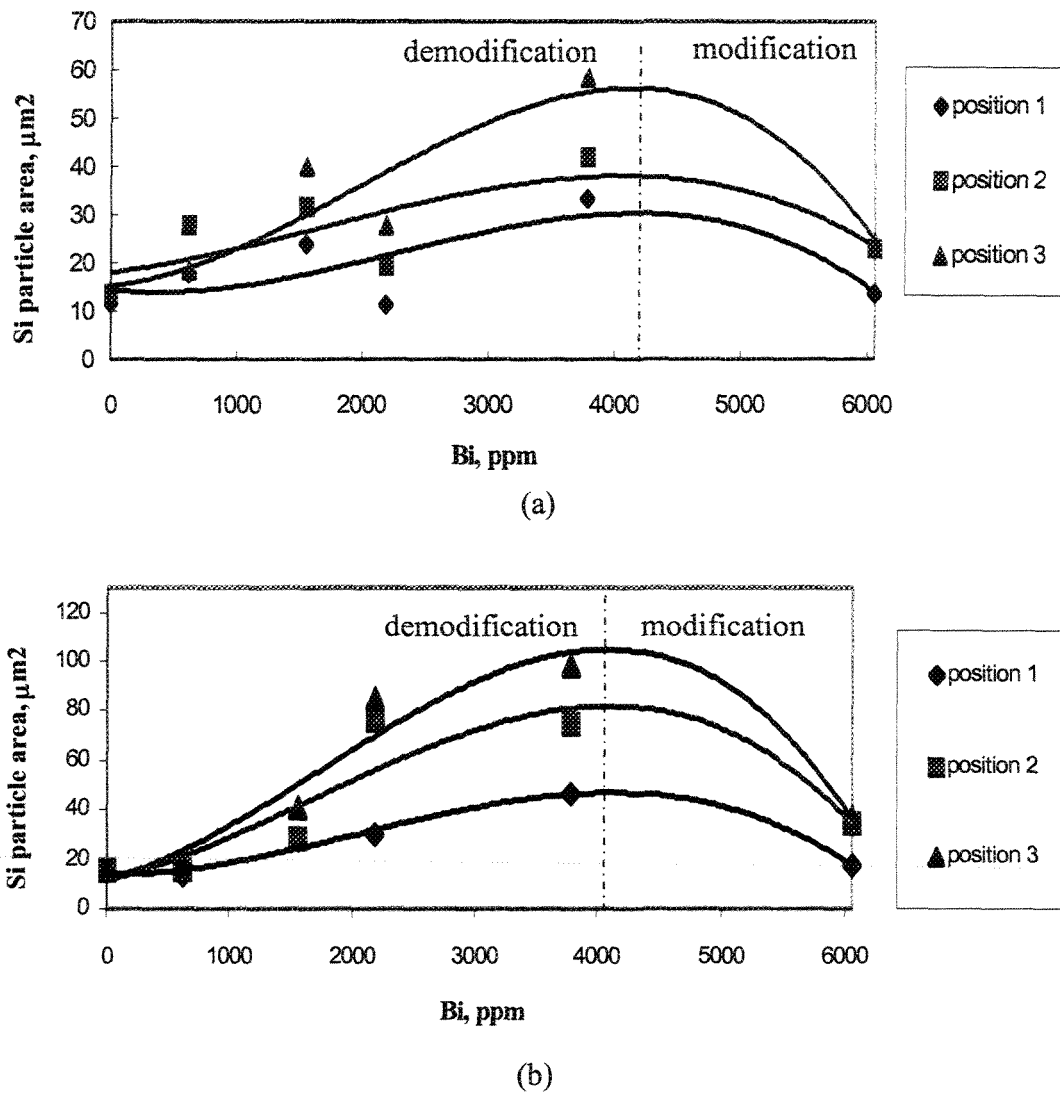


Figure 69. Variation in the average Si particle area in B alloy as a function of Bi addition obtained in a) small mold, and b) large mold samples. Positions 1, 2 and 3 in the legend correspond to the thermocouple positions in the casting from which the samples for metallographic examination were sectioned.

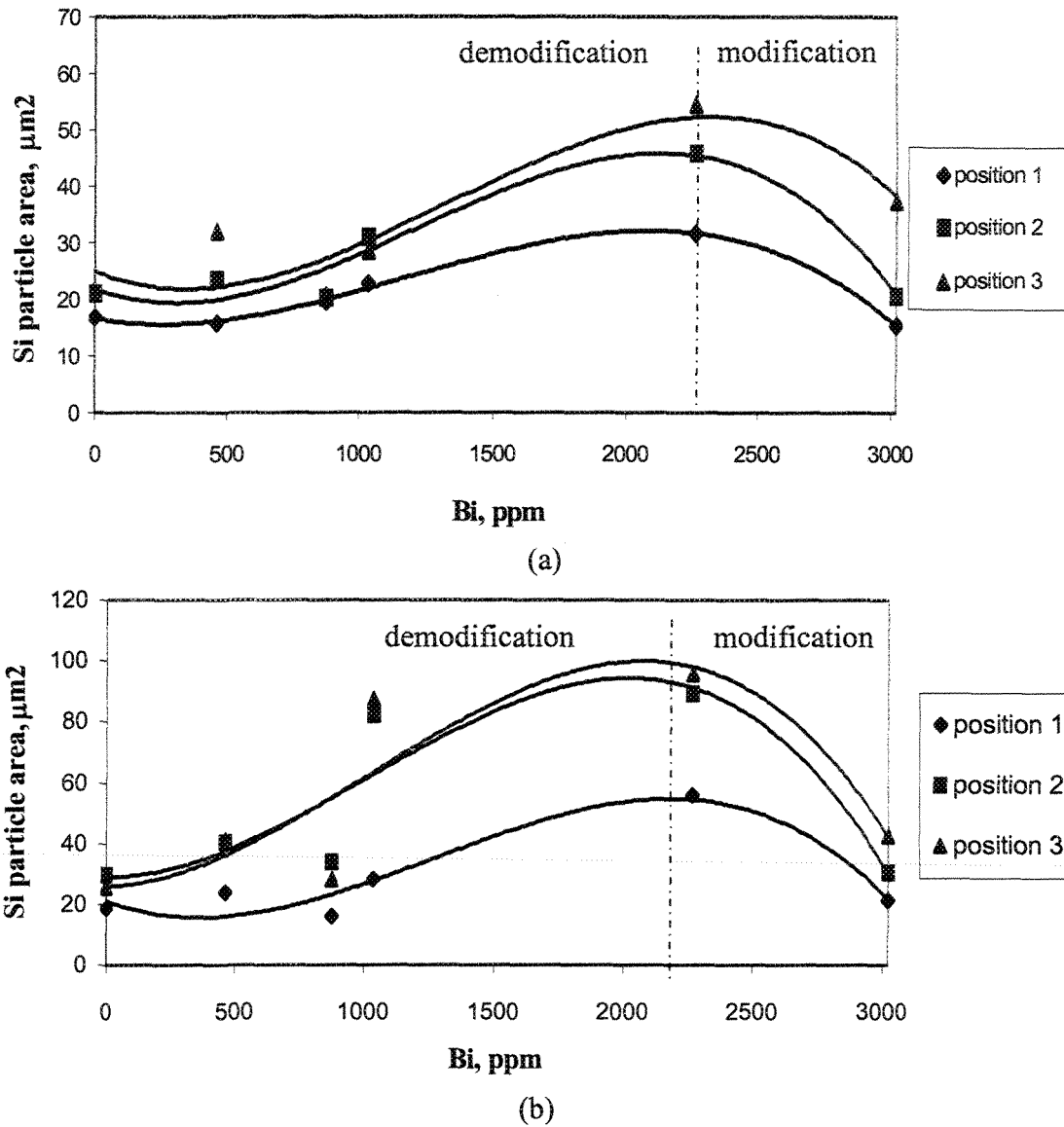


Figure 70. Variation in the average Si particle area in C alloy as a function of Bi addition obtained in a) small mold, and b) large mold samples. Positions 1, 2 and 3 in the legend correspond to the thermocouple positions in the casting from which the samples for metallographic examination were sectioned.

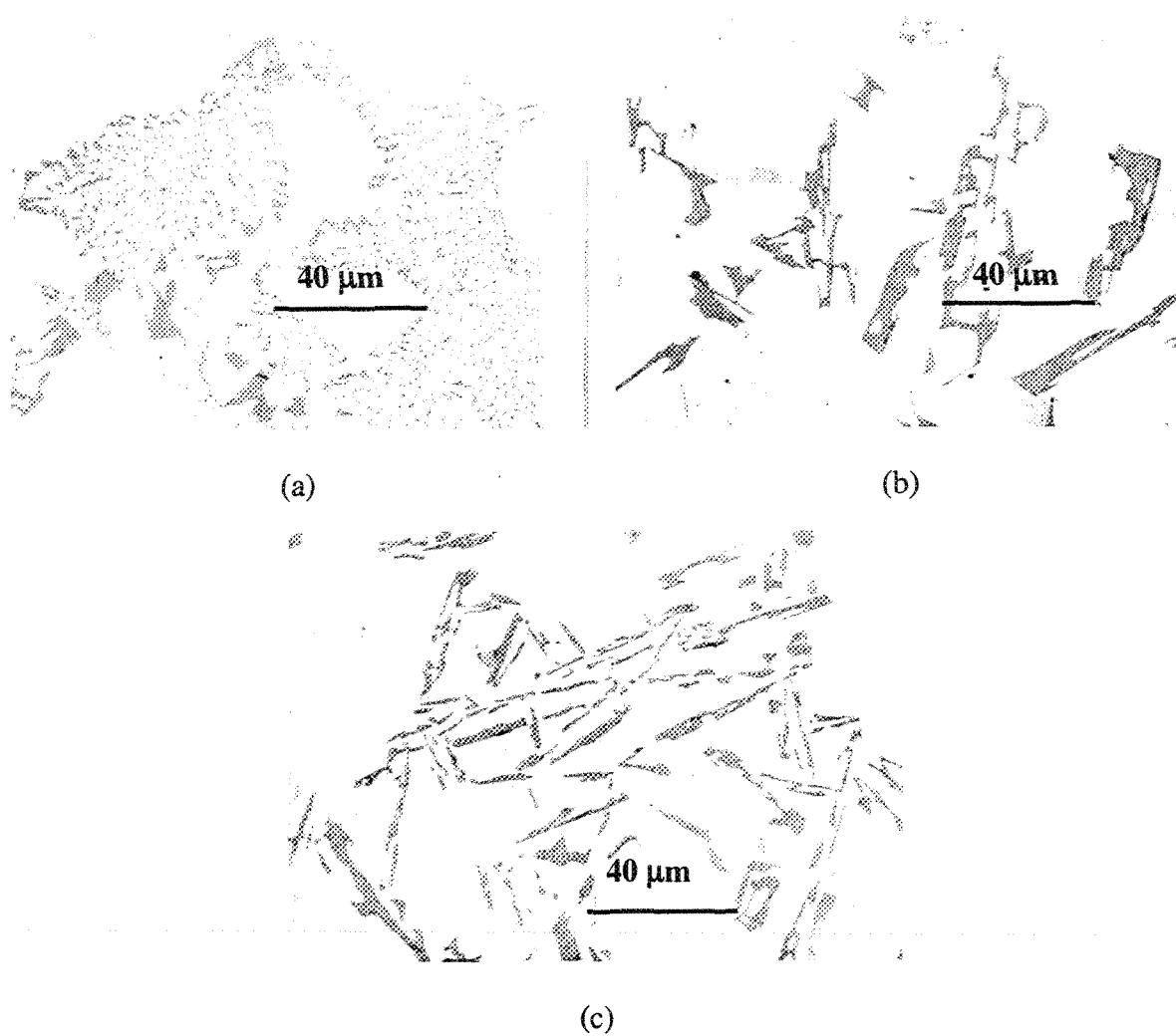


Figure 71. Eutectic Si structure observed in B alloy with (a) 0 ppm, (b) 1555 ppm, and (c) 6060 ppm Bi additions. Note the well-modified Si particles in (a) in the Sr-modified alloy, and the demodification and modification effects of Bi in (b) and (c) at the respective Bi levels.

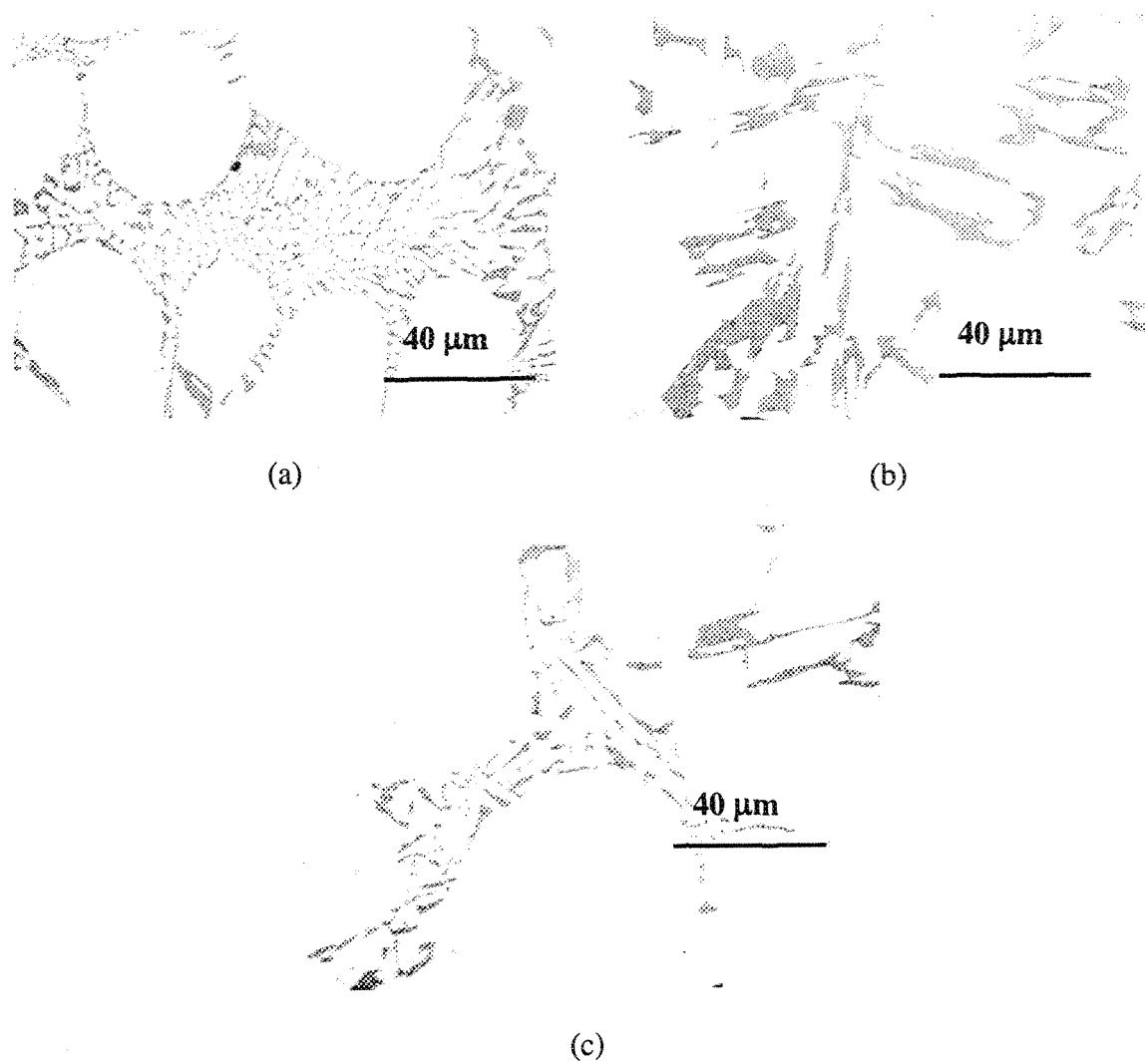


Figure 72. Eutectic Si structure in the C alloy with (a) 0 ppm, (b) 874 ppm, and (c) 3020 ppm Bi additions.

Coarse Si particles were almost always observed around Ca-compound particles (see circled areas in Figures 73 and 74). Table 13 summarizes these observations.

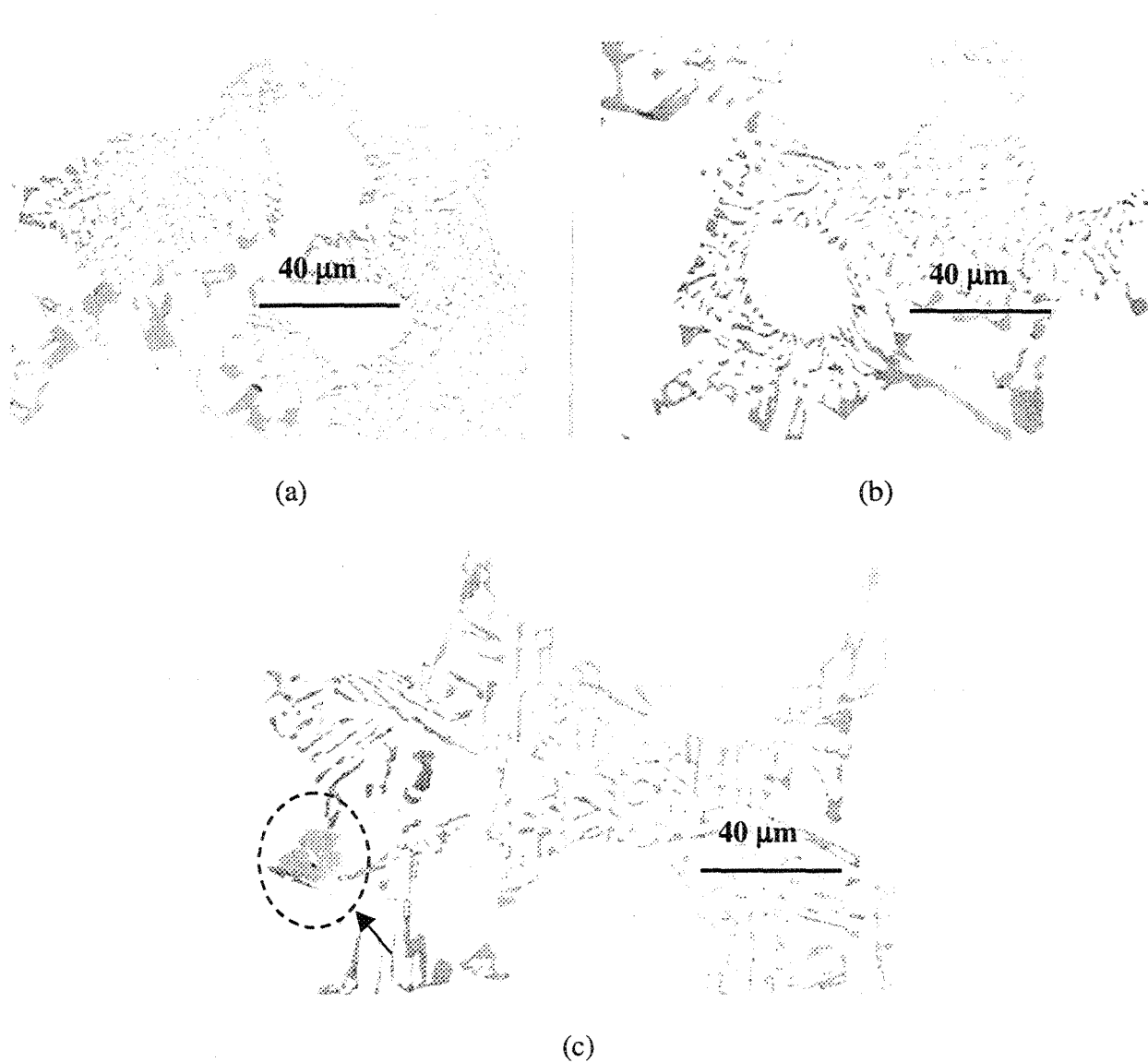


Figure 73. Eutectic Si structure in the B alloy with (a) 0 ppm, (b) 103 ppm, and (c) 465 ppm Ca additions. The circled area in (c) points to a Ca-compound particle.

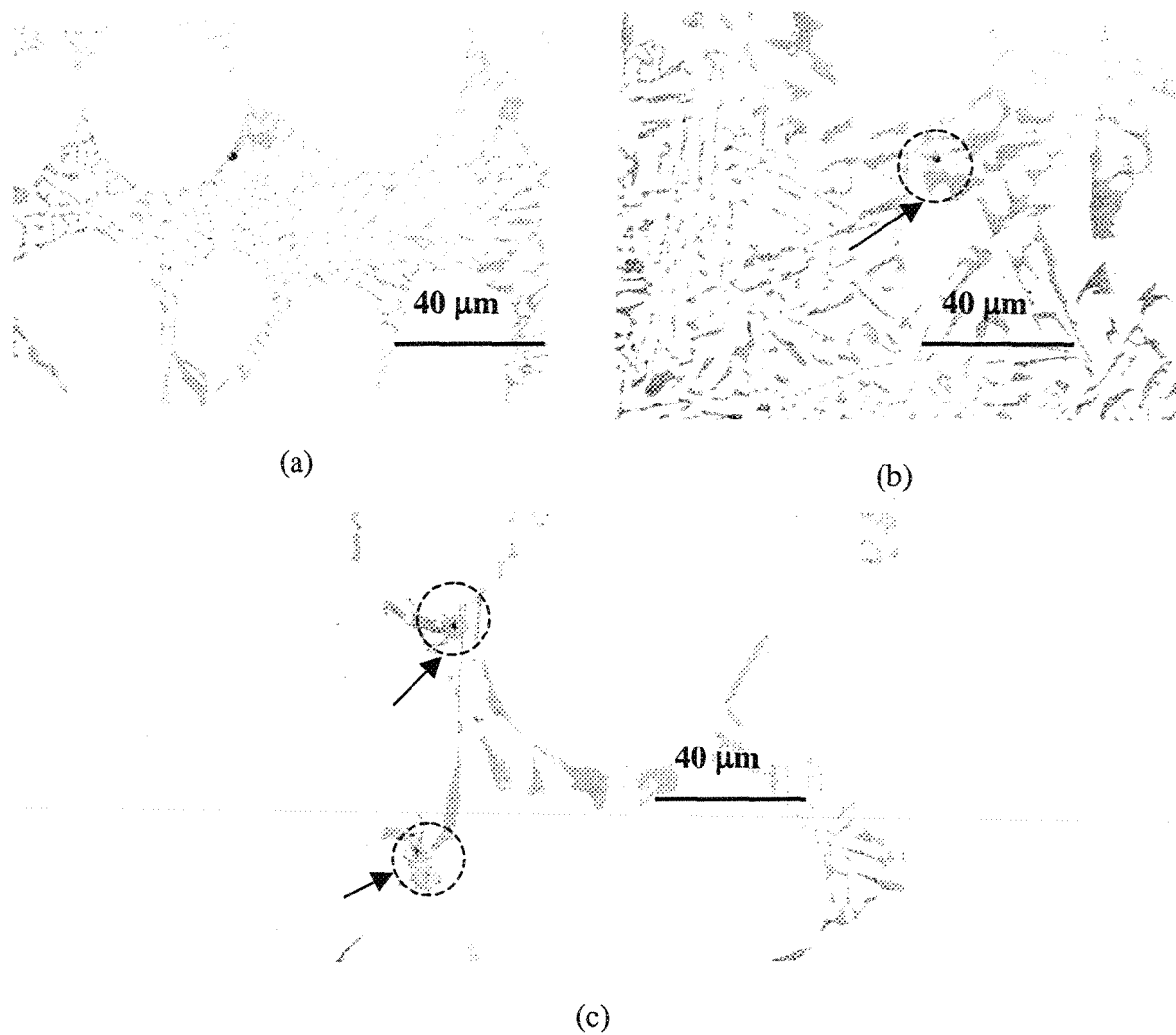


Figure 74. Eutectic Si structure in the C alloy with (a) 0 ppm, (b) 94 ppm, and (c) 486 ppm Ca additions. The circled areas point to a Ca-compound particle in each case.

Table 13 Average Si particle area and corresponding standard deviation obtained in B and C alloys with Ca addition

Sample code	Alloy	Si particle area, μm^2	
		Average	SD
B	B alloy	15.6	25.7
BC2	B alloy+103 ppm Ca	22.9	45.9
BC5	B alloy+465 ppm Ca	16.0	34.2
C	C alloy	25.6	58.6
CC2	C alloy+94 ppm Ca	27.2	38.2
CC5	C alloy+486 ppm Ca	45.7	66.3

4.3.2.2 POROSITY MEASUREMENTS

The percentage porosity in B and C alloys was affected to some extent with progressive Bi addition. Figure 75(a) shows the plot of percentage porosity versus Bi addition for B alloy, where Bi addition up to 6000 ppm increased the average percentage porosity to ~0.04% compared to 0.01% for the same alloy without Bi addition (large mold samples).

The average pore length was also affected, as shown in Figure 75(b), where the parameter decreased somewhat with Bi addition. The same effect was also observed in the case of C alloy, Figure 76. From Figures 75 and 76, it can be said that porosity formation in these alloys is hardly affected or, at most, affected only very slightly by Bi addition.

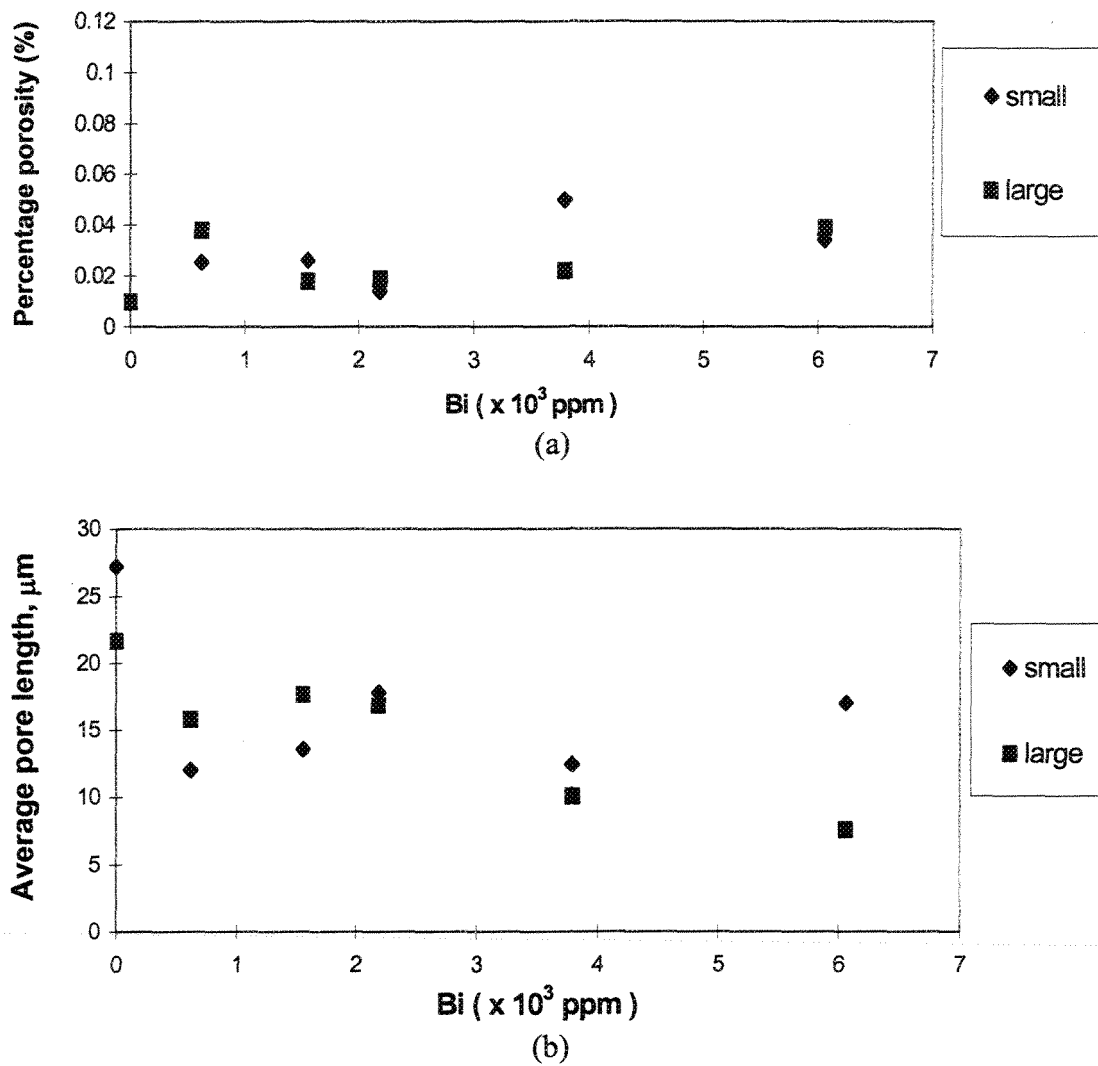


Figure 75. Variation in (a) percentage porosity, and (b) average pore length as a function of Bi addition in B alloy samples obtained from small and large mold castings.

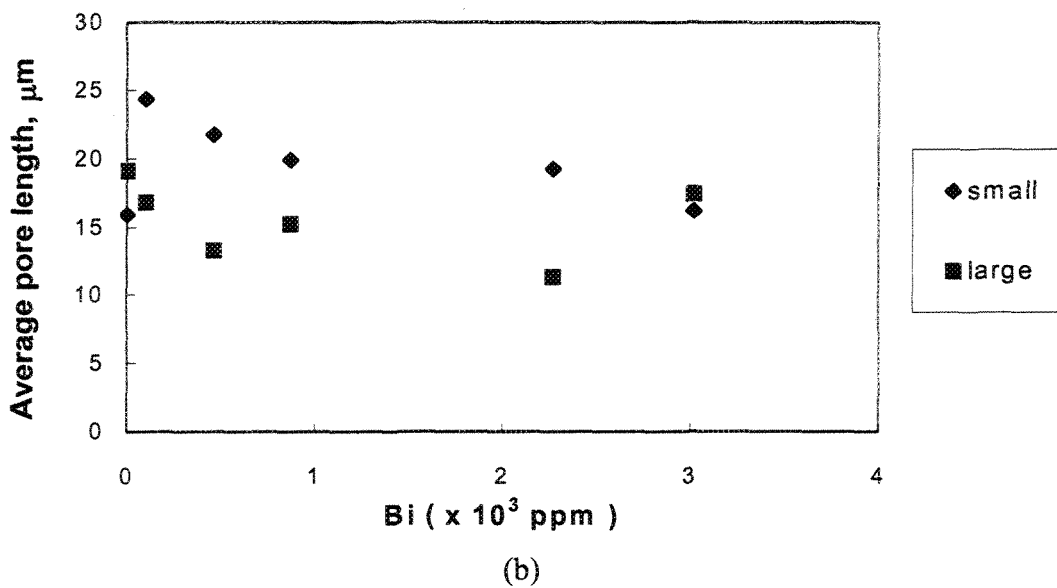
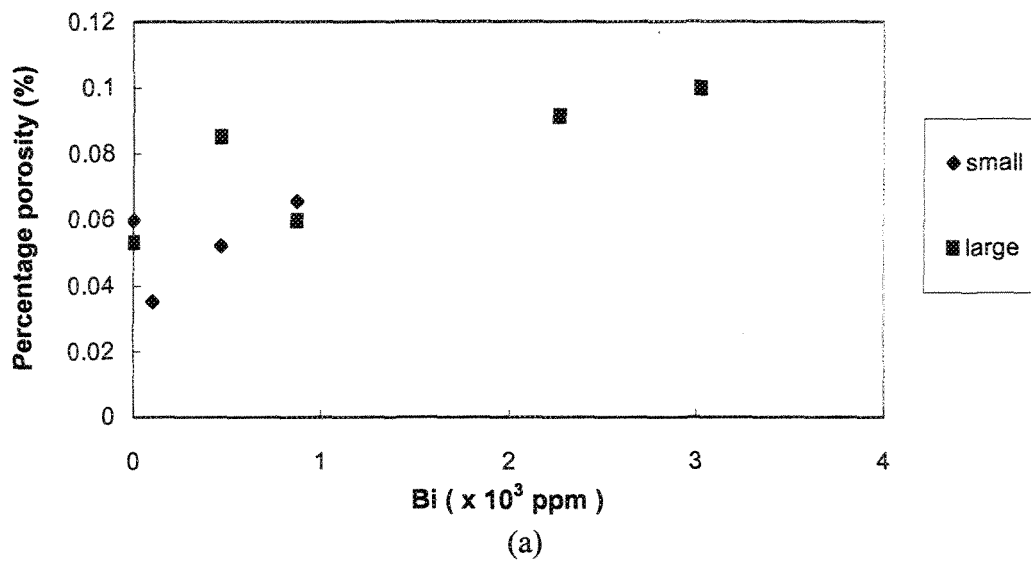


Figure 76. Variation in (a) percentage porosity, and (b) average pore length as a function of Bi addition in C alloy samples obtained from small and large mold castings.

With respect to the effect of Ca addition, again, no significant effect on the porosity was observed, as can be seen from Table 14. Any porosity associated with the Bi or Ca addition is related to the formation of their oxides and, to some extent, on the Ca particle size. This point will be elaborated upon in more detail in section 4.3.3.2.

Table 14 Percentage porosity for B and C alloys* with Ca addition

B alloy		C alloy	
Ca, ppm	% Porosity	Ca, ppm	% Porosity
0	0.01	0	0.06
52	0.04	63	0.05
103	0.04	94	0.07
465	0.05	486	0.04

* small mold samples

The very small amounts of porosity observed in these samples can be explained in terms of two factors:

i) Presence of fine micropores

The porosity associated with the Bi- and Ca-oxides is very fine microporosity (pore sizes less than 1 μm), as was determined when the samples were analyzed using electron probe microanalysis (section 4.3.3). Thus, these fine micropores could not be counted using the optical microscope-image analyzer system employed for quantitative porosity measurements.

ii) Effect of eutectic solidification mode on porosity formation

An increased level of porosity is generally encountered when Al-Si alloys are modified. The increased porosity can cause a reduction in the mechanical properties

(compared to those of the unmodified alloy), even though the eutectic silicon has been modified.

In spite of the different theories^{73,74,75,32} that have been proposed to explain this increase in porosity with modification, there is no consensus on the mechanism responsible for this effect. In a recent study, Dahle *et al.*⁷⁶ proposed that the nucleation and growth characteristics of the eutectic must be considered for a proper comprehension of said increase in porosity, given the fact that in the commonly employed casting alloys, the eutectic volume fraction ranges anywhere from 40 to 100 %. Their group has further proposed that the formation of the eutectic may significantly affect the permeability of the mushy zone, and have shown that a direct relationship between the eutectic solidification mode and porosity level and distribution is obtained.⁷⁶

Continuing this line of work, Knuutinen *et al.*⁷⁷ investigated the effect of Ba, Ca, Y and Yb additions on porosity formation in permanent mold castings of the type used by Dahle *et al.*⁷⁶ They found that Ca and Y additions caused the porosity to become increasingly concentrated in the hot spot regions observed in such castings. All additions were found to increase the porosity level (compared to the modified alloy) and also, the porosity increased with increase in the amount of addition.

Figure 77 shows an example of the appearance of hot spots in the macrographs of sectioned A356.0 alloy castings containing < 5 ppm, ~40 ppm, and ~150 ppm Ca. As these macrographs show, the porosity in the castings with the low and medium Ca additions are similar, whereas in the casting with ~150 ppm Ca, the pores are much larger and appear concentrated towards the centre of the hot spot.

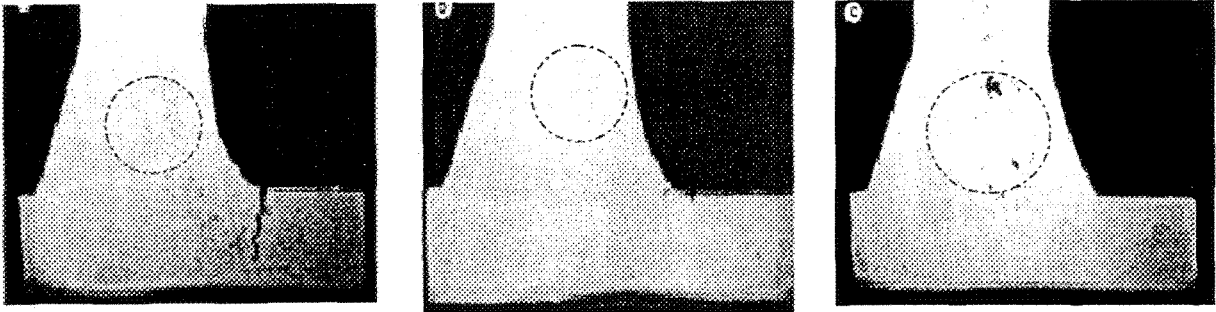


Figure 77. Macrographs of hot spots (circled) in castings containing (a) < 5 ppm Ca; (b) 40 ppm Ca; (c) ~150 ppm Ca.⁷⁷

From micrographs of samples quenched during the eutectic arrest, the authors found that the eutectic evolved with a dependency on the thermal gradient, *viz.*, from the surface towards the centre of the casting. Based on these observations and those of other researchers,^{78,79,60} Knuutinen *et al.*⁷⁷ have suggested that Ca causes the eutectic to evolve from the surface of the casting towards the centre of the hot spot. Such a eutectic solidification mode is expected to result in porosity being concentrated closer to the hot spot.

Similar to the observations of Knuutinen *et al.*,⁷⁷ hot spots were also observed in the small mold castings in the present study for the Ca-containing alloys. As Figure 78 shows, the concentration of micropores near the hot spot would suggest that the same reasoning would also apply in the present case, to explain the hot spot and associated porosity features observed in the figure.

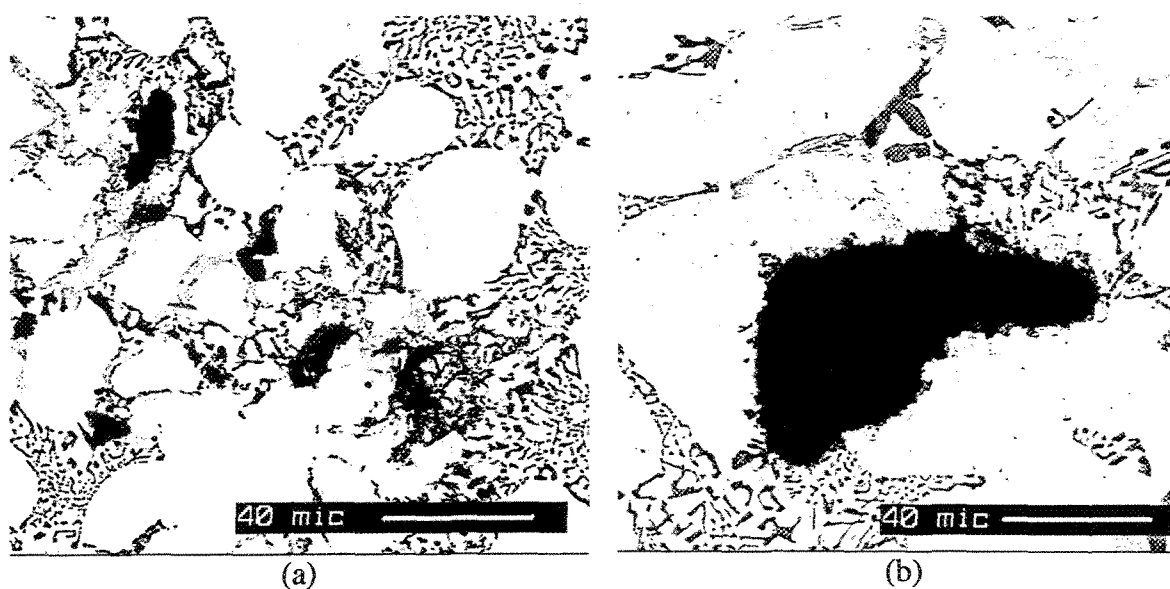


Figure 78. Examples of hot spot formation in (a) B alloy, and (b) BC5 alloy (B+465 ppm Ca) (small mold, position 1 samples).

In other studies carried out by Nogita *et al.*⁸⁰ the same observations were also noted in Na-modified alloys as those reported for Ca additions. In their studies on porosity formation in Al-9 wt% Si-3 wt% Cu alloys, Roy *et al.*⁷¹ obtained the same kind of hot spots associated with the small (0° angle) mold, using the same variable angle wedge mold used in our study. Such kind of hot spots disappeared as the mold angle was increased, *i.e.* with mold thickness, as it is clear from the X-ray radiographs for the TiB_2 grain refined version of this alloy, Figure 79. By comparing the castings obtained with cold and hot molds, it can be seen that increasing the mold temperature decreased the susceptibility for hot spot formation.

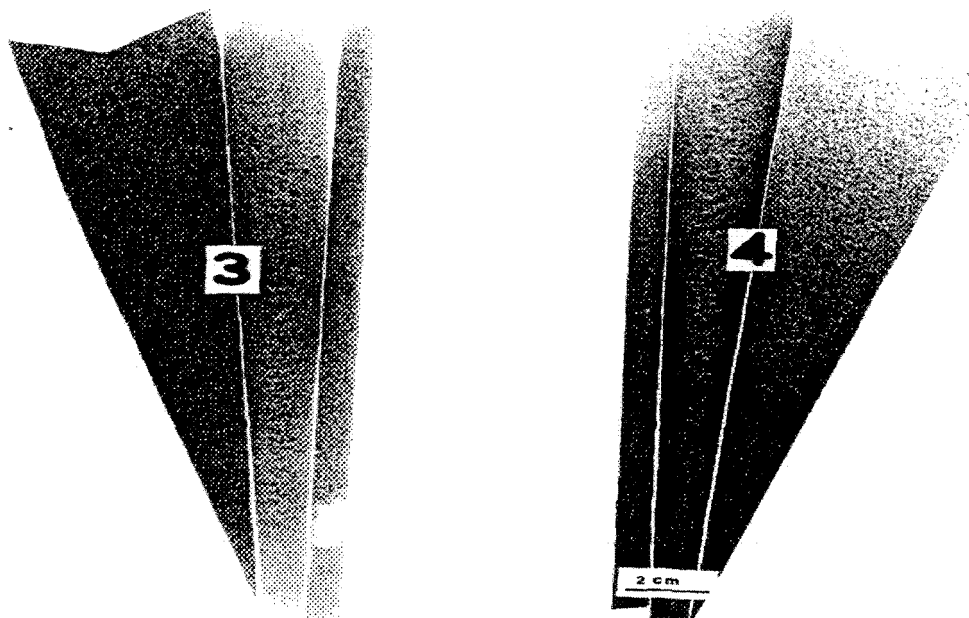


Figure 79. X-ray radiographs obtained from the TiB_2 grain refined (Al-9 wt% Si-3 wt% Cu) alloy samples, (a) cold mold, and (b) hot mold.⁷¹

As will be shown later (in section 4.3.3.1), the Bi-containing alloy castings obtained from the small mold also exhibited such hot spot-related microporosity features. It would be reasonable to assume that, in this case also, the same explanation would suffice.

4.3.3 ELECTRON PROBE MICROANALYSIS

In addition to the optical microscope – image analyzer system used for the porosity and Si particle measurements, the different alloy samples were also examined using a combined WD/ED electron microprobe analyzer to gain further information on the nature and size of the microporosity observed in these samples. At the same time, the composition of the particles and oxides formed with the Bi and Ca additions could also be determined.

4.3.3.1 BISMUTH ADDITION

Figure 80 shows the backscattered image obtained from BB2 alloy (B alloy + 2186 ppm Bi). The increase in percentage porosity observed in this sample arises from the microporosity associated with the formation of Bi oxide, which can be noted as the bright regions in the figure. The enlarged image to the right, taken from the circled area in Figure 80, shows this much more clearly. As can be estimated, the size of the micropore is in the order of $\sim 1 \mu\text{m}$. The presence of such fine micropores would explain the low values of percentage porosity observed in Figure 75.

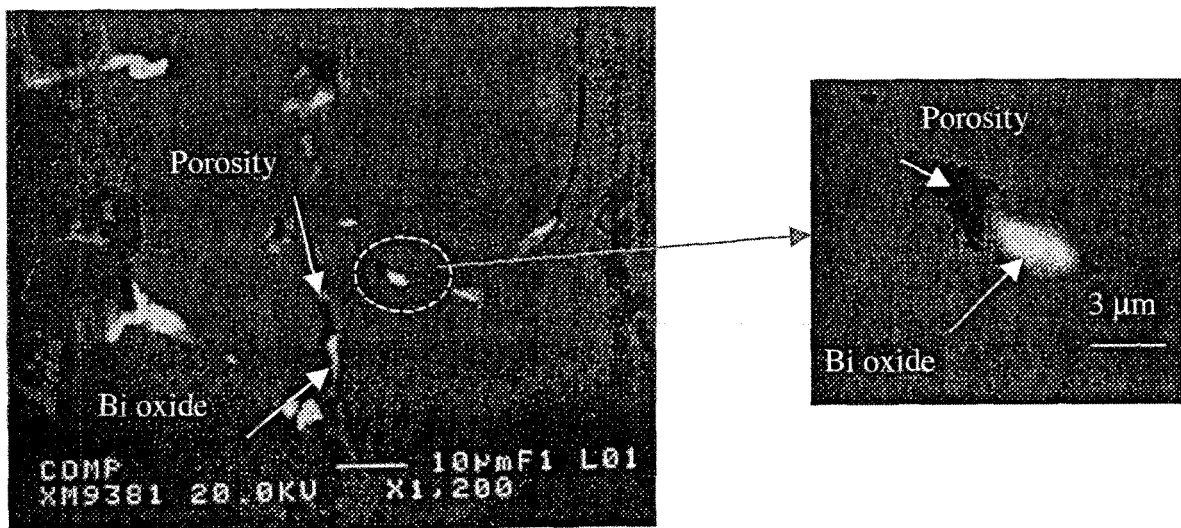


Figure 80. Backscattered image taken from BB2 alloy (B alloy + 2186 ppm Bi), large mold-position 2 sample.

The presence of Bi oxide was confirmed by the line scans taken for both Bi and O as shown in Figure 81. The increase in percentage porosity with the increase in Bi content is in agreement with the literature.⁵⁴

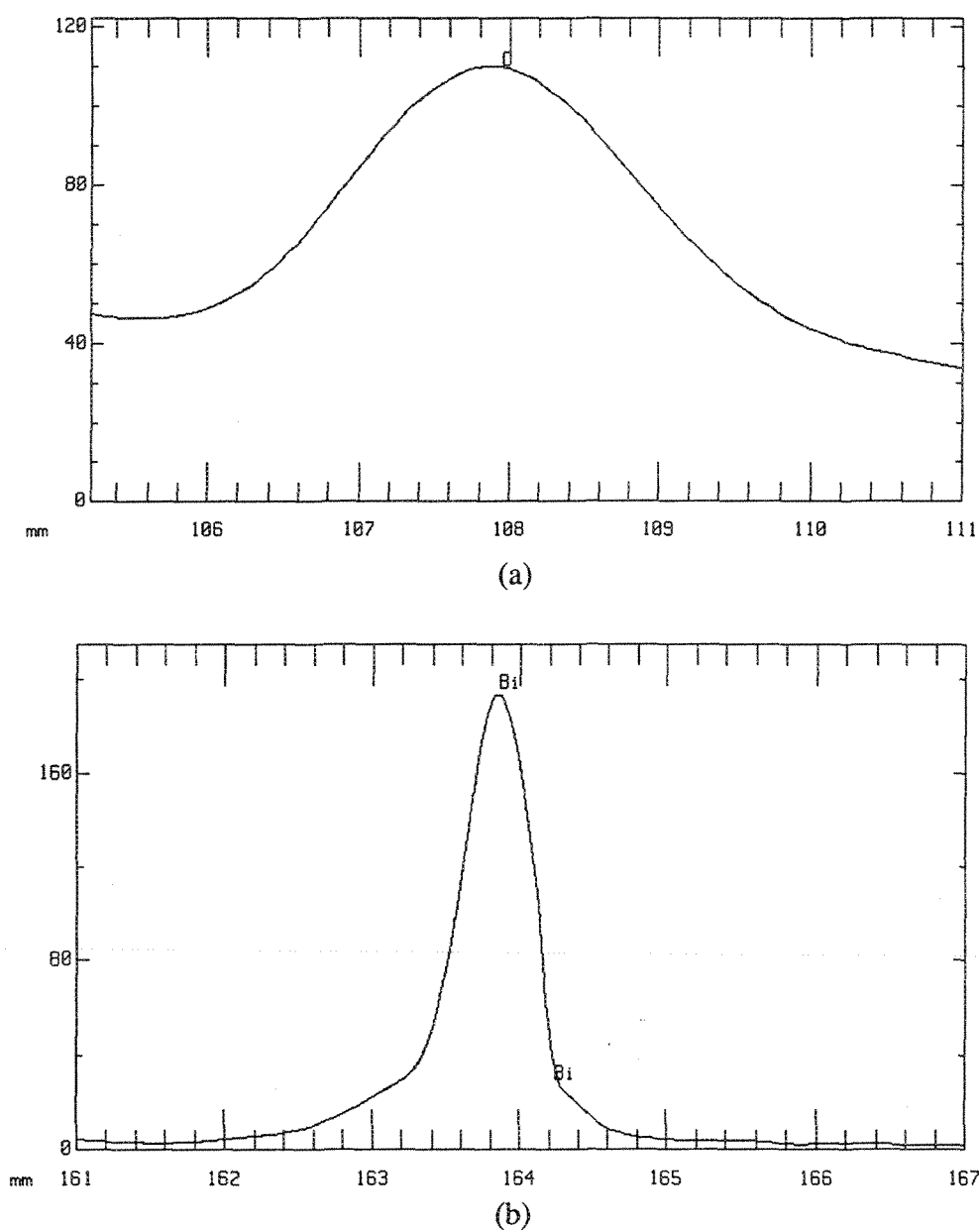


Figure 81. Line scans showing (a) O, and (b) Bi distributions from Bi oxides observed in BB2 alloy (B alloy + 2186 ppm Bi).

At higher Bi additions (3785 ppm and above) to the B alloy, in the case of the large mold samples, the average pore length was observed to decrease, as seen in Figure 75(b). This decrease may be explained in terms of the partial oxidation of the Bi particles resulting at high Bi additions. An example of this is depicted by the backscattered image of Figure 82, taken from BB6 alloy (B alloy + 6060 ppm Bi), showing a Bi particle (bright, circular region in the centre) that is partly oxidized, as evidenced by the diffused portion extending from the centre to the right hand side of the particle. It is interesting to observe the microporosity associated with the oxidized part of Bi particle, at the top right corner (circled).

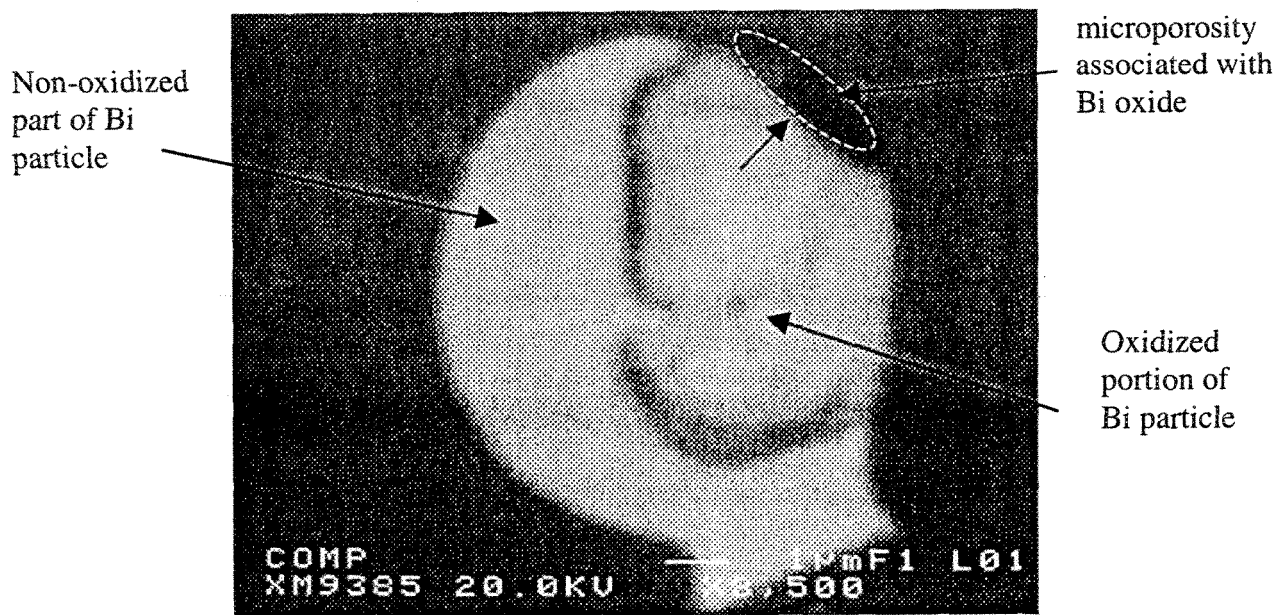


Figure 82. Backscattered image showing a Bi particle in BB6 alloy (B alloy + 6060 Bi, large mold sample).

Figure 83 is a composite of the backscattered image, and X-ray images of O, Sr and Bi elements obtained from the same area of the same sample. From the concentration of these elements in the oxidized area we can see that the oxide formed also corresponds to (Bi,Sr) oxide, as discussed previously in section 4.3.2.1. This would explain the 'demodification' effect of Bi on Sr in the B and C (Sr-containing) alloys, due to the formation of the (Bi,Sr) oxide. Figure 84 shows the corresponding EDX spectrum, revealing a strong Bi peak.

The same type of Bi oxide-induced porosity was also observed in the C alloy with Bi addition, as shown in Figure 85 for the CB2 alloy sample (C alloy + 1034 ppm Bi, large mold sample). Note the presence of Bi oxide particles (arrowed) within the pore and around its periphery.

The corresponding EDX spectrum is shown in Figure 86, where peaks for Sr and Bi can be clearly observed, in addition to those of Al, Si and Cu. Thus, it is reasonable to conclude that in Sr-modified 319 alloys containing Bi, the (Bi,Sr) oxides formed due to the presence of these elements contribute to porosity formation in the alloy.

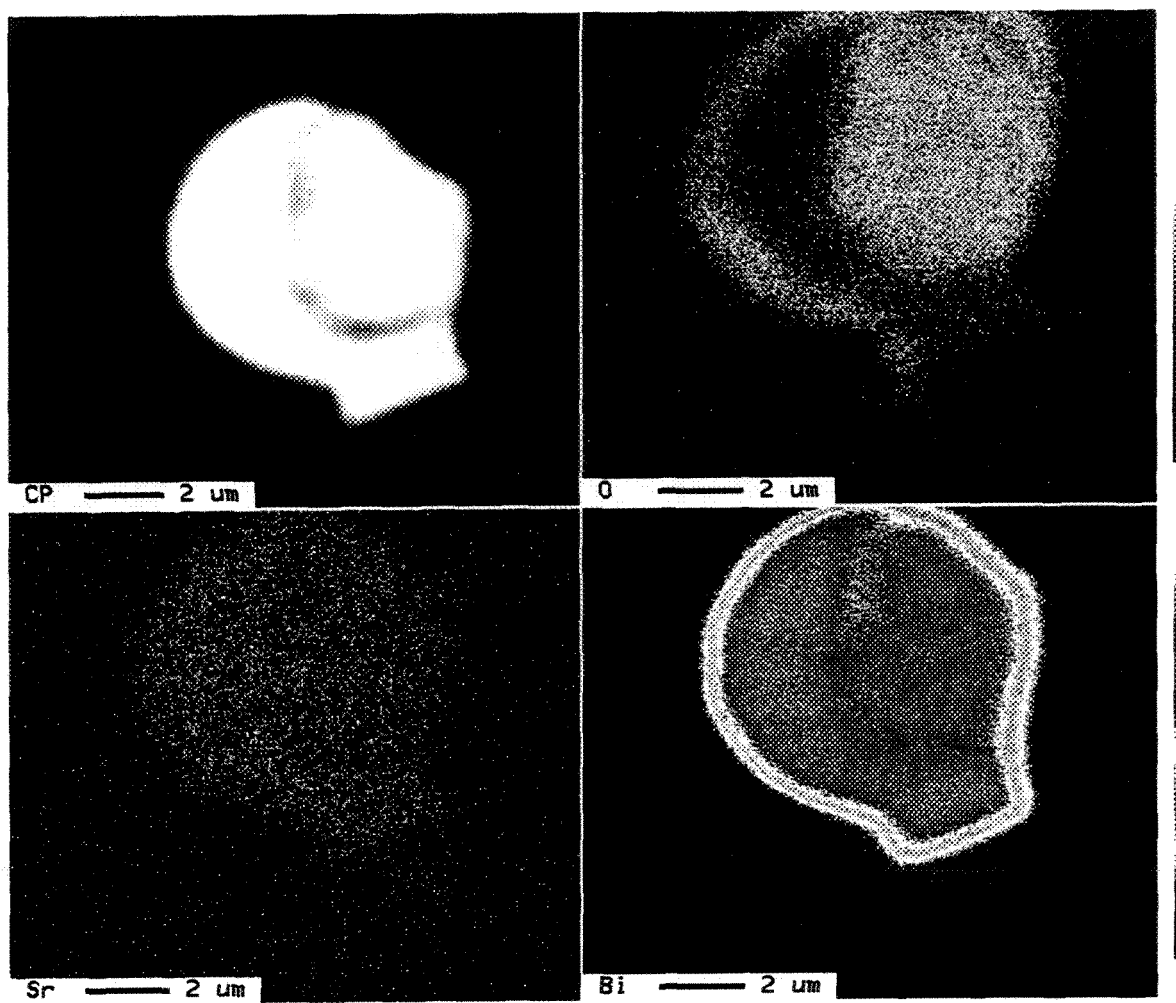


Figure 83. Backscattered image and X-ray images of O, Sr and Bi elements obtained from the Bi particle shown in Figure 82 (BB6 alloy).

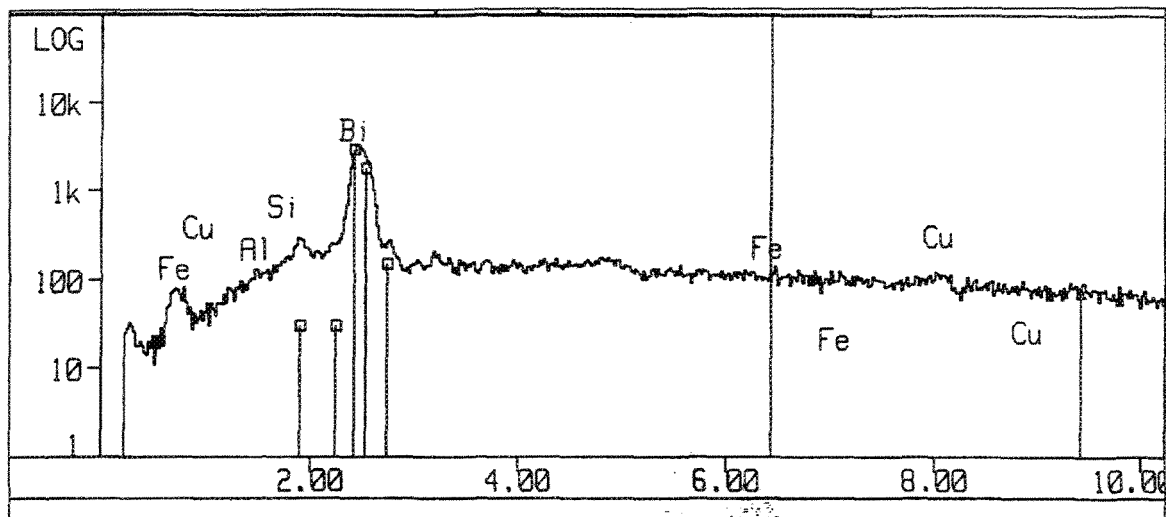


Figure 84. EDX spectrum obtained from the Bi particle shown in Figure 82 for BB6 alloy.

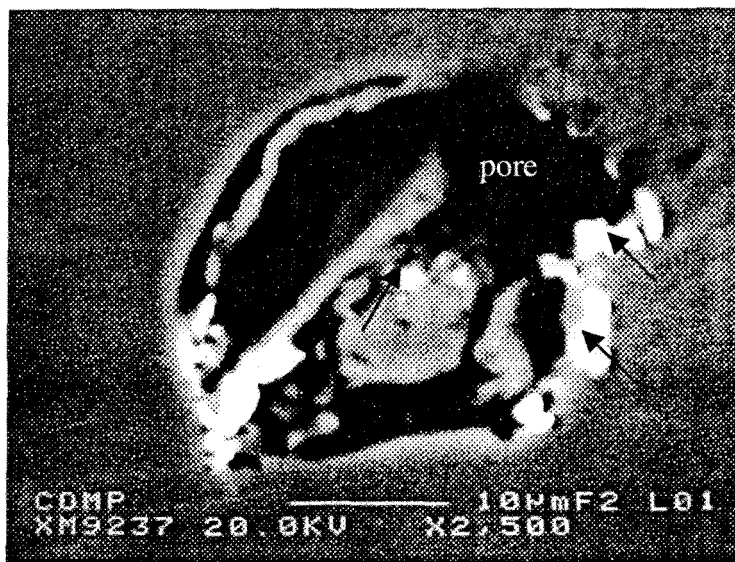


Figure 85. Backscattered image taken from CB2 alloy (C alloy + 1034 ppm Bi, large mold sample), showing Bi oxide particles (arrowed) within and around a pore.

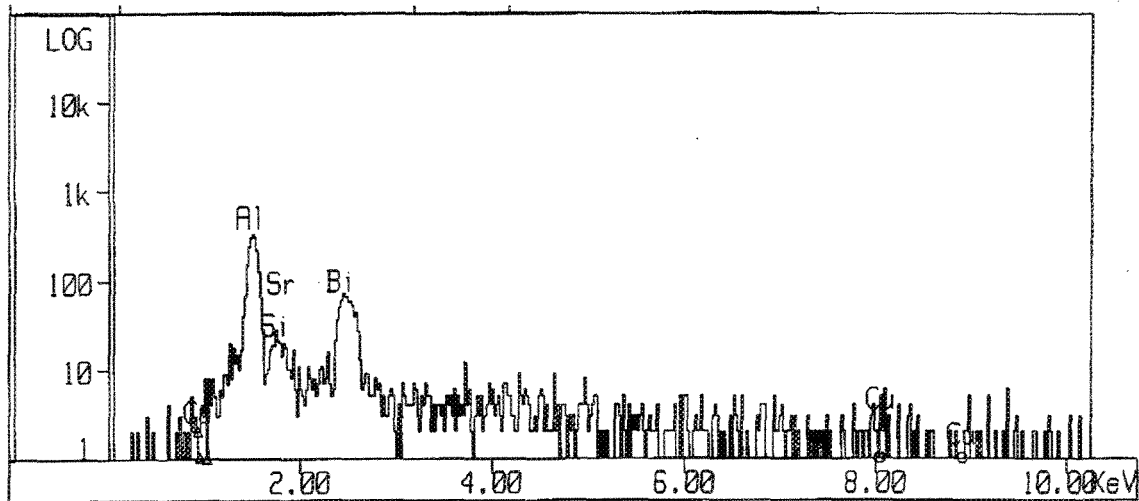


Figure 86. EDX spectrum corresponding to Figure 85, obtained from CB2 alloy.

An example of a hot spot observed in the CB2 alloy sample (C alloy + 1034 ppm Bi) obtained from the small mold casting is shown in Figure 87. Several fine pores are observed in the vicinity of the hot spot, together with Bi oxide particles (white). An enlargement of the circled region is shown alongside, and clearly reveals how microporosity is always associated with the Bi oxide particles. Again, this observation validates the low percentage porosity values exhibited by the Bi-containing B and C alloys.

As several such hot spots were observed in the Bi-containing alloy samples obtained from the small mold casting, it would be reasonable to assume that Bi influences microporosity migration to hot spot locations similar to Ca, as was discussed in section 4.3.2.2.

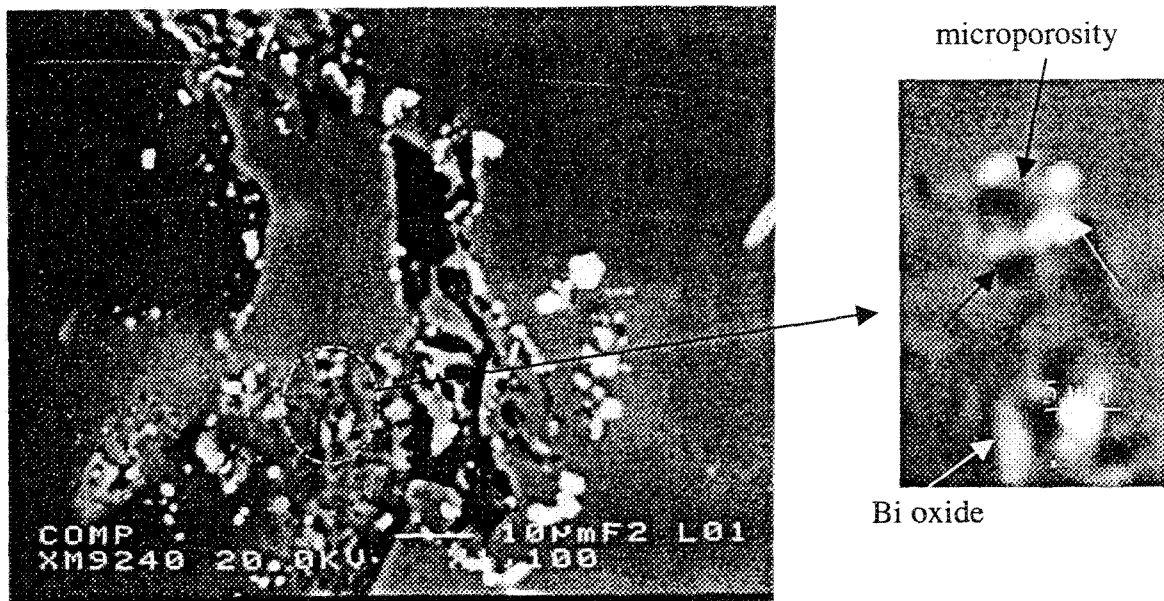


Figure 87. Backscattered image obtained from CB2 alloy (C alloy + 1034 ppm Bi, small mold sample), showing the presence of microporosity and Bi oxide particles (white) in the vicinity of a hot spot region.

4.3.3.2 CALCIUM ADDITION

With calcium addition to the B and C alloys, the same plate- and rod-type Ca-compound particles were also observed in the variable angle mold castings. While the most common particles in the Sr-modified B alloy were the rod-type particles (section 3.3.4.2), plate-like particles were also detected, the particle shape depending mainly on the type of nucleant (as was discussed in Chapter 3, section 3.3.4.2). Figure 88 shows examples of both particle types obtained in BC2 alloy (B alloy + 103 ppm Ca). The type of nucleant in the case of the plate-like particle could not be detected, as the particle completely covered the nucleant.

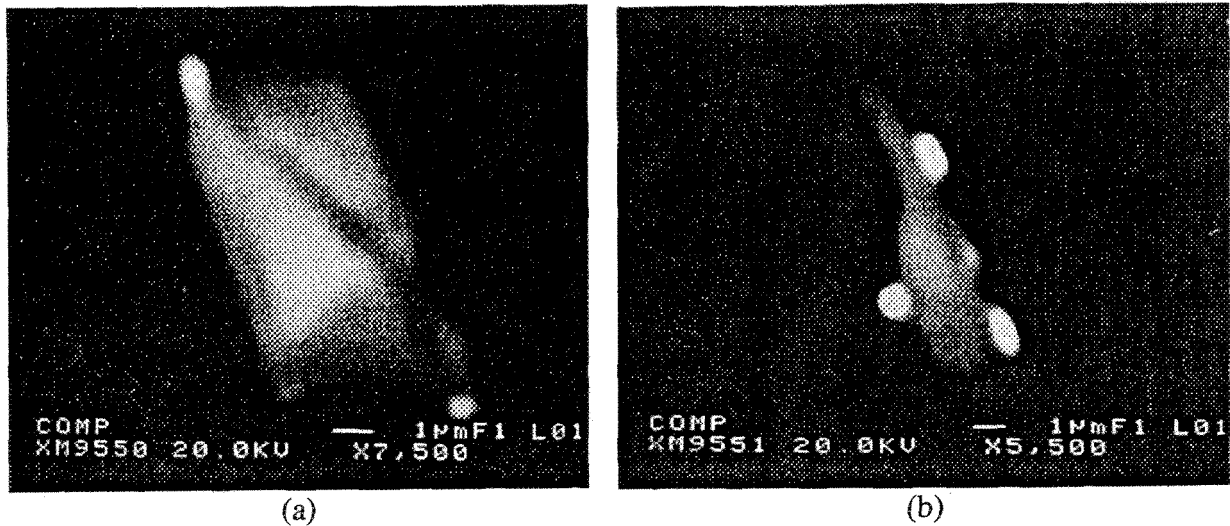


Figure 88. Ca-compound particles observed in BC2 alloy (B alloy + 103 ppm Ca) showing (a) plate-type, and (b) rod-type particles.

Table 15 gives the WDS analysis obtained from spot analysis of the surfaces of both particle types. The difference in Sr concentration between the two types is clear, which may be one of the factors attributing to the difference in their morphologies.

Table 15 Approximate composition (at%)*of the plate- and rod-type Ca-containing particles observed in BC2 alloy obtained from WDS analysis of the particle surface

Figure	Alloy Code	Element	At%	Suggested composition	Ca/Sr ratio
89(a)	BC2 (B alloy + 103 ppm Ca) Spot analysis taken from the plate-type particle	Al	42.4	Al ₅ (Ca,Sr)Si ₄ or Al ₅ CaSr _{1.4} Si ₄	0.7
		Si	35.15		
		Ca	8.5		
		Sr	11.1		
89(b)	BC2 (B alloy + 103 ppm Ca) Spot analysis taken from the rod-type particle	Al	40.5	Al ₄ (Ca,Sr)Si ₄ or Al ₄ CaSr _{2.5} Si ₄	0.4
		Si	42.9		
		Ca	10.8		
		Sr	4.33		

Similar to the case of Bi, the effect of Ca on percentage porosity was related to the formation/presence of Ca oxides. In addition, it was also observed that the finer the oxide particles, the more the pores that were observed. Figure 89 compares the Ca-containing compound observed in (a) B, and (b) C alloys, both of which contain ~500 ppm Ca. The coarse particle observed in (a) had a particle width of ~10-15 μm , whereas those observed in the form of a cluster around the micropores in (b) had an average size of about 1-3 μm .

Figure 90 shows the X-ray image of O corresponding to Figure 89(b). The concentrated oxygen region (circled) would suggest that the Ca-containing compound particles in Figure 89(b) are Ca oxide particles. WDS analysis corresponding to Figure 89(b) confirmed this to be true.

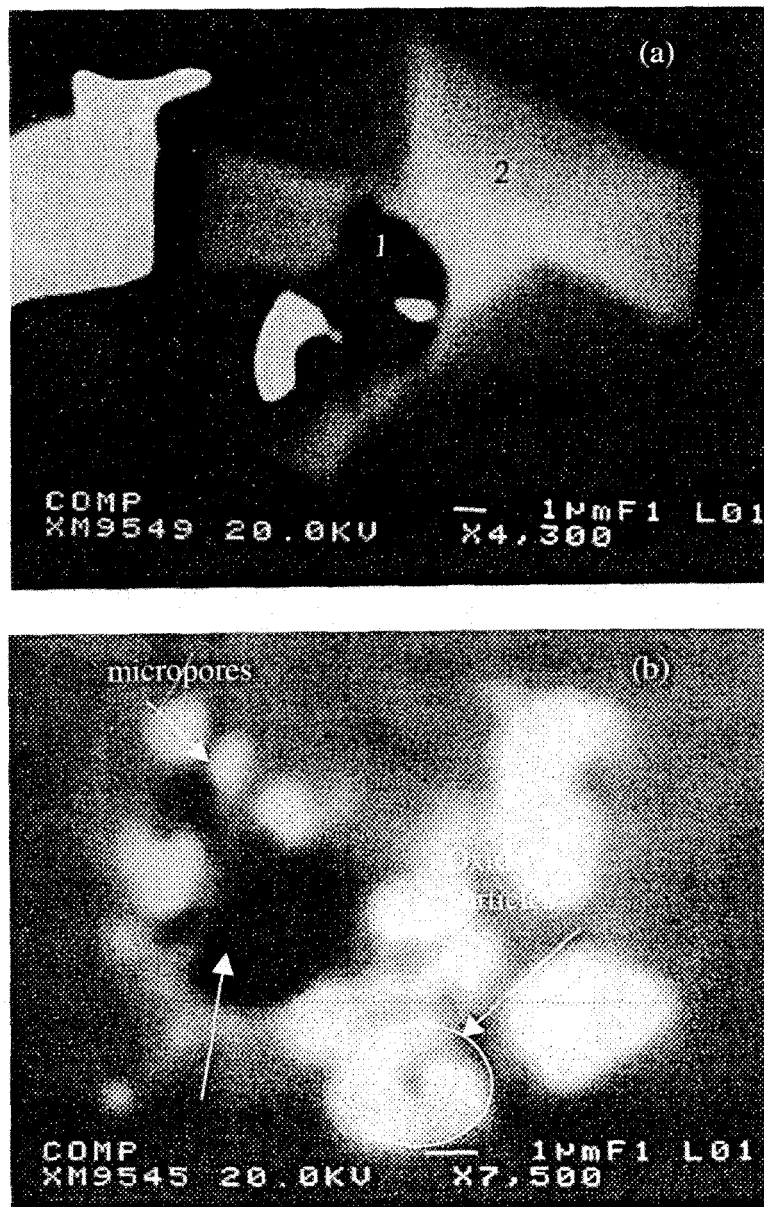


Figure 89. Backscattered images taken from (a) B, and (b) C alloy containing ~500 ppm Ca (large mold samples).

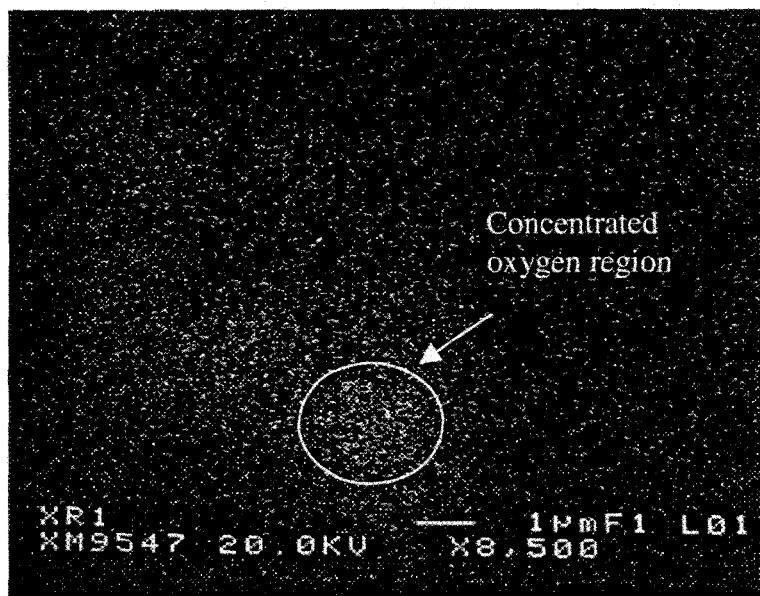


Figure 90. Backscattered image showing the oxygen distribution for the same particles illustrated in Figure 89(b).

Tables 16 and 17 show the WDS analysis results corresponding to the two cases shown in Figure 89. In Table 16, the spot analysis from positions 1 and 2 in Figure 89(a) corresponds to the centre and rim of the Ca compound particle, respectively. The high oxygen concentration observed in Figure 90 for the oxide particles of Figure 89(b) (circled areas) is in keeping with the WDS analysis given in Table 17. These observations again confirm that the microporosity observed in the B and C alloys with Ca (or Bi) additions are invariably associated with the presence of oxides.

Table 16 WDS analysis* corresponding to Figure 89(a), obtained from BC5 alloy (B alloy + 465 ppm Ca)

Alloy Code	Element	At%	Suggested composition	Ca/Sr ratio
BC5 (B alloy + 465 ppm Ca) Spot taken from the center (position 1)	Al	64.77	Al ₁₃ CaSr _{1.2} Si ₄	0.83
	Si	21.78		
	Ca	5.0	or	
	Sr	6.0	Al ₁₃ (Ca,Sr)Si ₄	
BC5 (B alloy + 465 ppm Ca) Spot taken from the rim (position 2)	Al	40.75	Al ₅ CaSr ₂ Si ₄	0.51
	Si	37.14		
	Ca	6.67	or	
	Sr	12.98	Al ₅ (Ca, Sr)Si ₄	

* Obtained from an average of 4 spots in each case

Table 17 WDS analysis* corresponding to Figure 89(b), obtained from CC5 alloy (C alloy + 486 ppm Ca)

Alloy Code	Element	At %	Suggested composition
CC5 (C alloy + 486 ppm Ca) Spot taken from the particle surface	O	37.8	CaO + other oxides
	Al	29.4	
	P	1.1	
	Si	19.6	
	Sr	4.8	
	Mg	2.4	
	Ca	4.5	

* Obtained from an average of 4 spots in each case

CONCLUSIONS

CONCLUSIONS

The effects of Bi and Ca as impurities in Al-Si-Cu 319 type casting alloys were investigated using different techniques. Based on the results obtained, the following conclusions could be drawn.

1. Bismuth always precipitates in the form of bismuth oxide due to its high oxygen potential, regardless of the Bi concentration or the chemical composition of the base alloy.
2. Bismuth counteracts the modification effect of Sr, as evidenced by the higher eutectic temperatures of 562°C at 2250 ppm Bi addition in B alloy, and 560°C at 5000 ppm Bi addition in C alloy, compared to 555°C in the Sr-modified 319 base alloy (B alloy). As a result, the Si appears in a coarse, acicular form instead of being fibrous. This observation is interpreted in terms of Bi-Sr or Bi-Mg-Sr interactions that reduce the amount of free Sr available for Si modification. These interactions are expected to take place in the molten state or during solidification, prior to the precipitation of the eutectic Si.

3. The addition of Bi to the Sr-modified 319 alloy leads to a gradual decrease in the eutectic undercooling from 1.2 °C until, at ~2250 ppm Bi addition, no undercooling is observed. At Bi addition exceeding 6500 ppm, an undercooling of 0.7 °C is observed, indicating that the Bi is now acting as a modifier.
4. The addition of 17 ppm Ca to Sr-modified 319 alloy leads to coarsening of the eutectic Si particles, due to the formation of the $\text{Al}_7(\text{Ca,Sr})\text{Si}_7$ compound. Further increase in Ca addition, up to 129 ppm, does not appear to produce further changes in the morphology or the dimensions of the eutectic Si particles.
5. The presence of Mg in Ca-containing high Mg 319 alloys (C alloy) results in changing the morphology and chemical composition of the Ca-containing phase (*i.e.*, from rod-type to plate-type). The chemical composition of the plate-type phase is close to $\text{Al}_2(\text{Ca,Sr})\text{Si}_2$, while that of the rod type is $\text{Al}_7(\text{Ca,Sr})\text{Si}_7$.
6. The presence of impurities, mainly AlP, $\text{Al}_2\text{O}_4\text{Mg}$, and MgO are found to act as nucleation sites for the plate-like Ca-containing phase. The growth of these plate-like particles takes place by an impurity-induced twinning mechanism.
7. Positive thermal gradient (upper thermocouple is at a higher temperature than the lower thermocouple) increases with the solidification time, reaching the maximum at complete solidification of the ingot. Thereafter, the thermal gradient declines.

8. The solidus interface velocity is affected by the rejection of solute atoms in front of the moving solid/liquid interface. This observation is more obvious in the small mold (0° angle) section than in the large mold (15° angle) section, due to the much higher velocity obtained in the former case.
9. Porosity formation in the Sr-modified and Sr-modified Mg-containing 319 alloys is affected only very slightly by Bi addition, a Bi addition of ~ 6000 ppm increasing the percentage porosity from 0.01% in Sr-modified 319 alloy to $\sim 0.04\%$.
10. In case of Ca additions, it is found that the porosity is mainly associated with Ca-oxide, rather than the Ca-compound particles. However, the porosity is also dependent to some extent on the particle size (*cf.* $\sim 10\text{-}15$ μm particle size for Ca-compound with $1\text{-}3$ μm for Ca-oxide).
11. Both BiO and CaO form very fine microporosity (less than 1 μm). Due to their fine size and also due to the concentration of such microporosity in/near the hot spots particularly in the case of the small mold castings, quantitative measurements of porosity are rendered difficult. This also explains the low percentage porosity values obtained in the B and C alloys with Bi and Ca additions.

SUGGESTIONS FOR FUTURE WORK

Based on the results obtained in the present study on the effect of Bi and Ca additions on the microstructural characteristics of 319 type alloys, it would definitely be of interest to extend the work to an investigation of the mechanical properties of these (and other Al-Si) alloys, such as the tensile, impact and fatigue properties. A study of the effects of the changes in the eutectic silicon particle characteristics and porosity (resulting from the presence of Bi and Ca) on these properties should prove extremely useful in finding the means to control the effect of tramp elements often present in commercial alloys. These studies could be further extended to cover the machinability characteristics - an important aspect in terms of the overall quality of the cast piece produced.

REFERENCES

REFERENCES

1. G.K. Sigworth, "Theoretical and Practical Aspects of the Modification of Al-Si Alloys," *AFS Transactions*, vol. 91 (1983), pp. 7-15.
2. *Aluminum: Properties and Physical Metallurgy*, J. E. Hatch (ed.), American Society for Metals, Metals Park, Ohio, (1984), pp. 224-225.
3. H. Toshihiro, K. Toshiro, N. Mitsuo and S. Yuichi, *Keikinzoku Gakkai Taikai Koen Gaiyo*, vol. 84 (1993), pp. 133-134.
4. T. Kobayashi, H. J. Kim and M. Niinomi, *Materials Science and Technology*, vol. 13 (1997), pp. 497-502.
5. A. Pennors, A.M. Samuel, F.H. Samuel and H.W. Doty, "Precepitation of β -Al₅FeSi Iron Intermetallic in Al-6%Si-3.5% Cu (319) Type Alloys: Role of Sr and P," *AFS Transactions*, vol. 106 (1998), pp. 251-264.
6. A.M. Samuel, P. Ouellet, F.H. Samuel and H.W. Doty, "Microstructural Interpretation of Thermal Analysis of Commercial 319 Al Alloy With Mg and Sr Additions," *AFS Transactions*, vol. 105 (1997), pp. 951-962.
7. F. Paray and J.E. Gruzleski, "Factors to Consider in Modification," *AFS Transactions*, vol. 102 (1994), pp. 833-842.
8. *Metals Handbook*, Ninth Edition, vol. 15: *Casting*, American Society for Metals, Metals Park, OH, (1987), pp. 159-161.
9. J.E. Gruzleski and B.M. Closset, *The Treatment of Liquid Aluminum-Silicon Alloys*, The American Foundrymen's Society, Inc., Des Plaines, IL, USA (1990), pp. 25-102.
10. D. Argo and J.E. Gruzleski, "Porosity in Modified Aluminum Alloy Castings," *AFS Transactions*, vol. 96 (1988), pp. 65-73.
11. A.V. Kurdyumov and S.V. Inkin, "Influence of Bismuth and Antimony on the Structure and Surface Tension of Alloy AL2," *Liteinoe Proizvodstvo*, No. 6 (1986), pp. 28-29.

12. S. Venkateswaran, R.M. Malliya and M.R. Seshadri, "The Effect of Trace Elements on the Cooling Curves, Microstructure and Mechanical Properties of Eutectic Aluminum-Silicon Alloy," *Cast Metals*, vol. 4, No. 2, pp. 72-82.
13. R. DasGupta, C.G. Brown and S. Marek, "Analysis of Overmodified 356 Aluminum Alloy," *AFS Transactions*, vol. 96 (1988), pp. 297-310.
14. N.R. Pillai and T.R. Anantharaman, "Elements of V Group as Modifiers of Aluminum-Silicon Alloys," *Transactions of the Metallurgical Society of AIME*, vol. 242 (1968), pp. 2025-2027.
15. *Metals Handbook*, Ninth Edition, vol. 15: *Casting*, American Society for Metals, Metals Park, OH, (1978), pp. 751-754.
16. S.Z. Lu, B. Lee and A. Hellwell, "Numerical Characterization of Microstructure Modified by Strontium in Al-Si Cast Alloys," *Proceedings of Materials Solutions Conference 98 on Aluminum Casting Technology*, pp. 291-296.
17. B.M. Closset, "Modification and Quality of Low Pressure Aluminum Castings," *AFS Transactions*, vol. 96 (1988), pp. 249-260.
18. P.D. Hess and E.V. Blackman, "Strontium as a Modifying Agent for Hypoeutectic Aluminum-Silicon Alloys," *AFS Transactions*, vol. 83 (1975), pp. 87-90.
19. B.M. Closset and J.E. Gruzleski, *AFS Transactions*, vol. 89 (1981), pp. 801-810.
20. G. Chai and L. Backerud, "Some Factors Affecting the Modification of Aluminum Silicon Alloys by Addition of Strontium Containing Master Alloys," *AFS Transactions*, vol. 100 (1992), pp. 847-854.
21. J.E. Gruzleski, "The Art and Science of Modification: 25 Years of Progress," *AFS Transactions*, vol. 100 (1992), pp. 673-683.
22. H. Beumler, A. Hammerstad, B. Wieting and R. DasGupta, "Analysis of Modified 319 Aluminum Alloy," *AFS Transactions*, vol. 96 (1988), pp. 1-10.
23. F.H. Samuel, P. Ouellet, A.M. Samuel and H.W. Doty, "Effect of Mg and Sr Additions on the Formation of Intermetallics in Al-6 Wt Pct Si-3.5 Wt Pct Cu-(0.45) to (0.8) Wt Pct Fe 319-Type Alloys," *Metallurgical and Materials Transactions A*, vol. 29A (1998), pp. 2871-2884.

24. A.M. Samuel and F.H. Samuel, "Modification of Iron Intermetallics by Magnesium and Strontium in Al-Si Alloys," *International Journal of Cast Metals Research*, vol. 10 (1997), pp. 147-156.
25. A.M. Samuel, H.W. Doty and F.H. Samuel, *Journal of Materials Science*, vol. 31 (1996), pp. 5529-39.
26. A.M. Samuel, J. Gauthier and F.H. Samuel, *Metallurgical and Materials Transactions A*, vol. 27A (1996), pp. 1785-98.
27. F.H. Samuel and A.M. Samuel, "Effect of Mg and Sr addition on the formation of iron-based intermetallics in Al-Si-Fe DC alloys", *Proc. Intl. Symposium on Light Metals*, Sudbury, Ontario, August 17-25, 1997, pp. 425-437.
28. A. M. Samuel, A. Pennors, C. Villeneuve, F.H. Samuel, H.W. Doty and S. Valtierra, "Effect of Cooling Rate and Sr-Modification on Porosity and Fe-Intermetallics formation in Al-6.5%Si-3.5%Cu-Fe alloys," *International Journal of Cast Metals Research*, vol. 13 (2000), pp. 231-253.
29. E.N. Pan, Y.C. Cherng, C.A. Lin and H.S. Chiou, "Roles of Sr and Sb on Silicon Modification of A356 Aluminium Alloys," *AFS Transactions*, vol. 102 (1994), pp. 609-629.
30. E.N. Pan, H.S. Chiou and G.J.Liao, "Effects of Modification and Solidification Conditions on the Feeding Behavior of A356 Al Alloy," *AFS Transactions*, vol. 99 (1991), pp. 605-621.
31. M. Garat, G. Laslaz, S. Jacob, P. Meyer, P.H. Guerin and R. Adam, "State-of-the-Art Use of Sb-, Na- and Sr-Modified Al-Si Casting Alloys," *AFS Transactions*, vol. 100 (1992), pp. 821-832.
32. G.K. Sigworth, C. Wang, H. Huang and J.T. Berry, "Porosity Formation in Modified and Unmodified Al-Si Alloy Castings," *AFS Transactions*, vol. 102 (1994), pp. 245-261.
33. S.T. Kao, E. Chang and L.C. Chan, "Effect of Hydrogen Content on Soundness of A356 Alloy Plate Casting," *AFS Transactions*, vol. 103 (1995), pp. 531-538.
34. Z. Zhang, X. Bian and X. Liu, "Heredity of Hydrogen in Al Alloys During Melting Process," *Materials Science*, vols. 331-337 (2000), pp. 307-312.

35. K. Tynelius, J.F. Major and D. Apelian, "A Parametric Study of Microporosity in the A356 Casting Alloy System," *AFS Transactions*, vol. 101 (1993), pp. 401-409.
36. G. Laslaz and P.Laty, "Gas Porosity and Metal Cleanliness in Aluminum Casting alloys," *AFS Transactions*, vol. 99 (1991), pp. 83-90.
37. N. Roy, "Etude parametrique de l'evolution de la porosite dans le system Al-9% Si-3% Cu", M. Eng. Thesis, UQAC, Chicoutimi, Qc, Canada, December 1994.
38. J.P. Anson and J.E. Gruzleski, "Effect of Hydrogen Content on Relative Shrinkage and Gas Microporosity in Al-7%Si Casting," *AFS Transactions*, vol. 107 (1999), pp. 135-142.
39. S.D. McDonald, K. Nogita, A.K. Dahle, J.A. Taylor and D.H. St.John, "Eutectic Solidification and Porosity Formation in Al-Si Alloys: Role of Sr." *AFS Transactions*, vol. 108 (2000), pp. 463-470.
40. A.N. Khorsani, "Gas Porosity in Aluminum Alloys", *Metal Casting and Surface Finish*, vol. (1996), pp. 35-39.
41. D. Emadi and J.E. Gruzleski, "Effect of Casting and Melt Variables on Porosity in Directionally Solidified Al-Si Alloys," *AFS Transactions*, vol. 102 (1994), pp. 307-312.
42. G. Boudreault, A.M. Samuel, F.H. Samuel and H.W. Doty, "Porosity formation in 319 aluminum alloy sand castings in relation to product quality for automotive applications," *Proc. Int. Symposium on Light Metals*, Sudbury, Ontario, August 17-25, 1997, pp. 369-384.
43. M. Serratos, D.R. Poirier and W. D. Lyman, "Effect of Stirring on Oxide Skins and Porosity in A356 aluminum Alloy," *AFS Transactions*, vol. 108 (2000), pp. 719-724.
44. F.H.Samuel, P. Ouellet and A. Simard, "Assessment of Melt Cleanliness and Analysis of Inclusions in Al-Si Alloys Using the Prefil Pressure Technique," *International Journal of Cast Metals Research*, vol. 12 (1999), pp. 17-33.
45. R. Fuoco, H. Goldenstein and J.E.Gruzleski, *AFS Transactions*, vol. 102 (1994), pp. 297-306.

46. P.D. Lee and J.D. Hunt, "Hydrogen Porosity in Directional Solidified Aluminum-Copper Alloys: In Situ Observation," *Acta Metallurgica*, vol. 45 (1997), No. 10, pp. 4155-69.
47. A.J. McAlister, *BAPD*, vol 5 (1984), pp. 247-250.
48. V.P. Sal'nikov and A.G. Zaigraikin, "Effect of Additions of Bismuth on the Properties of Aluminum Alloys," *Liteinoe Proivodstvo, Metalloved*, vol. 6 (1972), pp. 17-22.
49. N. Inoyama, K. Kkanehera and S. Yamamoto, "Influence of Te, Be, Ce and Bi on the formation of Modified Structure and Mechanical Properties in Eutectic Al-Si Cast Alloys," *Imono*, vol. 64 (1992), No.9. pp. 619-625.
50. A.V. Kurdyumov, S.V. Inkin, R. Bekher and I. Bekher, "Influence of Certain Elements on Structure and Surface Tension of Grade Al14 Alloys After Sodium and Strontium Treatments," *Soviet Casting Technology*, No. 7 (1988), pp. 17-19.
51. N.P. Pillai and T.R. Anatharaman, "Elements of V Group as Modifiers of Aluminum-Silicon Alloys," *Transactions of the Metallurgical Society of AIME*, vol. 242 (1968), pp. 2025-2027.
52. J.I. Cho and C.R. Loper, "Limitation of Bismuth Residual in A356.2 Al," *AFS Transactions*, vol. 108 (2000), pp. 359-367.
53. C.J. Machovec, G.E. Byczynski, J.W. Zindel, L.A. Godlewski, "Effect of Bi-Sr Interactions on Si Morphology in a 319-Type Aluminum Alloy," *AFS Transactions*, vol. 108 (2000), No. 76, pp. 439-444.
54. D.Kube, F. Josef, S. Siegered and A. Achen, "Effect of Antimony and Bismuth on the Grain Refinement and Porosity of the Alloy AlSi9Cu, Part2: Influence of Additional Elements on the Refining and Porosity of the Step Bars, Summary and Conclusions", *Giesserei*, vol 85 (1998), No. 10, pp. 38-42.
55. A.V. Kurdyumov and S.V. Inkin, "Influence of Certain Elements on Structure and Surface Tension of Grade AL4 Alloys After Sodium and Strontium Treatments", *Liteinoe Proizvodstvo*, No. 7 (1988), pp. 10-18.
56. C.R. Loper and J.I. Cho, "Influence of Trace Amounts of Calcium in Aluminum Casting Alloys, Review of literature," *AFS Transactions*, vol. 108 (2000), pp. 585-592.

57. M. Nagao, K. Kunii and K. Oosumi, "Effect of Bismuth with Calcium in Molten Aluminum Alloys," *Keikinzoku Gakkan Taikan Koen Gaiyo*, vol. 89 (1995), pp. 113-114.
58. Y. Tsumura, A. Sakakibara, K. Toyoda and S. Hara, "Influence of Ca on Al-Si Casting Alloys", *Journal of Japan Institute of Light Metals*, vol. 22 (1972), No. 6.
59. K. Hiroshi and A. Yoji, "Effects of Calcium on Hydrogen Absorption of Molten Al-Si Alloy," *Journal of Japan Foundry Engineering Society*, vol. 67 (1997), pp. 556-561.
60. E. Velasco, F. Hernandez, J.G. de la Rosa, S. Valtierra, J.F. Mojica and R. Colas, "Effect of Calcium on the Microstructure of a Cast Aluminum Alloy," *Light Metals 1998*, B. Welch (ed.), TMS, Warrendale, PA, 1998, pp. 993-1001.
61. S. Holecek, "Calcium Effect on the Foundry Properties of Eutectic Al-Si Alloys," *Slevarensvi*, vol. 1 (1976), pp. 9-10.
62. M.A. Moustafa, F.H. Samuel, H.W. Doty and S. Valitierra, "Effect of Mg and Cu Additions on the Microstructural and Tensile Properties of Sr-modified Al-Si Eutectic Alloys," *International Journal of Cast Metals Research*, vol. 14 (2002), pp. 235-253.
63. A. T. Joenoes and J.E. Gruzleski, *International Journal of Cast Metals Research*, vol. 4, (1991), pp. 62-71.
64. A. M. Samuel and F. H. Samuel, *Actes de colloque franco-canadien de septembre 1995*, A. Thorel, J. Masounave et M. Suéry (eds.), Les Presses de l'École des Mines de Paris, (1997), pp. 81-92.
65. M. Nagao, K. Kunii, K. Oosumi, *Keikinzoku Gakkan Taikan Koen Gaiyo*, vol. 89 (1995), pp. 113-114.
66. *Oxidation Potentials*, W. M. Latimer (ed.), Prentice-Hall, Inc., Englewood Cliffs, N. J., 1952, pp. 121-136.
67. H. Huang and J.T. Berry, "Evaluation of Criteria Functions to Minimize Microporosity Formation in Long-Freezing Range Alloys", *AFS Transactions*, vol. 101 (1993), pp. 669-675.
68. K. Tynelius, "A Parametric Study of the Evolution of Microporosity in Al-Si Foundry alloys", Doctor of Philosophy Thesis, Drexel University, (1992).

69. N. Roy, P.R. Louchez and F.H. Samuel, "Statistical analysis of porosity in Al-9wt%Si-3wt%Cu-X alloy systems", *Journal of Materials Science*, vol. 31 (1996), pp. 4725-4740.
70. R. W. Heine, C.R. Loper and P. C. Rosenthal, *Principles of Metal Casting*, American Foundrymen's Society, second edition, McGraw-Hill, New York (1967).
71. N. Roy, A.M. Samuel and F.H. Samuel, "Porosity Formation in Al-9 Wt Pct Si-3 Wt Pct Cu Alloy Systems: Metallographic Observations", *Metallurgical and Materials Transactions A*, vol. 27A, 1996, pp. 415-429.
72. A.M. Samuel, P. Ouellet, F.H. Samuel, H.W. Doty, "Microstructural Interpretation of Thermal Analysis of Commercial 319 Al; Alloy with Mg and Sr Additions", *AFS Transactions*, vol. 105 (1997), pp. 951-961.
73. D. Argo and J.E. Gruzleski, "Porosity in Modified Aluminum Alloy Castings," *AFS Transactions*, vol. 96 (1988), pp. 65-74.
74. Q.T. Fang and D.A. Granger, "Porosity Formation in Modified and Unmodified A356 Alloy Castings, *AFS Transactions*, vol. 97 (1989), pp. 989-1000.
75. H. Iwahori, K. Yonekura, K.Y. Yamamoto and M. Nakamura, "Occuring Behavior of Porosity and Feeding Capabilities of Sodium and Strontium-Modified Al-Si alloys," *AFS Transactions*, vol. 98 (1990), pp. 167-173.
76. A.K. Dahle, J. Taylor and D.A. Graham, "The Role of Eutectic Growth Mode in Porosity Formation in Al-Si alloys," *Aluminum Transactions*, vol. 3 (2000), pp. 17-30.
77. A. Knuutinen, K. Nogita, S.D. McDonald and A.K. Dahle, "Porosity Formation in Aluminum Alloy A356 Modified with Ba, Ca, Y, and Yb", *Journal of Light Metals*, vol. 1 (2001), pp. 241-249.
78. S.Holecek, "Einfluss verschiedener Kalziumgehalt auf das Lunkerverhalten eutektischer Aluminum-Silizium-Legierungen," *Aluminium*, vol. 84 (1973), pp. 811-812.
79. A. Abdollahi and J.E. Gruzleski, "An Evolution of Calcium as a Eutectic Modifier in A357 alloy", *International Journal of Cast Metal Research*, vol. 11 (1998), pp. 145-155.

80. K. Nogita, S.D. McDonald, J.W. Zindel and K.Dahle, "Eutectic Solidification Mode in Sodium Modified Al-7mass%Si-3.5mass%Mg Casting Alloys", *Materials Transactions*, vol. 42 (2001), pp. 1981-1986.